Manufacturing and characterization of microcapsules obtained by the PGSS process from water in oil emulsions stabilized by emulsifiers

Dissertation zur Erlangung
des Grades Doktor-Ingenieur

der Fakultät für Maschinenbau
der Ruhr-Universität Bochum
von

Luca Davico
aus Torino

Bochum 2018

Dissertation eingereicht am: 12.11.2018
Tag der mündlichen Prüfung: 17.12.2018
Erster Referent: Prof. Dr.-Ing. E. Weidner
Zweiter Referent: Prof. Dr.-Ing M. Petermann

List of publications

Part of the following works was used in chapter 4 “Apparatus and methods”:

L. Davico, R. Scholz, T. Vöpel, S. Kareth, E. Weidner, Effect of Emulsifiers in hard Fat Microcapsules Generated From an Emulsion, Proceedings of EMSF 2016.

T. Vöpel, R. Scholz, L. Davico, M. Gross, S. Büning, S. Kareth, E. Weidner, S. Ebbinghaus, Infrared laser triggered release of bioactive compounds from single hard shell microcapsules, Chemical communications (Cambridge, England) 51 (2015) 6913–6916.

Other publications:
R. Scholz, L. Davico, V. Jakobi, S. Kareth, A. Rosenhahn, E. Weidner, Verkapselungseffizienz und Freisetzungsverhalten fettbasierter Mikrokapseln mit lipophilen Emulgatoren, Chemie Ingenieur Technik 90 (2018) 562–567.

Acknowledgements

This work was possible thanks to the financial support from the People programme (Marie Curie Actions) of the European Union's Seventh Framework Programme FP7/2007–2013/ under REA grant agreement no. 316959 (DoHip project, ''Training Program for the Design of Resource and Energy Efficient Products by High Pressure Processes'').

I would like to thank my supervisor Prof. Dr.-Ing. E. Weidner from the Ruhr-Universität Bochum for the opportunity to work in the Chair of Process Technology. I am grateful for his scientific advices, guidance and support.

My gratitude also goes to Prof. Dr.-Ing. M. Petermann for his help, discussing my research activity.

Thank you to Dr. S. Kareth for her support and encouragement in these years.

Many thanks to all the professors of the DoHip project. Especially I want to thank Prof. A. Martín of the University of Valladolid for his assist during my PhD exchange in Spain.

My gratitude to all the companions and friends of the DoHip project. Thanks to Alba, Alejandro, Amit, Candela, Daniel, Elvira, Gyorgy, Joana, Markus, Milica and Sara for all the time spent together discussing our projects, laughing or enjoying a beer. I want to thank Sara in particular, for her friendship and assistance during this time in Germany.

Thanks to the colleagues of the Chair of Process Technology and Solid Process Engineering. Many thanks to my office colleagues, Dr. R. Scholz and K. Grübel.

Thanks to all the people collaborating in the C2 Resolv group, in particular Dr. T. Vöpel and Dr. V. Jacobi for their cooperation.

Many thanks to all the students that assisted me in these years: D. Gerasimova, N. Roß, S. Ruiz, A. Meinhardt, S. Singh, R. Flug and K. Aoun.

Special thanks to the friends I made in Bochum, supporting each other in foreign land. Thanks Audrey, Davide, Elisa, Francesco and Irene.

Last but not least I want to express my gratitude to my family for their support and encouragement regardless of the distance. Grazie, vi voglio bene!

Luca Davico

Abstract

Recently, growing attention is paid to the use of supercritical fluids, more frequently $scCO_2$, in high pressure processes for the generation of powderous composites, encapsulating active substances (core) into a solid fat or polymer (shell). Those active substances, e.g. vitamins, medical drugs and flavours, can be rather expensive. At least a part of it is lost during the processing. Overarching aim of this work is to understand the parameters causing the losses and to find ways to reduce that loss. The use of a dense gas enables the production of solvent-free capsules as CO_2 is **G**enerally **R**ecognized **A**s **S**afe (GRAS-Fluid). The **P**article from **G**as **S**aturated **S**olutions (PGSS) process has been proven to be suitable for the generation of water filled microcomposites. This work focuses on improving the understanding of the PGSS process concerning encapsulation, investigating the role of additives in the sprayed material, such as emulsifiers, and the process parameters.

Prior to performing PGSS-experiments, the phase behaviour of Witepsol W31 (shell material) and CO_2 was studied at different temperatures and pressures. The experimental results were then modelled with the **G**roup **C**ontribution **E**quation of **S**tate (GCEoS). The same EoS was employed to model the three-phase system W31 (shell) - H_2O (core) - CO_2.

Performance of the emulsifiers with the shell material was assessed using the **M**elt **D**ispersion **T**echnique (MDT), which requires the preparation of a double emulsion **W**ater in **O**il in **W**ater (W/O/W). The produced capsules were molten with a microscopy technique combined with high speed image acquisition and laser induced heating. Between the chosen emulsifier PGPR 4125 at 5% w/w in shell material showed a good compatibility with Witepsol W31, enhancing the encapsulation and slowing down the release of the NaCl solution.

Capsules produced with the PGSS technique showed a higher encapsulation of NaCl compared to the MDT capsules, but faster release due to the smaller dimensions and the presence of holes in the shell material while solidifying in the spray tower. From these experiments a way to estimate the loading efficiency of water in the microcomposites has been found. This opens the pathway to improved operating conditions with minimised losses of highly priced active ingredients, by knowing the thermophysical properties of the materials involved in the process and the process parameters.

Finally, an economic evaluation for a PGSS plant that produces 10 t/day of capsules. Sensitivity analyses, up to 100 t/day, were performed as well as the study of a PGSS plant with a 90% recycle of CO_2. The total added value cost per kg of liquid-filled capsules is in the same range like the costs for producing powders from pure substances.

Notation

Latin and danish alphabet

Symbol	SI unit	Description
A	J	Helmholtz energy
A	m^2	Heat transfer area
c_p	kJ/(kg K)	Heat capacity
CF	-	Correction factor
d	m	Diameter
d_c	cm/mol	Critical diameter
EE	-	Encapsulation efficiency
g	-	Attractive energy parameter
h	J	Enthalpy
H	-	Auxiliary quantities
k	-	Binary interaction parameter
L	m	Length
LE	-	Loading efficiency
m	kg	Mass
$\dot{m}$	kg/s	Mass flow
MC	%	Moisture content
MW	g/mol	Molecular weight
MW^*	g/mol	Modified molecular weight
n	mol	Mole
O	-	Oil
P	Pa	Pressure
$\dot{Q}$	W	Power
q	-	Number of surface fragments
R	J/(K mol)	Gas constant
T	K	Temperature
T^*	K	Arbitrary reference temperature
U	J/(s K m^2)	Overall heat transfer coefficient
V	m^3	Volume
w	kg	Weight
w	J	Work
W	-	Water
x	-	Mass or mole fraction in heavy phase
y	-	Mass or mole fraction in light phase
Z	-	Compressibility factor
Ø	m	Diameter of pipes

Greek alphabet

Symbol	SI unit	Description
α	-	NRTL non-randomness parameter
γ	N/m	Surface tension
θ	-	Surface fraction
λ	kJ/kg	Latent heat of solidification/evaporation
ν	-	Number of groups
π	-	pi
ρ	kg/m^3	Density
σ	m^2	Surface area
φ	-	Fugacity coefficient

Pedices and indices

Pedices		Indices	
Symbol	**Description**	**Symbol**	**Description**
bulk	Bulk	*att*	Attractive
c	Critical	*C*	Configurational
Caps	Capsules	*ideal gas*	Ideal gas
CO_2	Carbon dioxide	*fv*	Free volume
cyl	Cylinder	*residual*	Residual
degas	Degasified	‘	Conditions ‘
dry	Dry	‘’	Conditions ‘’
em	Emulsifier		
empty	Empty		
ext	External		
filt	Filtered		
full	Full		
H_2O	Water		
i	Substance i		
melt	Melting		
NaCl	Sodium chloride		
p	Pressure		
sample	Sample		
tot	Total		
wat	Water		
wet	Wet		
W31	Witepsol W31		
10	10 %		
50	50 %		
90	90 %		

Table of content

List of tables

List of Figures

1 Introduction

Microencapsulation is defined as a "technology of packaging solids, liquids, or gaseous materials in miniature, sealed capsules that can release their contents at controlled rates under specific conditions" [1]. The final product of microencapsulation, referred to as microcapsule, is characterized by at least two materials, the shell material and the core material. Different compounds with value for the use in the food, cosmetic or pharmaceutical industry [1–6] can be used as core materials. Examples of these compounds are aromas [7], vitamins [8] or proteins [9]. Encapsulation is a way to increase the shelf life, to improve stability and to control the release of the encapsulated active compounds.
In the last decades particular attention has been paid to supercritical fluids and high pressure processes for the generation of powderous composites [10]. In particular, supercritical or compressed CO_2 has been proven to be a promising alternative to the various solvents commonly employed in encapsulation techniques, with the advantage of being a GRAS (**G**enerally **R**ecognized **A**s **S**afe) component, helping in producing solvent-free capsules. Different techniques and processes are available, each of them exploiting a distinct effect and behaviour between the substances involved with CO_2.

The **P**articles from **G**as **S**aturated **S**olution (PGSS) process has been employed as a high pressure encapsulation technology method. Previous studies showed that powders from polymers and fat could be easily obtained with this process [11–14]. Furthermore PGSS processes can be used to generate microcomposites, ranging from water encapsulated in fat to liquors in chocolate [11].

In this work Witepsol W31, a solid fat with a melting point of 35-37 °C, was employed as shell material. The core material was a 9% w/w solution of NaCl in water. NaCl was used as a tracer to study of the encapsulation efficiency of the process and to verify the release pattern of the encapsulated material in water. Emulsifiers, like Span 65 or PGPR 4125, were also added to the shell material to investigate their effect on the encapsulation efficiency and the release of the encapsulated substance.

Prior to performing the experiments, the phase behaviour of Witepsol W31 and CO_2 was studied at different temperatures and pressures (chapter 5). The experimental results were then modelled with the **G**roup **C**ontribution **E**quation of **S**tate (GCEoS), firstly introduced by Skyold-Jørgensen [15,16]. The same EoS was employed to model the three-phase system W31-H_2O-CO_2, providing information hardly obtainable via experiments.

Subsequently (chapter 6), the performance of the emulsifiers was assessed using the **M**elt **D**ispersion **T**echnique (MDT), which firstly requires the preparation of an emulsion between the molten shell material, the emulsifier and the core material. Once this is achieved warm water is added and a double emulsion **W**ater in **O**il in **W**ater (W/O/W) is

produced. By adding cold water and bringing the temperature of the double emulsion under the melting point of the shell material, capsules are formed. Two different amounts of emulsifiers were employed (1% and 5% w/w in respect to the shell material). The produced capsules were also molten with a microscopy technique combined with high speed image acquisition and laser induced heating. In order to work with this instrument a fluorescent protein was added to the core material, so it was possible to observe the behaviours of the capsules generated with different emulsifiers.

In chapter 7 the PGSS technique is employed. Firstly powder of Witepsol W31 was generated, with a two-fold aim: to verify that the shell material behaved similarly to other fats [13,17,18] and to observe the effects of different parameters, such as temperature and pressure before expansion, which could be modified in the PGSS plant. After that, the generation of microcomposites proved to be possible and the results were similar to previous findings [17,18] on different substances or emulsifiers. A way to estimate the loading efficiency of water in the microcomposites starting from the spraying conditions is illustrated. This proved to be quite reliable when compared to the experimental results of the present and previous works [17,18].

Finally, chapter 8 contains an economic evaluation for a PGSS plant that produces 10 t/day of capsules. To achieve this, the evaluation method described in [19] was employed. Sensitivity analyses, up to 100 t/day, were performed as well as the study of a PGSS plant with a 90% recycle of CO_2.

2 State of the art

Microencapsulation techniques proved to be a suitable technique for the protection of sensitive substances from degradation or to facilitate their transport [20,21]. It can also help to control the release of the encapsulated substances like aromas [7], vitamins [8] or proteins [9]. Different methods are available in industry, ranging from chemical methods like coacervation or in-situ polymerization to physical processes as extrusion or spray-drying [22,23].

2.1 - Supercritical fluid processes

Supercritical fluids processes have shown potential as methods to produce powders and to achieve encapsulation [14,24]. One of the advantages of these processes is the possibility to work at lower operative temperatures for thermolabile substances. Moreover, if the chosen fluid is inert (e.g. CO_2), it is possible to reduce or completely eliminate the use of other solvents (in applications that require a solvent), which could be contaminants in the final product. By varying the process parameters, the final product properties can be tuned [14,18,25].

Microcomposites or microcapsules generated by supercritical fluids processes can be obtained by exploiting different behaviour of the supercritical fluids and the materials involved. For example CO_2 and polymers/fats solubilize into each other. Therefore different techniques can be employed depending on the phase in which the method operates.

A showcase of the different methods and techniques will be presented in the next paragraphs. Each of them will focus on how a supercritical/high pressure fluid is used and which role it plays in the generation of powders and capsules.

2.1.1 - Rapid Expansion of Supercritical Solutions (RESS)

In the RESS process the supercritical fluid is chosen to exploit its solvent power and in particular the great change in solvent power due to pressure changes. As shown in fig. 1, the supercritical fluid dissolves the solute and then it is rapidly expanded which brings the solute to precipitate in pulverous form [10,14,26–28]. The technology can be adapted for the formation of composites as well; this can be achieved by dissolving both the shell and core material in the supercritical fluid.

One of the major limitations of the RESS technology is the poor solubility of substances in supercritical fluids like CO_2; this limitation can be overcome by adding a co-solvent. Moreover, in case of composites generation, the morphology and the content of the encapsulated material are very difficult to control because of the rapid expansion [25,27,29].

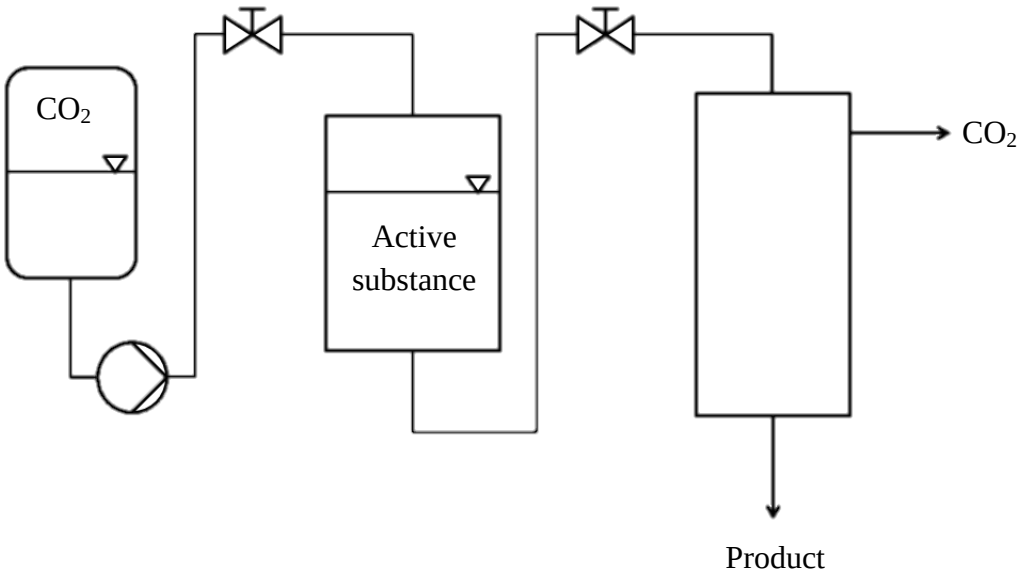

Figure 1 - RESS process

2.1.2 - Supercritical Anti Solvent (SAS)

Opposite to the RESS process, in the SAS process (fig. 2) the supercritical fluid is used as an anti-solvent. The substance to pulverize is dissolved in a liquid solvent. This is then saturated with the supercritical fluid which leads to the precipitation and pulverization of the solute due to an anti-solvent effect, i.e. it reduces the solubility of the material that is required to be powderised in the solvent so that it precipitates [10,14,26,30].

The powder is collected on a filter which is placed in the bottom of the autoclave.

To obtain composites with the SAS technology the core and shell material can be co-precipitated at the same time in the same solvent. If the chosen carrier and core substances are not both soluble in the same solvent it is possible to use two different solvents. Nevertheless the two solutions have to undergo the SAS process at the same time [25,31,32].

The presence of a solvent, most of the time an organic solvent, is one of the disadvantages of this technique because it requires an extra step in order to remove the solvent from the final product. On the other hand, the solvent may be beneficial to the overall process because it improves the solvent power when compared to the supercritical gas alone.

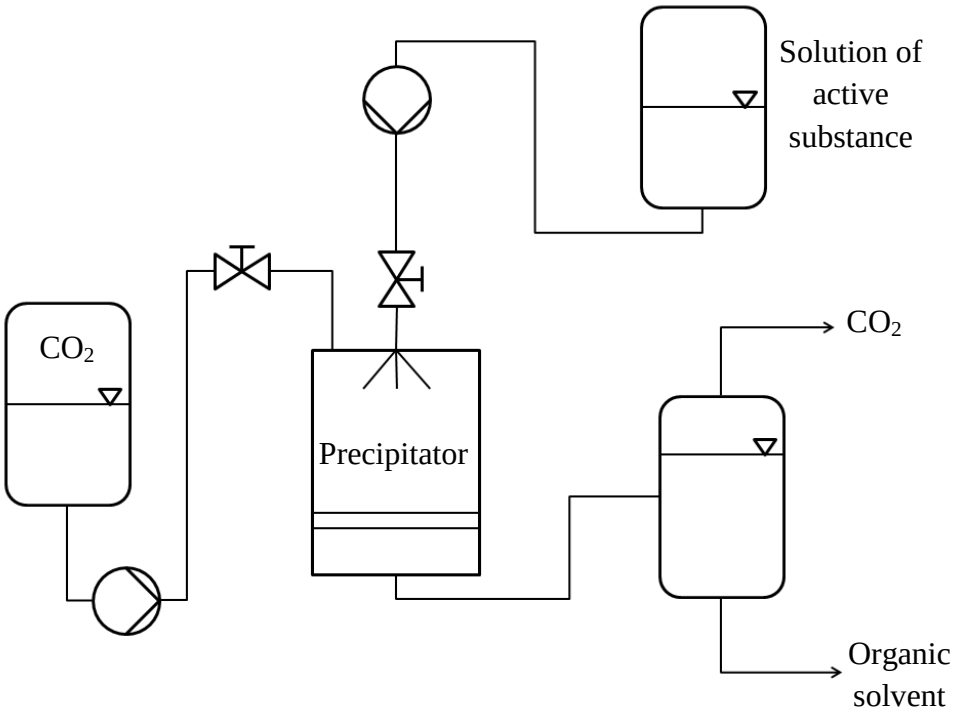

Figure 2 - SAS process

2.1.3 - Supercritical Fluid Extraction of Emulsions (SFEE)

A supercritical fluid can also be used for its anti-solvent properties in the SFEE.

This technology was firstly introduced by Perrut et al. [33], who dissolved a water soluble component in the dispersed phase of a W/O emulsion. An organic solvent and supercritical CO_2 where used together to dry the emulsion and form particles.

The principle behind is similar to the SAS process, as well as the equipment required (figure 3). The main difference between the SAS technique and the SFEE is the presence of an emulsion instead of a solution of the substance to be micronized, which requires an extra step in the preparation of the initial materials. Moreover the **P**article **S**ize **D**istribution (PSD) of the dispersed phase of the emulsion introduces a new controlling parameter besides pressure, temperature, concentrations and flow rates. Another difference is that in general the product obtained from this process is liquid, which then requires further steps to obtain the final product as powder [25,34].

It is possible to operate in semi continuous (the setup is shown in fig. 3) or in batch mode. In the last case the emulsion is loaded in the precipitator and the supercritical fluid is bubbled through it. If CO_2 has a sufficiently high flow then it is possible to completely evaporate both the aqueous fraction of the emulsion and the organic solvent, leading to the direct production of dry powder.

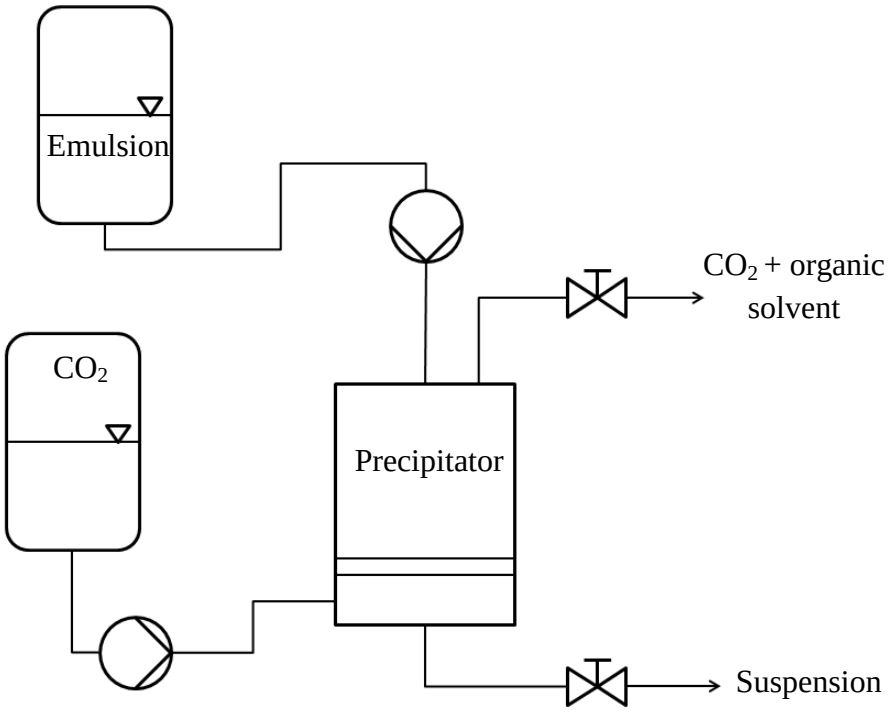

Figure 3 - SFEE process

2.1.4 - Particles from Gas Saturated Solutions (PGSS)

In the PGSS process the supercritical fluid is dissolved in the material to be micronized. This changes the properties of the material, which renders it easier to be micronized. The material, which has to reach liquid state, is heated to the required temperature and pressurized to the designated pressure when it is mixed with the supercritical fluid, for example CO_2. This mixture is then expanded to ambient pressure and the expanding gas removes heat due to the Joule-Thomson effect, and the material solidifies [35,36].

PGSS can be performed as a batch (fig. 4) or as a continuous process (fig. 5). In the first case the chosen material and CO_2 are premixed in a tank at the chosen temperature and pressure. This solution is then expanded. In the second case, the substances are heated and pumped separately and the mixing takes place before the expansion, e.g. via static mixer.

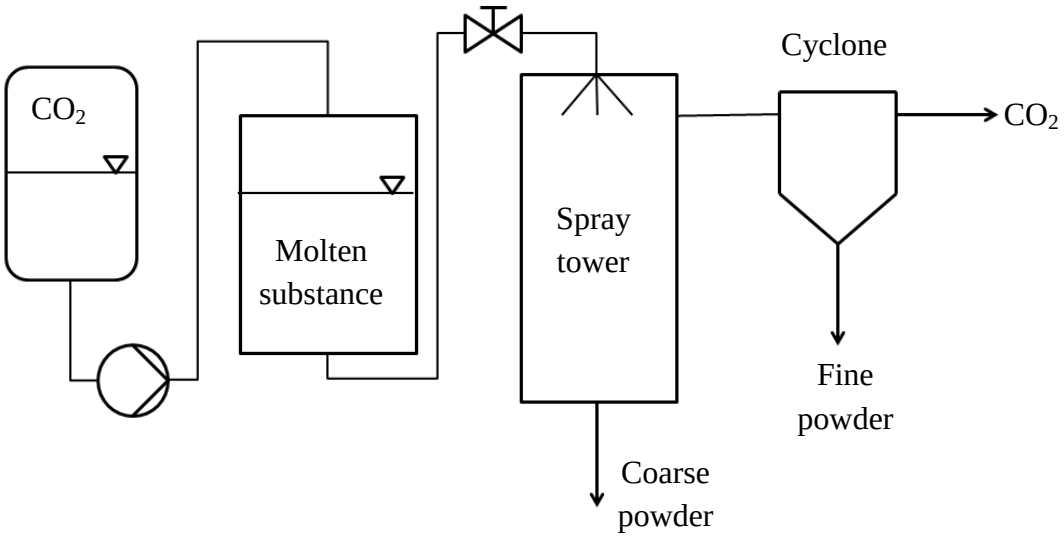

Figure 4 - Discontinuous PGSS

To generate composites via the PGSS process different approaches can be used:

1. The substance that will act as shell is premixed with supercritical CO_2. It is then pumped and mixed with the core material before the expansion [18,37];
2. Shell material, core material and CO_2 are brought to the required T and p separately and mixed before the expansion [11,17,38];
3. An emulsion of the shell material and of the core material is previously prepared and then pumped to be mixed with CO_2 before the expansion (this work).

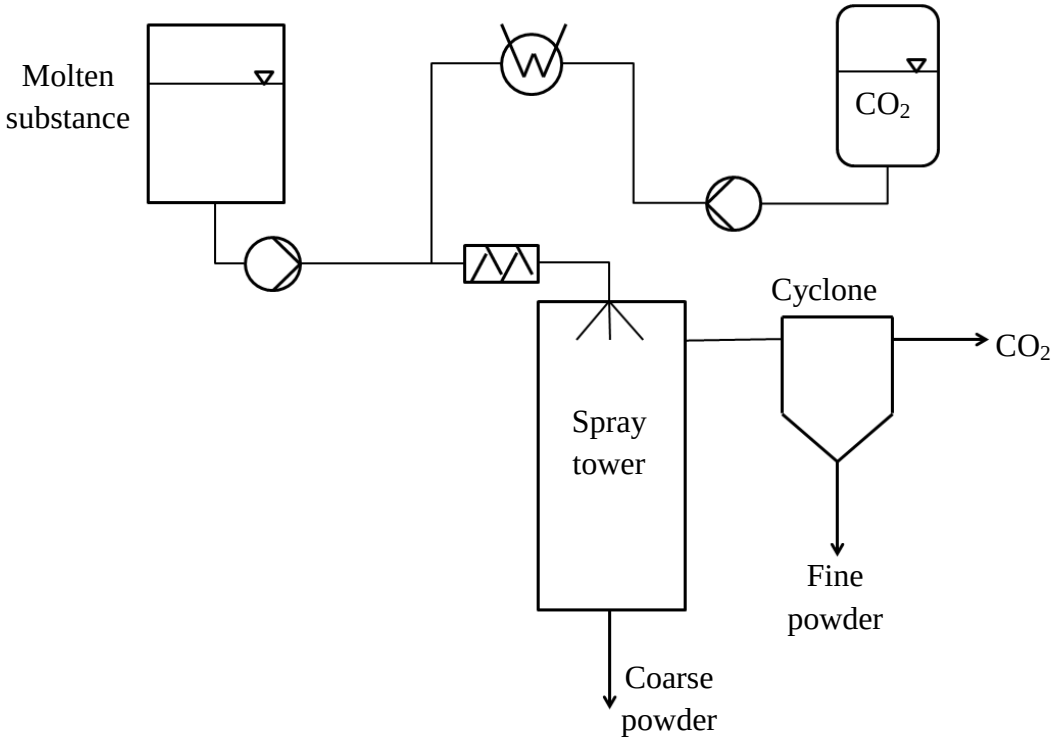

Figure 5 - Continuous PGSS

2.2 - Emulsion

An emulsion is defined as "a dispersion of two immiscible liquids" [39]. The liquid that is dispersed inside the other may be referred to as dispersed phase or internal phase, while the other phase is referred to as continuous phase or external phase. In this work the liquids are an aqueous phase and an oily phase, therefore two kinds of emulsions are possible depending on which is the dispersed phase and which is the continuous phase. It is possible to form a **W**ater in **O**il emulsion (W/O) in which the aqueous phase is the internal phase or an **O**il in **W**ater emulsion (O/W) in which the oily phase is the dispersed phase.

2.2.1 - Formation of an emulsion

In order to disperse one of the liquid into the other it is necessary to provide energy, otherwise the molecules would stay in their respective phase and would not disperse. The energy required is represented in eq. 1

$$dw = \gamma d\sigma \tag{1}$$

where dw is the work needed, γ is the surface tension and $d\sigma$ is the new generated surface area. From Eq. (1) it can be observed that to reduce the energy required to obtain an emulsion it is possible to choose to have bigger droplets, therefore reducing the generation of new surface area $d\sigma$, or intervening on the surface tension γ, adding in the system substances that reduce it [40].

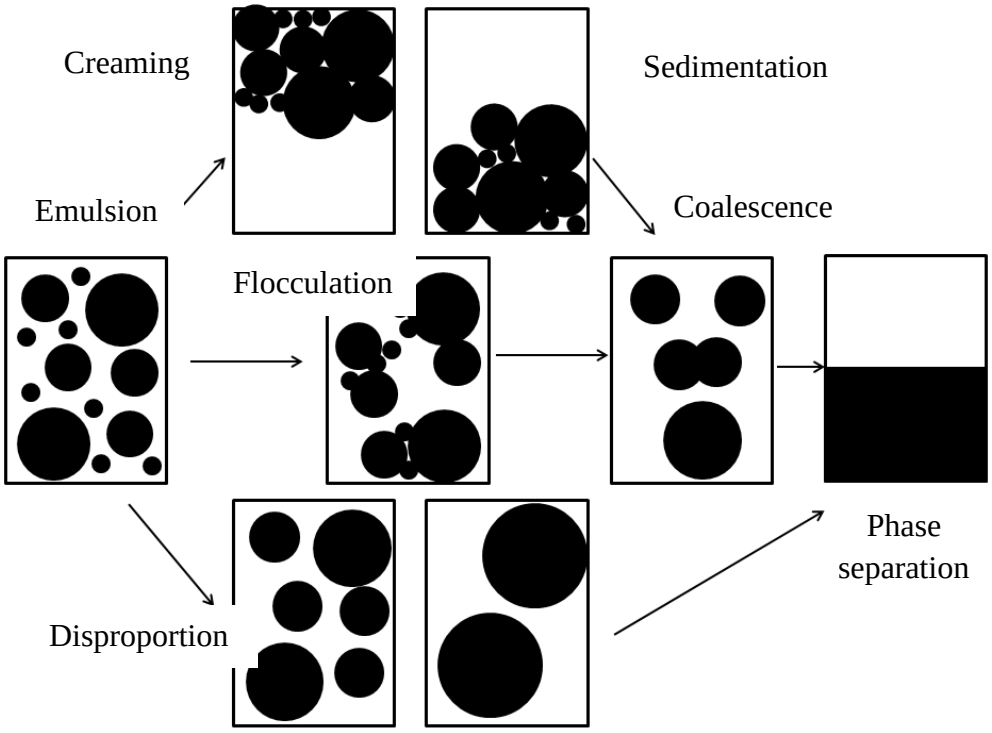

Figure 6 - Destabilization mechanics. Redrawn from [40].

An emulsion is a thermodynamically unstable system and eventually both phases will separate.

Three processes (fig. 6) are causing the breakage of the emulsion [40]:

- Sedimentation or creaming: the density difference between the two phases brings the dispersed phase to rise (creaming) or to sediment (sedimentation).
- Disproportionation: in order to reduce the potential energy at the interface, the droplets decrease the surface area with the diffusion of the smaller droplets into the largest.
- Flocculation and coalescence: when two droplets encounter one another they may flocculate and coalesce.

To help the formation and stabilization of an emulsion an extra component is added to the two phases: an emulsifier.

2.2.2 - Emulsifiers

Emulsifiers belong to the family of the surfactants. The name comes from the crasis of the words "*surf*ace *act*ive age*nts*". This implies that these substances play a certain role at the surface/interface of different phases. In general they are formed by a hydrophilic head that interacts with the aqueous phase and a lipophilic tail which is attracted by the oily phase [41]. The surfactants can be classified based on a number called HLB, the **H**ydrophilic-**L**ipophilic **B**alance. This concept has been first introduced by Griffin [42,43] in order to classify surfactants in relation to their behaviour and solubility in water. This classification takes into consideration that any surfactant is a molecule composed by a hydrophilic and a lipophilic part and that the proportion between the two can indicate the behaviour that the surfactant may exhibit. Griffin developed an experimental method to determine the HLB value of the surfactants [42] and a way to calculate the HLB value of non-ionic surfactant based on their type [43]. Davies [44] continued this work and developed a new formula to calculate the HLB values of surfactants (ionic or not) based on the chemical formula, assigning an HLB group number to hydrophilic and lipophilic groups (an extract of this work is shown in table 1).

Table 1 - Extract of Group number for the HLB calculation from [44]

Hydrophilic groups	Group number
N (tertiary amine)	9.4
Ester (sorbitan ring)	6.8
Ester (free)	2.4
-COOH	2.1
Lipophilic groups	
-CH- $-CH_2-$ CH_3- =CH-	-0.475

From the group numbers it is possible to calculate the HLB value of a chosen surfactant using Eq. 2

$$HLB = \sum hydrophilic\ group\ numbers - n * (lipophilic\ group\ number) + 7 \quad (2)$$

where *n* is the number of lipophilic groups in the molecule of the surfactant.

The HLB value purpose is only to indicate for which application the surfactant is most suitable for rather than how good it is in the system. Table 2 summarizes the use of a surfactant according to its HLB value. The value of HLB ranges from 1-20. Low HLB emulsifiers are soluble in oil while high HLB emulsifiers are soluble in water.

Table 2 - Classification of surfactant based on HLB value

HLB value	Application
3.5 - 6	W/O emulsifier
7 - 9	Wetting agent
8 -18	O/W emulsifier
13-15	Detergent
15-18	Solubilization

2.2.3 - Role of emulsifiers

Emulsifiers play different roles in an emulsion. Due to their amphiphilic nature, emulsifiers tend to occupy the area which forms the interface between the two phases. This has two major effects on the emulsion [40]:

1) it reduces the surface tension, therefore less energy is required to generate an emulsion;
2) it increases the stabilization of the emulsion.

The stabilization mechanism depends on the nature of the emulsifier. In case of an anionic or cationic emulsifier it prevents coalescence due to the formation of an electric double layer. The ionic emulsifier accumulates at the interface and charges it, thus increasing the repulsion potential between the droplets. When the emulsifier is non-ionic the stabilization is provided by the formation of a steric barrier. At the interface the emulsifier orientates itself with the lipophilic tail in the oil phase and the hydrophilic head in the water phase. By forming a densely packed layer at the surface, coalescence can be prevented. The effectiveness of an emulsifier against demulsification depends on how it is packed at the surface and on the substances involved.

2.3 - Microcomposites

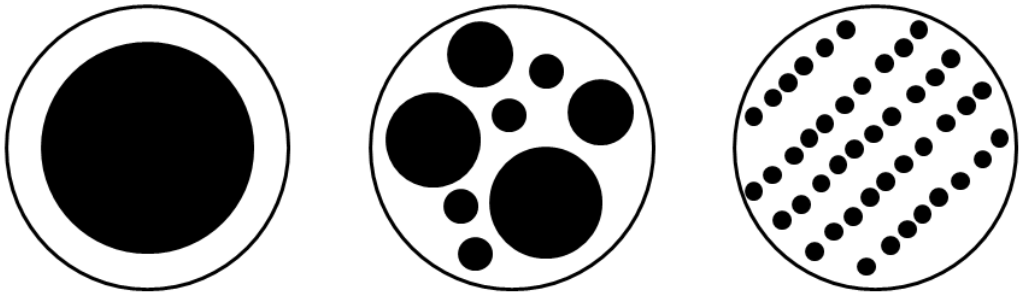

Mononuclear capsule Polynuclear capsule Matrix capsule

Figure 7 - Types of composites

The products obtained from the PGSS process are pulverous microcomposites. The term composite refers to a mixture of at least two substances, one being a solid material, the shell material, and the other one, as a solid, liquid or gas, is called core material [17]. The powder is referred to as a closed composite when the liquid is entrapped inside the shell material. When the entirety of the core material is concentrated in a specific area of the shell material, the composite is referred to as a "core-shell" or "mononuclear" type. If the core material is distributed inside the shell material in more than one domain (e.g. a droplet), it belongs to the "matrix" type when the droplets are non-randomly distributed, otherwise they are referred to as "polynuclear" [22]. The opposite are the open composites, where the liquid is outside the shell material but bound to it. The liquid may be bound in different ways, for example by adhesion or entrapped between particles.

In case of microcomposites produced with the PGSS process, Hanu [24] showed through a low field H-NMR analysis of the microcapsules obtained from spraying hydrogenated castor oil as shell material and water that the liquid can be entrapped in different ways. By analysing the relaxation times the author identified three types of water. The one that showed the major mobility was water accumulated between particles, easily lost through evaporation. The other two types showed less mobility, the water being entrapped in the matrix of the shell material or directly bond to the shell material. This last one may due to the affinity between the shell material, in the work of Hanu hydrogenated castor oil, and water. Hydrogenated castor oil is also known as PEG-40, which may also be used as an emulsifier and has a HLB value of 15, sign of high affinity with water. This affinity could explain the higher water content in PEG-40/water capsules compared to the one of tripalmitin/water.

3 Materials

In this chapter the materials employed for this work will be summarized. The main capsule components were Witepsol W31, employed as shell material, and water as core material. Sodium chloride was utilized as indicator, as well as enhanced yellow fluorescent protein. The emulsion was prepared with different emulsifiers: Span 65, Span 80, Tween 80 and polyglycerol polyricinoleate 4125 (shortened to PGPR). In order to obtain particles or microcomposites with a PGSS process, compressed and supercritical CO_2 was employed.

3.1 - Witepsol W31

Witepsol W31 is a white hard fat at ambient temperature. It is a mixture of triglycerides (65-80 %), diglycerides (10-35 %) and monoglycerides (1-5 %). The monoglycerides contained are not sufficient to produce stable emulsions, therefore the presence of an emulsifier is required. It melts at 35-37 °C and it has a yellow-brown color. Witepsol W31 was obtained from CREMER OLEO GmbH & Co. KG (Germany), now IOI Oleo GmbH. In this work Witepsol W31 is used as the shell material for the microcomposites. Some characteristics of Witepsol W31 are summarized in table 3 [45].

Table 3 - Material data of Witepsol W31 at ambient pressure

	Value	**Unit**
Melting point	35÷37	°C
Hydroxyl number	31	mg KOH/g
Acid number	0.2	mg KOH/g
Saponification value	225 - 240	mg KOH/g
Density (25 °C)	956.3	kg/m³
Density (40 °C)	933.1	kg/m^3
Viscosity (40 °C)	39.8	mPas

3.2 - Water

Water is a taste-, color- and odorless substance. It solidifies at 0 °C and evaporates at 100 °C when at ambient pressure. Water reaches supercritical conditions at 374 °C and 22 MPa. In this work deionized water has been used as the core material of the microcomposites. In table 4 some relevant characteristics of water are collected [46].

Table 4 - Material data of water at ambient pressure

	Value	Unit
Density (25 °C)	997.042	kg/m³
Viscosity (25 °C)	0.890	mPas
Molar mass	18.01	g/mol

3.3 - NaCl

Sodium chloride (NaCl) is a salt composed in a 1:1 ratio of Na^+ and Cl^- ions. NaCl was obtained from Fischer Chemicals (U.K.). It has been used as a marker in the internal water phase because its presence changes the conductivity of the water. It also proved of particular interest for the development of emulsions for sodium-reduced liquid-processed foods [47]. The characteristics of NaCl are summarized in table 5 [46]

Table 5 - Material data of NaCl at ambient pressure

	Value	Unit
Molar mass	58.44	g/mol
Solubility in water (0 °C)	35.7	100 parts
Solubility in water (100 °C)	39.8	100 parts

3.4 - Enhanced Yellow Fluorescent Protein

Enhanced **Y**ellow **F**luoroscent **P**rotein (eYFP) is a modification of the **G**reen **F**luorescent **P**rotein (GFP). Like other fluorescent proteins it is used in fluorescence microscopy as reporters in cells or animals. It has a melting point of 78 °C. Specifically, when excited at 514 nm it emits fluorescent light up to 527 nm [53].

In this work it has been used as core material, in order to observe both the melting process of the capsules and what happens to them in the presence of different emulsifiers.

3.5 - Span 65

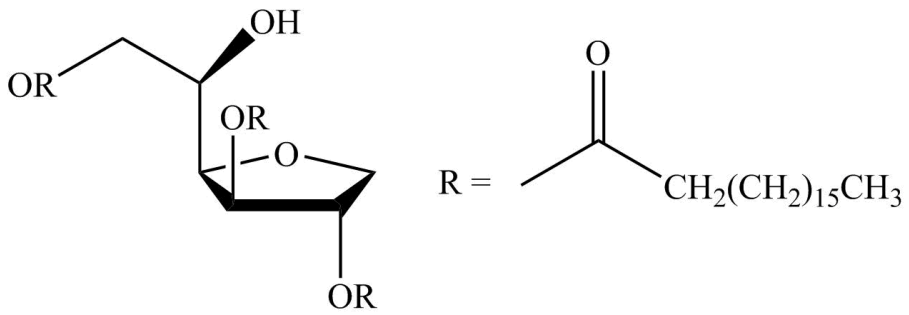

Figure 8 - Structure of Span 65

Sorbitan tristearate, sold under the trade name Span 65, is a white waxy powder at room temperature with a HLB value of 2.1, and therefore suitable for the preparation of W/O emulsions. It melts at 60 °C [48].

This nonionic emulsifier is approved by the EU as a food additive (identification number: E492) and it is used, for example, in the production of ice cream or baked foods. The product used in this work comes from the company Sigma Aldrich GmbH. An overview of the most important material data is given in table 6 (Sigma Aldrich GmbH, 2013). The water content was measured via Karl-Fischer Titration.

Table 6 - Information on Span 65

	Value	**Unit**
Chemical formula	$C_{60}H_{114}O_8$	
Molar mass	963.55	g/mol
Water content	0.0039 ±0.0004	g/g

3.6 - Span 80

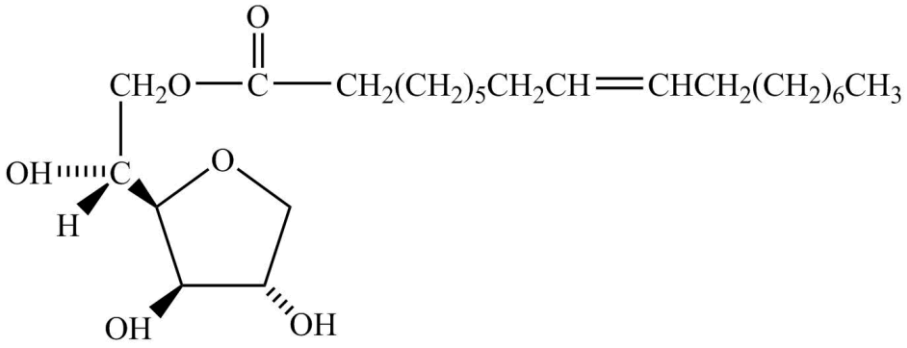

Figure 9 - Structure of Span 80

Sorbitan monooleate, sold under the trade name Span 80, is a yellow, odorless liquid having a HLB value of 4.3 [49], and therefore suitable for the preparation of W/O emulsions. [50].

Table 7 - Information on Span 80

	Value	**Unit**
Chemical formula	$C_{24}H_{44}O_6$	
Molar mass	428.62	g/mol
Water content	0.0037 ±0.0001	g/g

This nonionic emulsifier is approved by the EU as a food additive (identification number: E 494) and it is used, for example, in the production of ice cream or baked foods. The product used in this work comes from the company Sigma Aldrich GmbH. An overview of the most important material data is given in table 7 (Sigma Aldrich GmbH, 2013).

3.7 - PGPR 4125

PGPR 4125 is a type of polyglycerol polyricinoleate with an HLB value of around 4.7 [51]. In fig. 10 a structure for a generic PGPR is shown. Depending on the number of *m* and *n* different kind of PGPR can be distinguished. It is approved by EU (identification number E476) as, for example, viscosity reducer in ice cream. It was kindly provided by Palsgaard (Denmark). At ambient conditions it is a yellow viscous fluid.

Table 8 - Information on PGPR

	Value	**Unit**
Chemical formula	$(C_3H_{5O2})_n(C_{18}H_{32O2})_m$	
Molar mass	Depends on the composition	
Water content	0.0011	g/g

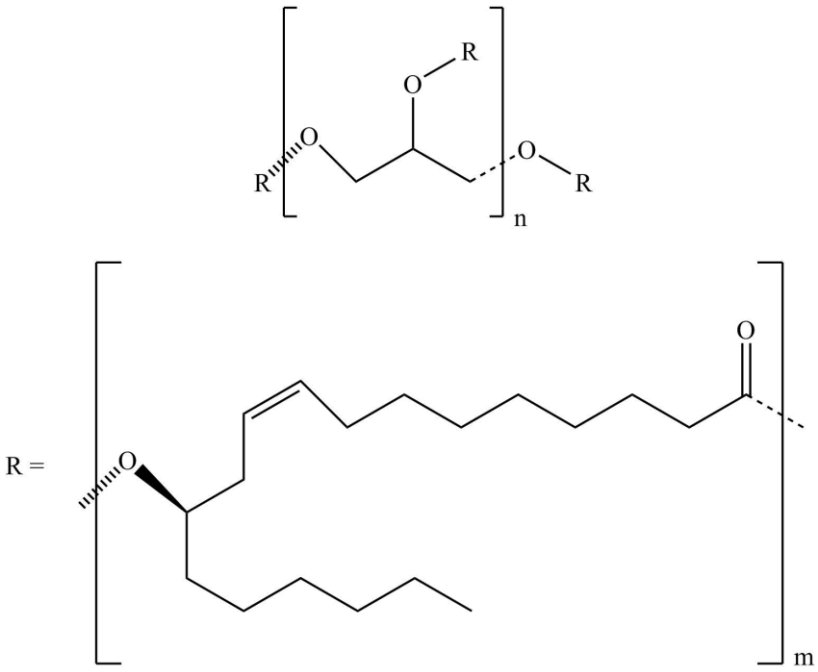

Figure 10 - Structure of a generic PGPR

3.8 - Tween 80

Behind the industrial name Tween 80 hides polysorbate 80, or Polyoxyethylensorbitanmonooleate. It has an HLB value of 15 and thus is particularly suitable for the preparation of O/W emulsions. The product comes from the company SIGMA Aldrich GmbH. At ambient conditions it has a yellowish hue and it is an odorless liquid. In the EU it is supplied with the identification number E433 as a food additive and is frequently used for the production of ice cream.

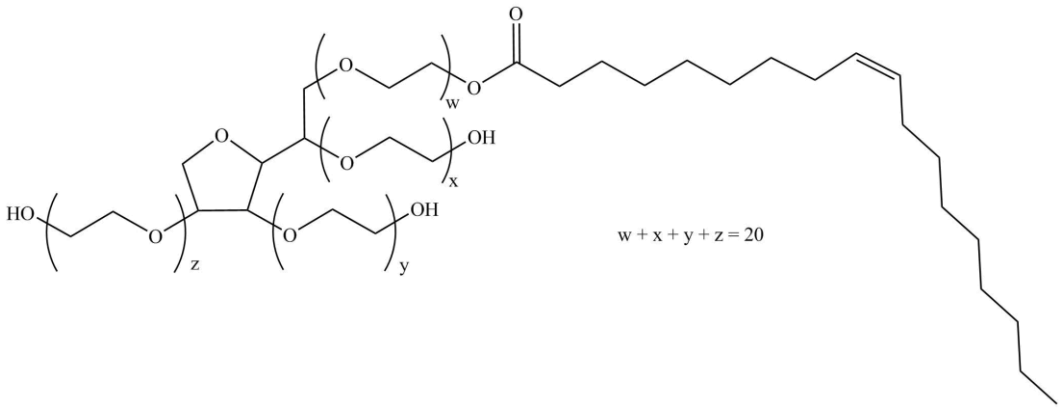

Figure 11 - Structure of Tween 80

Table 9 - Information of Tween 80

	Value	Unit
Chemical formula	$C_{64}H_{124}O_{26}$	
Molar mass	1310	g/mol
Soluble in water	yes	

3.9 - CO_2

Carbon dioxide is an odour-, colourless and inert gas at ambient conditions. Carbon dioxide, or CO_2, has a molar mass of 44.01 g/mol. When in supercritical condition it exhibits the density as a liquid while having the viscosity of a gas. Critical conditions are reached at relatively moderate conditions: T_c = 304.2 K and p_c = 7.38 MPa. Carbon dioxide was supplied by the company Yara GmbH & Co. KG, Germany.

In this work its properties have been calculated with the commercially available software FLUIDCAL [52].

Table 10 - Information on CO_2

	Value	Unit
Density (25 °C)	1.78	Kg/m3
Critical temperature	31.04	°C
Critical pressure	73.82	bar
Molar mass	44.01	g/mol
Purity	99.9	Vol %
Water content	< 50	ppm

4 Apparatus and methods

In this chapter the apparatuses and methods employed to perform the experiments will be shown. It will be described how the phase equilibrium was studied. The preparation of the microcomposites, with or without supercritical CO_2, will follow and at the end the various methods and apparatuses used to characterize the obtained composites will be detailed.

4.1 - Phase equilibrium measurements

The phase equilibrium study of the system CO_2 and Witepsol W31 have been performed in a stainless steel view cell (New Ways of Analytics, Germany). The cell is a horizontal cylinder equipped with a sapphire window both in the front and the rear which enabled the observation of its inside volume. The view cell can work up to a temperature of 200 °C and 75 MPa.

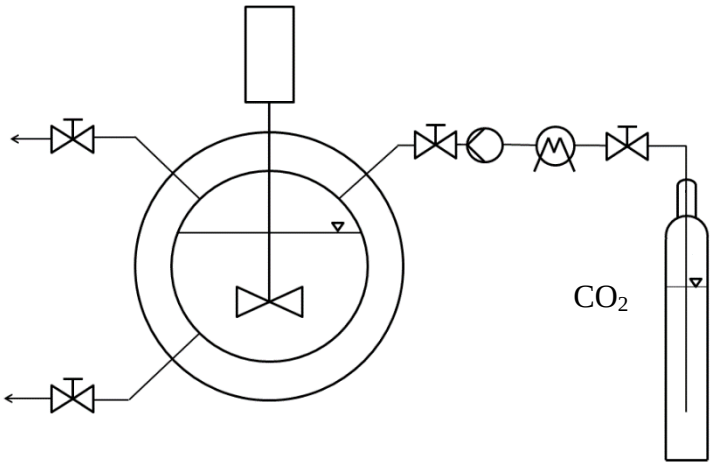

Figure 12 - Scheme of the view cell

Around 15 ml of W31 were inserted inside the view cell and then CO_2 was fluxed inside the cell to remove air, which could alter the results of the analysis. The top of the view cell was closed by inserting a magnetic stirrer. The system was heated to the chosen temperature with two cartridge heaters (Horst GmbH, Germany) inserted in two boring present in the cell. The entire cell was insulated to minimize the temperature losses. Once T was reached and constant, CO_2 is pumped inside the cell until the desired pressure was achieved. To control the operating conditions, the temperature was measured and regulated by a K-Type thermocouple connected to a controller (HT MC1-10A, HORST GmbH, Germany), while pressure was measured by a digital pressure transmitter (S-11, Wika Alexander Wiegand SE & Co. KG, Germany).

The stirrer was activated and W31 and CO_2 mixed. Due to the solubility of CO_2 in W31 a drop in pressure is always observed. Therefore, more CO_2 has to be introduced in the system to attain the desired conditions. Re-established the operating conditions, the system was left to mix for about 1 hour. The magnetic stirrer was then shut off and

everything was let to rest for a minimum of one hour and a half. All happened at isobaric and isothermal condition. Due to density differences two phases were formed: one sedimented at the bottom, the other moved at the top. The resting time was considered sufficient when, by observation through the sapphire glass, no bubbles were present in the bottom phase and there were no droplets in the top phase: the phase separation had been completed. Samples of the two phases were taken in order to quantify the composition. The heavy phase was removed from a valve positioned at the bottom of the cell, while the light phase was removed from the top of the cell. To keep the cell in isobaric and isothermal condition while sampling, the rear part of the cell was movable, which allowed for controlling the volume of the cell. By reducing the volume of the cell the pressure of the system could be kept constant even if samples were taken. The volume of the cell could be varied between 54 cm^3 and 24.7 cm^3.

The samples were collected in glass test tubes. The difference in pressure between the view cell and the environment leads to degasification of the samples, so glass traps were set to let the gas go through a volumetric gas meter (ELSTER Group, GmbH, Germany). This measurement was combined with gravimetric analysis in order to evaluate the composition of the phases. To help degasification of the samples, these were heated with a heat gun, to release the gas that may have been entrapped in the W31 that solidified in the tubes. The glass tubes were weighed three times each using an analytical balance (AB204-S, Mettler-Toledo GmbH, Germany). The mass of the empty tubes (m_{empty}), the mass with the sample after collection (m_{sample}) and the mass of the sample after degasification with heat (m_{degas}) are collected.

The mass of W31 (m_{W31}) presents in the sample was calculated as:

$$m_{W31} = m_{degas} - m_{empty} \tag{3}$$

while the mass of CO_2 (m_{CO_2}) was calculated as

$$m_{CO_2} = m_{sample} - m_{degas} + \rho_{CO_2} \cdot V_{CO_2} \tag{4}$$

where ρ_{CO_2} is the density of carbon dioxide at ambient conditions as calculated by the software FLUIDCAL [52] and V_{CO_2} is the volume measured by the volumetric gas meter. The mass fractions were easily calculated with this information. In the case of CO_2, the mass fraction in the heavy and light phase equals to

$$x_{CO_2}, y_{CO_2} = \left(\frac{m_{CO_2}}{m_{CO_2} + m_{W31}}\right) \tag{5}$$

The mass fractions of the W31 (x_{W31}, y_{W31}) could be calculated in the same way, by changing the term at the numerator with m_{W31}. Otherwise, since the total of the mass fractions is also equal to 1, one could use:

$$x_{W31} = 1 - x_{CO_2}\ ;\ y_{W31} = 1 - y_{CO_2} \tag{6}$$

4.2 - Microcomposites by melt dispersion technique (MDT)

Preliminary tests on the efficacy of the emulsifiers have been performed by preparing microcomposites with the melt dispersion technique [4,54,55]. For this specific set of experiments, 5 g of Witepsol W31 were melted at a heating temperature of 40 °C in a beaker. The required amount of emulsifier (to achieve 1 or 5% w_{em}/w_{W31}) was added into the beaker before melting W31. W31 and emulsifier were then mixed together. To the molten sample, a NaCl solution (9% w/w) was added to obtain a core/shell ratio of 0.2. The content of the beaker was mixed with a magnetic stirrer for 5 minutes, keeping the T constant. Then distilled water at 40 °C was added to the mixture while stirring. The mass ratio between the fat and the distilled water was 1:6. This led to the formation of a W/O/W emulsion. After 5 minutes of stirring, 80 g of cold water (approximately 4 °C) were added to decrease the temperature of the emulsion. The temperature reached was always below the melting temperature of the hard fat, which solidified. To avoid drop coalescence the water was added while stirring. The microcapsules were separated by filtration using MN 615 ¼ Ø 185 mm filters (MACHEREY-NAGEL GmbH & Co. KG, Germany). Eventually, the powder was washed twice and the washing water was collected for future measurements. The capsules were left to dry for one night and then collected in sample bottles. All tests were performed at least three times [56].

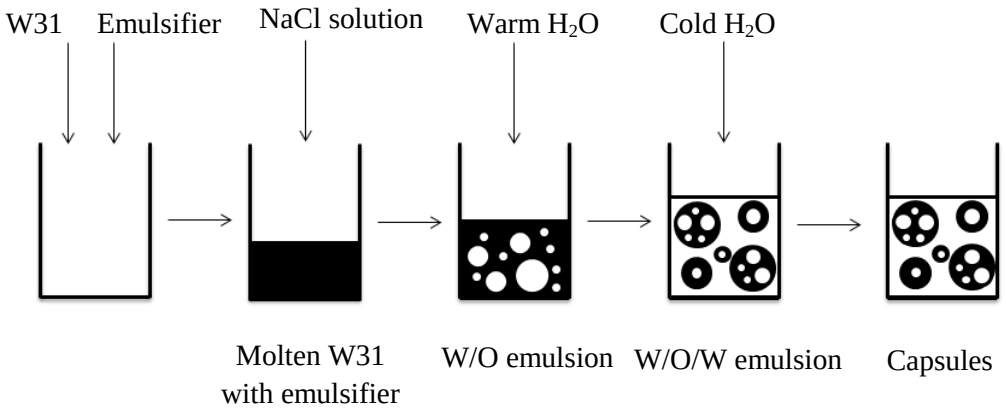

Figure 13 – Melt Dispersion Technique experiments setup

4.3 - Microcomposites by PGSS process

Molten Witepsol W31 and the chosen emulsifier were mixed on a stirring plate at 60 °C for at least 1 h in order to ensure complete homogeneity. Then, to achieve the selected water/oil (W/O) ratio, the NaCl solution was added and everything was stirred on a stirring plate for 10 min. The final step was a 5 min stirring via an Ultra-Turrax T 50 Basic (IKA Werke GmbH & Co. KG, Germany) at a speed of 8800 1/min.

The emulsion was loaded in a tank contained in an oven to keep the temperature constant. It was then pumped to the nozzle block and before being sprayed it came in contact with

CO_2. Through the nozzle, the mixture was expanded in the spray tower where the W31 solidified and microcomposites were formed. A plastic bag was placed inside the spray tower to simplify collection of the product. The expanded carbon dioxide was sent to the environment after filtering of the smaller particles [57].

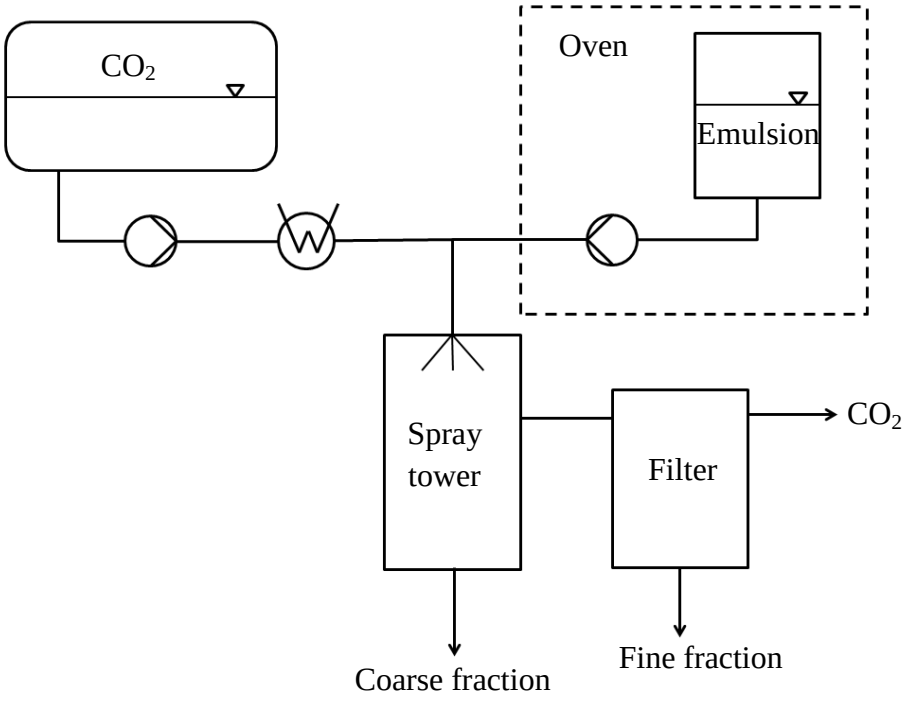

Figure 14 - Scheme of the PGSS plant used in this work

4.4 - Characterization of the product

In this section the different techniques employed to characterize the powder and the composites produced via the MDT or the PGSS process are described. Regarding the MDT, the focus of the analyses was on the encapsulation efficiency (EE) and the release of NaCl, while for the products of the PGSS process these studies were backed up with the investigation of other characteristics such as particle size and distribution, density, morphology and moisture content, from which the loading efficiency (LE) was obtained.

4.4.1 - Particle size distribution (PSD)

The particle size and the distribution were analysed using a Mastersizer 2000 (Malvern Instruments GmbH, Germany). The device can determine particle sizes of powders and suspension based on the laser diffraction method. The particles enter an optical measuring cell where a laser beam is present. The presence of the particles diffracts the laser beam and by detecting the scattering pattern it is possible to mathematically determine the particle size of the particles. The scattering pattern depends on the size of the particles, because this affects the angle of diffraction and the intensity pattern. Mathematical methods to determine the particle size are for example the Fraunhofer approximation or

the Mie scattering theory. The choice of the mathematical model depends on the size of the particles. Since the diffraction depends on the morphology of the particles it is assumed that they are spherical. The two models tend to be in agreement in the following cases:

- all particles are larger than 50 µm;
- particles are opaque and in the range 2 to 50 µm [58].

In this work the Mie model has been chosen, since it enables the measurements of the smaller particles produced by the PGSS process. The Mie theory requires to know the refractive index of the medium and the material which were 1.333 and 1.4495 respectively [59].

The PSD measurements were performed in wet state using the Hydro 200 MU module (Malvern Instruments GmbH, Germany). The medium was water with 10 ml of a 10 % (w/w) Tween 80 solution to avoid agglomeration of the particles when in water. Firstly, the background spectrum of the medium was measured, then the particles were inserted into the dispersing unit and ultrasound at 20 kHz are activated for around 4-5 minutes until a light attenuation between 10 and 20 % is reached. The measurements were then carried out 3 times per sample and the PSD was obtained.

The size distribution provided by the software is volume-based, for particles with a diameter ranging from 0.02 µm to 2000 µm. The data usually considered in PSD are the so called d_{10}, d_{50}, d_{90} and the span value. D_{10} is the diameter required to obtain 10% of the total volume of the particles by summing all particles with that diameter or less. The same is valid for d_{50} and d_{90}, which corresponds to the 50% and the 90% of the total volume respectively. The span value is used as an indication of the width of the size distribution and it is calculated as:

$$span = \frac{d_{90} - d_{10}}{d_{50}} \quad (7)$$

The larger is the span value, the broader is the size distribution.

4.4.2 - Bulk density

The bulk density is an important property of powders and powderous composites because it gives useful information regarding packing, storage and transport of the material. The bulk density indicates the ratio between the mass of the powder and the volume it occupies.

The bulk density has been measured according to DIN EN 543 [60]. A cylinder of known mass and volume is filled with powder that was previously inserted in a funnel above the cylinder. Then, the excess powder is removed with a spatula in order to have the powder at the same level as the cylinder. It is important not to press the powder inside the cylinder.

Finally, the weight of the full cylinder is measured and the bulk density can be determined as:

$$\rho_{bulk} = \frac{m_{full} - m_{empty}}{V_{cyl}} \quad (8)$$

where m_{full} is the mass of the cylinder full with powder, m_{empty} is the mass of the cylinder alone and V_{cyl} is the volume of the cylinder.

4.4.3 - Morphology

The morphology of the powder was observed through images taken by a Scanning Electron Microscope (SEM), specifically a LEO Gemini 1530 (Zeiss, Germany) or a Gemini2 Merlin (Zeiss, Germany)

This type of instrument allows observing and imaging the surfaces of the analyzed samples. Briefly, electromagnetic lenses focus an electron beam one the sample's surface, the image of which can be generated by detecting the secondary electrons that the surface emits in response to the beam [61]. The evolution of the instrument made it possible to inspect non-conductive samples without previous application of a conductive coating, e.g. gold.

For each experiment at least three images were taken.

4.4.4 - Water concentration

The composites produced by PGSS were analysed in respect to their concentration of water, in order to obtain data regarding the loading efficiency (LE), i.e. how much water is present in the composites in comparison to the emulsion they were generated from.

The moisture content was measured by Karl-Fischer Titration using the 870 KF-Titrino Plus from Metrohm, Switzerland. The water standard used for titer determination was Hydranal® Eichstandard 5.00, the titrating agent was Hydranal®-Composite 5 and the working medium, used to solubilize the shell material completely, was Hydranal® Lyposolver CM. All were purchased from Fluka, United States.

Karl-Fischer titration is a method for volumetric water determination. The titrating agent is inserted at volume steps and it reacts with water. When the value measured reaches the predefined endpoint the titration is stopped [62]. By knowing the volume dosed of titrating agent the apparatus can calculate the water content of the sample and from it it is possible to determine the loading efficiency of the process.

The L.E. was calculated as:

$$LE = \frac{m_{wat,caps}}{m_{wat,tot}} = \frac{x_{wat,caps} / (1 - x_{wat,caps})}{x_{wat,tot} / (1 - x_{wat,tot})} \quad (9)$$

where $m_{wat,caps}$ is the mass of water cointained in the capsules, $m_{wat,tot}$ is the total mass of water in the emulsion, which can be calculated as presented in the second part of the equation in order to confront the same quantity of W31 and emulsifier. In the left part of the formula $x_{wat,caps}$ is the moisture content measured with the Karl-Fischer Titration and $x_{wat,tot}$ is the moisture content of the emulsion.

The moisture content was also measured via a moisture analyser (model HB43-S, Mettler-Toledo GmbH, Germany). The device calculates the moisture content based on the thermogravimetric principle. An aluminium pan is tared on the balance present in the moisture analyser and it is then filled with the sample (around 3 g). The filled pan is inserted in the analyser and an integrated halogen heating module melts the sample. In order to guarantee the melting of the shell material and the complete evaporation of water a working temperature of 115 °C was chosen. Moreover a switch criterion of 5 was selected which ensures that the measurement is stopped only when the mass loss of the sample is less than 1 mg over a time of 140 s.

At the end of the measurement the moisture analyser displays the moisture content (MC), which is calculated as:

$$MC = \frac{m_{wet\ sample} - m_{dry\ sample}}{m_{wet\ sample}} \cdot 100\% \quad (10)$$

where $m_{wet\ sample}$ is the mass of the sample before starting the moisture analyser and $m_{dry\ sample}$ is the mass left after the water is evaporated.

4.4.5 - NaCl encapsulation and release

To calculate the encapsulation efficiency (EE) and the release from the composites the conductivity of salt in water was measured with the conductometer 3310 from WTW GmbH, Germany.

When in water NaCl dissociates in two ions, Na^+ and Cl^-. The presence of ions increases the conductivity of water. There is a direct correlation between conductivity and concentration of ions. Therefore by knowing this relation it is easy to measure the conductivity and calculate back the concentration of the ions. A calibration curve was obtained for the system NaCl-H_2O before performing the measurements. Because of the use of different batches of NaCl for the capsules produced via the melt dispersion technique and the PGSS, two different calibration curves have been employed.

For the particles produced with the MDT, the conductivity was measured in the external water after filtering and from the washing water. The amount of NaCl is calculated via the calibration curve and then subtracted from the total amount of NaCl: the difference is the quantity of NaCl present in the capsules. Another measurement was performed by melting 0.3 g of capsules in 30 g of H_2O in glass probes. The system was left to cool down and filtered. The conductivity in the water was then measured and the quantity of NaCl present in the capsules is calculated.

The EE was evaluated as:

$$EE_{ext.wat.} = \frac{\frac{m_{NaCl_{tot}}}{m_{W31}+m_{em}} - \frac{m_{NaCl_{ext.wat.}}}{m_{caps}}}{\frac{m_{NaCl_{tot}}}{m_{W31}+m_{em}}} \quad (11)$$

$$EE_{melt} = \frac{\frac{m_{NaCl_{filt.wat.}}}{m_{caps}}}{\frac{m_{NaCl_{tot}}}{m_{W31}+m_{em}}} \quad (12)$$

where $m_{NaCl_{tot}}$ is the total mass of NaCl introduced in the system, $m_{NaCl_{ext.wat.}}$ is the mass of NaCl present in the external and washing water, $m_{NaCl_{filt.wat.}}$ is the mass of NaCl present in the filtered water of the melting experiments, m_{W31} is the mass of Witepsol W31 in the emulsion, m_{em} is the mass of emulsifier in the emulsion and m_{caps} is the mass of the capsules inserted in the probe [56].

For particles obtained from the PGSS process the encapsulation efficiency was analysed using two different methods. The first procedure requires melting 0.3 g of capsules in 30 g of deionized water, stirring for around 3 h, and in the end measuring the conductivity in the water after filtering the capsules (same method as for calculating the EE_{melt}). The second one instead is performed by inserting 0.3 g of capsules in 30 g of distilled water in a glass probe, manually shaking for 2 min and then measuring the conductivity in the water after filtering the capsules.

The EE was evaluated as:

$$EE_{melt} = \frac{\frac{m_{NaCl_{filt.wat.}}}{m_{caps}}}{\frac{m_{NaCl_{tot}}}{m_{W31}+m_{em}}} \quad (13)$$

$$EE_{ext.wat.} = \frac{\frac{m_{NaCl_{tot}}}{m_{W31}+m_{em}} - \frac{m_{NaCl_{ext.wat.}}}{m_{caps}}}{\frac{m_{NaCl_{tot}}}{m_{W31}+m_{em}}} \quad (14)$$

where $m_{NaCl_{tot}}$ is the total mass of NaCl introduced in the system,$m_{NaCl_{filt.wat.}}$ is the mass of NaCl present in the filtered water of the melting experiments, $m_{NaCl_{ext.wat.}}$ is the mass of NaCl present in the external water after shaking the samples for 2 minutes, m_{W31} is the mass of Witepsol W31 in the emulsion, m_{em} is the mass of emulsifier in the emulsion and m_{caps} is the mass of the capsules inserted in the probe.

The release investigations were performed in a similar way: 0.3 g of capsules were inserted in probes and 30 g of deionized water were added. Subsequently, the probes were shaken with the Digital Orbital Shaker Sea Star (Heathrow Scientific, LLC, U.S.A.) for the selected times at 200 rpm. Finally, the capsules were filtered and the conductivity in the water was measured [56].

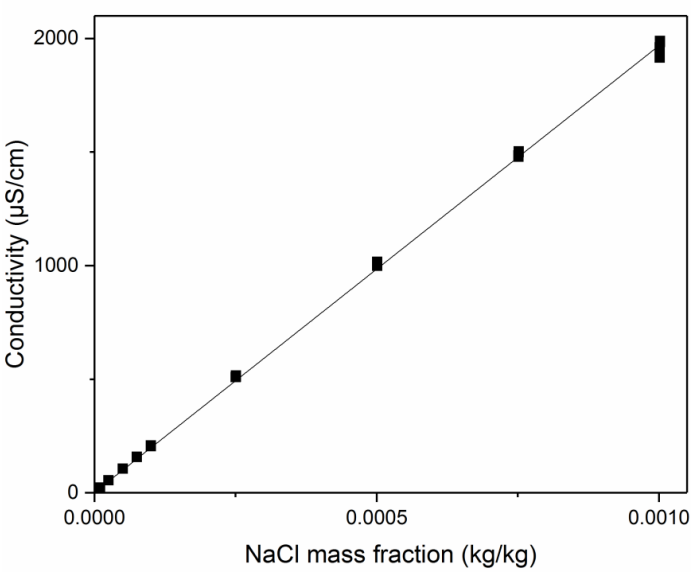

Figure 15 - Calibration curve for capsules obtained via double emulsion technique

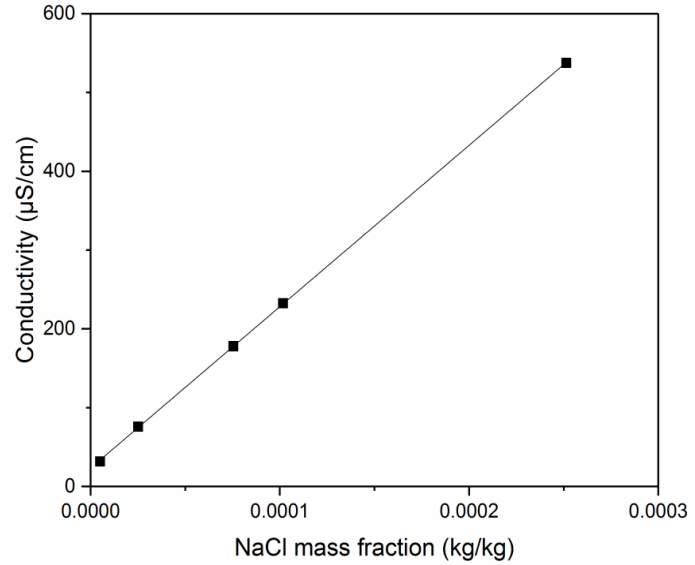

Figure 16 - Calibration curve for capsules obtained via PGSS

4.4.6 - Fluorescence imaging and temperature controlled release

Fluorescence imaging was done using a Zeiss Axio Observer Z1 inverted microscope equipped with a Colibri 2 LED light source (Carl Zeiss AG, Germany). All experiments were performed at a constant room temperature of 24-25 °C. The samples were heated using a 2200 nm infrared laser (m2k-laser GmbH, Germany). The temperature dependent fluorescence of Rhodamine B was used as a measure for the temperature of the heated solution. A heating profile with 25 individual steps each with a temperature increase of 1 °C each were used [53]. For the release experiments the microcapsules were added into DPS buffer and loaded into ibidi µ-Slides VI with a channel height of 400 µm (ibidi GmbH, Germany). Data analysis was done using Zeiss Axiovision, OriginPro 9g (OriginLab, USA) and ImageJ [53].

5 Phase equilibria

The knowledge of phase equilibria of fatty oils/lipids and supercritical fluids is important in industrial processes. Furthermore, the possibility of modelling and predicting phase equilibria is very appealing, because it enables a deeper understanding of the system behaviour with only a limited amount of experimental work. However, predictions need to be sufficiently reliable, especially if the system studied contains at least a high-molecular weight compound (the oil or lipid) and a low-molecular weight fluid (e.g. supercritical CO_2), as it is the case in this work.

The study of such a system is not trivial, due to the presence of a lipid mixture. Indeed, the representation of a lipid mixture chemical structure is not easy. This is true also in the case of Witepsol W31. There are two possible solutions: one is to represent the lipid as a mixture of simple triglycerides (tristearin, trimystirin, etc…) based on the fatty acid composition of the original mixture; the other is to represent the mixture as a single pseudo-component, with the same molecular weight and degree of unsaturation of the original mixture [63]. The latter was the solution adopted in [63] and chosen for this work.

5.1 - The Group Contribution-Equation of State

In the current work, phase equilibria were modelled using the Group Contribution Equation of State (GC-EoS). The GC-EoS was firstly proposed by Skjold-Jørgensen in 1984 [16]. It was derived by combining four well-known equations and principles in phase equilibrium thermodynamics: the Carnahan-Starling expression for hard spheres, the group contribution principle, the non-random two-liquid (NRTL) equation and the van der Waals equation of state [15].

The following part of this section is adapted from [15,16,63].

All thermodynamic properties of interest in phase equilibria calculation can be derived by differentiation of the configurational Helmholtz function with respect to composition or density.

The Helmholtz energy (A) is the sum of two parts: the first depending on the ideal gas behaviour $\left(A^{ideal\ gas}\right)$, the second due to intermolecular forces $\left(A^{residual}\right)$:

$$A = A^{ideal\ gas} + A^{residual} \tag{15}$$

For the GC-EoS the interest is focused only on the residual part. The residual Helmholtz energy is obtained by the contribution of two terms: a free volume term (A^{fv}) and a contribution from attractive intermolecular forces (A^{att}):

$$A^{residual} = A^{fv} + A^{att} \tag{16}$$

For the free volume term the assumption of hard sphere behaviour for the molecules is made. Therefore every substance *i* present in the system is characterized by a hard sphere diameter d_i. By adapting a Carnahan-Starling type of hard sphere expression for mixtures, the free volume contribution is expressed as:

$$\left(\frac{A}{RT}\right)^{fv} = 3\left(\frac{\lambda_1\lambda_2}{\lambda_3}\right)(Y-1) + \left(\frac{\lambda_2^3}{\lambda_3^2}\right)(-Y + Y^2 - \ln Y) + n \ln Y \tag{17}$$

where:

$$Y = \left(1 - \frac{\pi\lambda_3}{6V}\right)^{-1} \text{ and } \lambda_k = \sum_j^{NC} n_j d_j^K \tag{18}$$

where λ is an auxiliary geometric quantity, n_j is the number of moles of component *j*, *n* is the total number of moles, *NC* is the number of components and *V* is the total volume.

It is assumed that the hard sphere diameter *d* is temperature dependent:

$$d_j = 1.065655 d_{cj}\left[1 - 0.12\, exp\left(\frac{-2T_{cj}}{3T}\right)\right] \tag{19}$$

where d_{cj} is the value of the hard-sphere diameter at the critical temperature T_{cj} for the pure component *j*.

The attractive-energy parameter is calculated with an expression similar to the NRTL model for the excess Helmholtz function:

$$\left(\frac{A}{RT}\right)^{att} = -\left(\frac{z}{2}\right)\sum_i^{NC} n_i \sum_j^{NG} \nu_j^i q_j \sum_k^{NG} \theta_k \left(\frac{g_{kj}\tilde{q}\tau_{kj}}{RTV}\right) / \sum_l^{NG} \theta_l \tau_{lj} \tag{20}$$

where

$$\tilde{q} = \sum_i^{NC} n_i \sum_j^{NG} \nu_j^i q_j \,,\ \theta_j = \left(\frac{q_j}{\tilde{q}}\right)\sum_i^{NC} n_i \nu_j^i,\ \tau_{ij} = exp\left[\alpha_{ij}\Delta g_{ij}\tilde{q}/(RTV)\right] \tag{21}$$

and

$$\Delta g_{ij} = g_{ij} - g_{jj} \tag{22}$$

where *z* is the numbers of nearest neighbours to any segment (set to 10), ν_j^i is the number of groups of type *j* in molecule *i*, θ_j the surface fraction of group *j*, q_j the number of surface fragments assigned to group *j*, NG the number of different groups, $\tilde{q}$ the total number of surface segments, g_{ij} the attraction energy parameter for interactions between group *i* and *j*, and α_{ij} the NRTL non-randomness parameter.

The interactions between unlike segments are defined by $g_{ji} = k_{ji}\left(g_{ii}g_{jj}\right)^{1/2}$, where k_{ij} is the binary interaction parameter. It is assumed that the interactions parameters are temperature-dependent.

$$g_{ii} = g_{ii}^*[1 + g_{ii}'(T/T_i^* - 1) + g_{ii}'' ln(T/T_i^*)] \tag{23}$$

$$k_{ij} = k_{ij}^{*}\left[1 + k_{ij}' ln\left(T/T_{ij}^{*}\right)\right] \quad (24)$$

$$T_{ij}^{*} = 0.5\left(T_{i}^{*} + T_{j}^{*}\right) \quad (25)$$

T_i^* is an arbitrary but fixed reference temperature for group i.

It is then possible to write the configurational Helmholtz function (A^C) as:

$$\left(\frac{A^{c}}{RT}\right)_{T,n} = -nlnV + \left(\frac{A^{R}}{RT}\right)_{T,V,n} \quad (26)$$

where $\left(\frac{A^{R}}{RT}\right)_{T,V,n} = \left(\frac{A}{RT}\right)^{fv} + \left(\frac{A}{RT}\right)^{att}$ (27)

By deriving the configuration Helmholtz functions it is possible to calculate the properties necessary for the phase equilibria calculation.

The compressibility factors (Z) are derived by differentiating with respect to volume:

$$Z = -v\frac{\partial}{\partial V}\left(\frac{A^{c}}{RT}\right)_{T,n} = Z^{fv} + Z^{att} + 1 \quad (28)$$

where

$$Z^{fv} = -v\left[3\left(\frac{\lambda_1\lambda_2}{\lambda_3}\right) + \left(\frac{\lambda_2^3}{\lambda_3^2}\right)\left(2Y - 1 - \frac{1}{Y}\right) + \frac{n}{Y}\right]\left(\frac{\partial Y}{\partial V}\right)_{T,n} \quad (29)$$

$$\left(\frac{\partial Y}{\partial V}\right)_{T,n} = -Y^2\pi\frac{\lambda_3}{6V^2} \quad (30)$$

$$Z^{att} = -\left(\frac{z}{2n}\right)\sum_{j=1}^{NG}\bar{v}_j q_j \left(H_{5_j} + H_{2_j} - \frac{H_{2_j}H_{6_j}}{H_{4_j}}\right)\Big/ H_{4_j} \text{ (28) and } \bar{v}_j = \sum_{i=1}^{NC} v_j^i n_i \quad (31)$$

The auxiliary quantities H will be defined at the end of this section.

The fugacity coefficients (φ) are derived from the expression for the residual Helmholtz function at constant volume:

$$\ln\varphi_i = \frac{\partial}{\partial n_i}\left(\frac{A^{R}}{RT}\right)_{T,V,n_{k\neq i}} - \ln Z = \ln\varphi_i^{fv} + \ln\varphi_i^{att} - \ln Z \quad (32)$$

where

$$\ln\varphi_i^{fv} = 3\left(\frac{\lambda_1\lambda_2}{\lambda_3}\right)(Y-1)\left[\frac{\lambda_1'}{\lambda_1} + \frac{\lambda_2'}{\lambda_2} - \frac{\lambda_3'}{\lambda_3} + \frac{Y'}{Y-1}\right] + \left(\frac{\lambda_2^3}{\lambda_3^2}\right)(-Y + Y^2 - \ln Y)\left(3\frac{\lambda_2'}{\lambda_2} - 2\frac{\lambda_3'}{\lambda_3}\right) + \left(\frac{\lambda_2^3}{\lambda_3^2}\right)\left(2Y - 1 - \frac{1}{Y}\right)Y' + \ln Y + \left(\frac{n}{Y}\right)Y' \quad (33)$$

where $\lambda_k' = d_i^k$ and $Y' = \frac{Y^2\pi d_i^3}{6V}$;

and

$$\ln \varphi_i^{att} = -\left(\frac{z}{2}\right)\left[\sum_j^{NG} PS_{ij}\frac{H_{2_j}}{H_{4_j}} + \sum_j^{NG}\theta_j\frac{H_{3_{ij}}+MS_iH_{5_j}}{H_{4_j}} - \sum_j^{NG}\theta_j H_{2_j}\frac{H_7-MS_iH_{4_j}+MS_iH_{6_j}}{H_{4_j}^2}\right] \quad (34)$$

The auxiliary quantities are defined as follows:

$$PS_{ij} = \nu_j^i q_j \quad (35)$$

$$MS_i = \sum_j^{NG} PS_{ij} \quad (36)$$

$$H_{2_j} = \sum_k^{NG}\theta_k\tau_{kj}g_{kj}\tilde{q}/VRT \quad (37)$$

$$H_{3_{ij}} = \sum_k^{NG} PS_{ik}\tau_{kj}g_{kj}\tilde{q}/VRT \quad (38)$$

$$H_{4_j} = \sum_k^{NG}\theta_k\tau_{kj} \quad (39)$$

$$H_{5_j} = \sum_k^{NG}\theta_k\tau_{kj}(g_{kj}\tilde{q}/VRT)\alpha_{kj}\Delta g_{kj}\tilde{q}/VRT \quad (40)$$

$$H_{6_j} = \sum_k^{NG}\theta_k\tau_{kj}\alpha_{kj}\Delta g_{kj}\tilde{q}/VRT \quad (41)$$

$$H_{7_{ij}} = \sum_k^{NG} PS_{ik}\tau_{kj} \quad (42)$$

5.2 - Phase Equilibria of Binary Systems

The great advantage of the GC-EoS is given by the possibility to represent a wide variety of substances by using their corresponding functional groups. A functional group is a group of molecules composing a substance. For example ethanol, whose molecular composition is CH_3-CH_2-OH, is composed of -CH_3, -CH_2 and –OH as functional groups [46]. Each functional group is characterized by the pure group parameters:

- T* (K) → arbitrary but fixed reference temperature;
- q → number of surface-area segments per mole;
- g*
- g‘
- g“

  → parameters to calculate the attractive-energy parameter.

T* and q are fixed parameters, while the g parameters can be modified.

The GC-EoS considers also the interaction between the functional groups; therefore also the binary interaction groups are parameterized:

- k → temperature dependent group-group interaction;
- α → non-randomness parameter.

These parameters have been experimentally evaluated and regressed in various works [15,16,63–65].

Two more data are necessary to proceed with the modelling of phase equilibria. This time they refer directly to the molecule and not the functional groups that compose it:

- T_c → critical temperature (K);
- d_c → critical diameter (cm/mol).

5.3 - Witepsol W31-CO_2

In order to use the GC-EoS it is necessary to know the structure of the molecules that will be studied. Witepsol W31 is a mixture of different triglycerides characterized by a melting point of around 37 °C. As explained in the introduction, the molecule of Witepsol W31 was described as a single pseudo-component. Unfortunately the real composition of Witepsol W31 is not known. However, ranges of composition are known: mainly C12 fatty acids (45 - 55%) with certain amounts of C14 (10 - 20%), C16 (10 - 15%) and C18 (10 - 20%); monoglycerides: 1 - 5% diglycerides: 15 - 25% triglycerides: 70 - 80% [e-mail conversation with producer].

By averaging these values the pseudo-component for Witepsol W31 was obtained following the method suggested in [63].

The pseudo-component has the following structure:

$$[(CH_2COO)_2CHCOO](CH_2)_{32}(CH_3)_3$$

Witepsol W31 can be seen as a triglyceride with no unsaturated bonds, in between trimystirin and tripalmitin. The molecular weight of this molecule is 667.05 g/mol.

To obtain the T_c and d_c of this molecule a comparison with other triglycerides has been done. For the critical diameter, the correlation proposed in [66] has been used. Bottini et al. correlated the d_c to the molecular weight (MW) of alkanes and triglycerides. It is important to notice that in the case of triglycerides the MW has to be modified according to the following formula, in order to make a comparison with alkanes possible:

$$MW^* = MW - 3\,MW_{COO} + 3\,MW_{CH2} \qquad (42)$$

From figure 17, the corresponding d_c for the pseudo-component of Witepsol W31 was found to be equal to 10.36 cm/mol.

A similar technique was used to determine the T_c, but this time with saturated triglycerides only. In this case it was not necessary to correlate with MW*, but simply with MW. The T_c values of different triglycerides were taken from [67].

From figure 18, the corresponding T_c for the pseudo-component of Witepsol W31 was found to be equal to 919.71 K.

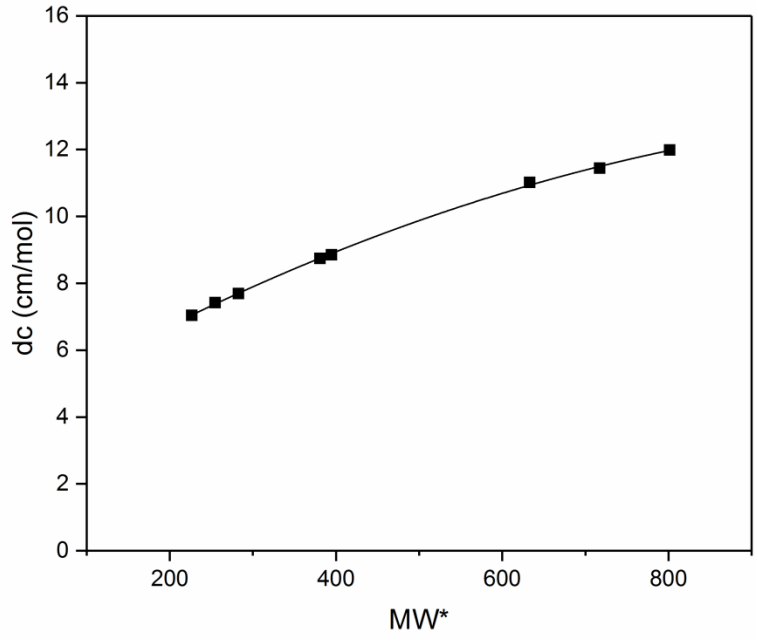

Figure 17 - Correlation between d_c and MW* for alkanes and saturated triglycerides. Modified from [66]

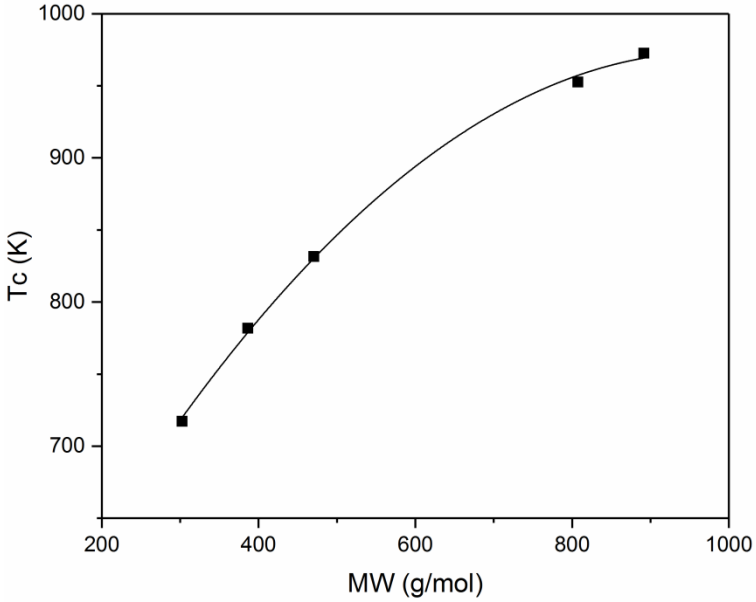

Figure 18 - Correlation between T_c and MW for saturated triglycerides.

Table 11 - Pure group parameters used for the system Witepsol W31-CO_2. TG is the group [$(CH_2COO)_2CHCOO$] [67]

Group	**T* (K)**	***q***	***g****	***g'***	***g''***
CO_2	304.2	1.261	531890	-0.5780	0.0000
CH_3	600.0	0.848	316910	-0.9274	0.0000
CH_2	600.0	0.540	356080	-0.8755	0.0000
TG	600.0	3.948	346350	-1.3460	0.0000

Table 12 - Interaction parameters used for the system Witepsol W31-CO_2 [67].

i	j	k_{ij}^{*}	k_{ij}'	α_{ij}	α_{ji}
CO_2	CH_3	0.98	0.15	3.0	3.0
CO_2	CH_2	0.93	0.15	3.0	3.0
CH_3	CH_2	1.00	0.00	3.0	3.0
TG	CH_3/CH_2	0.74	0.15	3.0	3.0
TG	CO_2	1.00	0.15	3.0	3.0

The pure group parameters and binary interactions (tables 11 and 12) needed for the system were taken from the work of [67], where a parametrization study for triglycerides in supercritical CO_2 was performed. Their results were initially used to model the system tristearin and CO_2 with the GC-EOS. This was done to verify the parameters, because tristearin is a pure substance, compared to Witepsol W31. The results, not reported here, were very good and comparable with the experimental results of [18], therefore the same parameters were used to model the system Witepsol W31-CO_2.

The results are shown in fig. 19 and a comparison with some experimental data is provided in table 13.

Table 13 - Comparison between experimental data and prediction from the GC-EoS of Witepsol W31-CO_2 (xCO_2 in mol%).

T (°C)	**P (bar)**	**xCO_2, exp. (%)**	**St. Dev. (%)**	**xCO_2, GCEOS (%)**	**Rel. Diff. (%)**	**Rel. Err.**
50	50	67.17	1.57	67.06	0.11	0.16%
50	80	79.94	1.24	79.27	0.67	0.84%
50	100	83.58	0.69	83.67	0.09	0.10%
50	150	86.94	1.06	88.14	1.20	1.38%
65	50	63.76	4.76	61.85	1.91	2.99%
65	100	79.55	0.64	79.37	0.18	0.23%
65	150	84.89	0.25	86.03	1.14	1.35%
80	50	56.47	2.34	57.30	0.83	1.47%
80	100	75.49	0.52	75.36	0.13	0.18%
80	150	81.89	1.47	83.32	1.43	1.75%

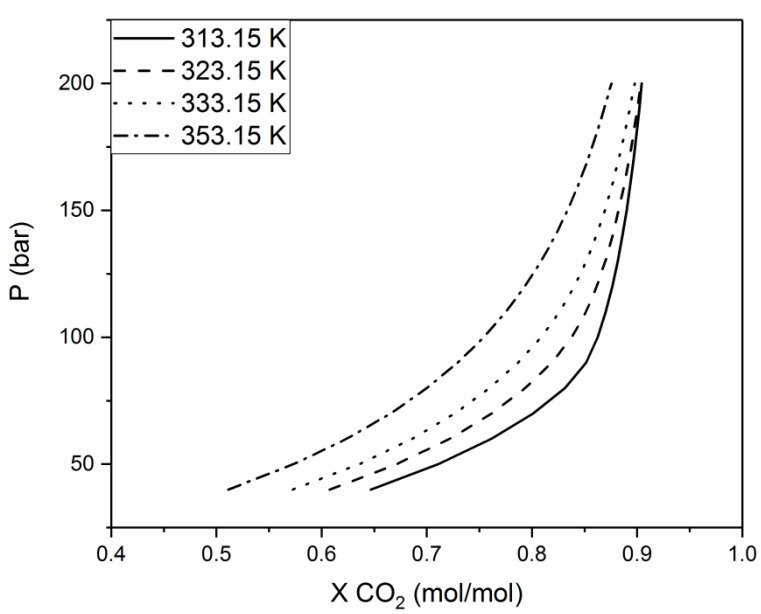

Figure 19 - Results of phase equilibria prediction of the system Witepsol W31-CO_2 with the GC-EoS. Only the heavy phase is shown for simplicity

By having a look at fig. 19 and table 13 it is possible to observe that the solubility of CO_2 into Witepsol W31 increases by increasing pressure, but decreases when increasing temperature. This is observed both in the experiments and the simulations. This behaviour has been observed in any system comprising a triglyceride and CO_2 [13,17,18].

Moreover, table 13 shows that the GC-EoS is suitable to model the phase behaviour of mixtures containing triglycerides and carbon dioxide. The relative error is very low, sign of a good reliability.

5.4 - H_2O-CO_2

The system H_2O-CO_2 was also modelled with the GC-EoS. This time the parameters collected in [65] did not provide satisfactory results when compared with experimental data (figure 20) from [68], whose data were chosen because they fell in the range of interest of p and T for this work. It has to be said that the concentration of CO_2 in water is very low; therefore these errors are justifiable and the work of [65] was based not only on [68] data.

In order to improve the modelling of the phase equilibria of the system H_2O-CO_2 the interaction parameters between the two functional groups were optimized, by using the function *fminsearch* in Matlab to minimize the relative error between experimental data and modelled data (in both the liquid and the gas phase).

Table 14 - Pure group parameters used for the system H_2O-CO_2 [65].

Group	**T* (K)**	***q***	***g****	***g'***	***g''***
CO_2	304.2	1.261	531890	-0.5780	0.0000
H_2O	647.3	0.866	1697000	-0.6707	0.0000

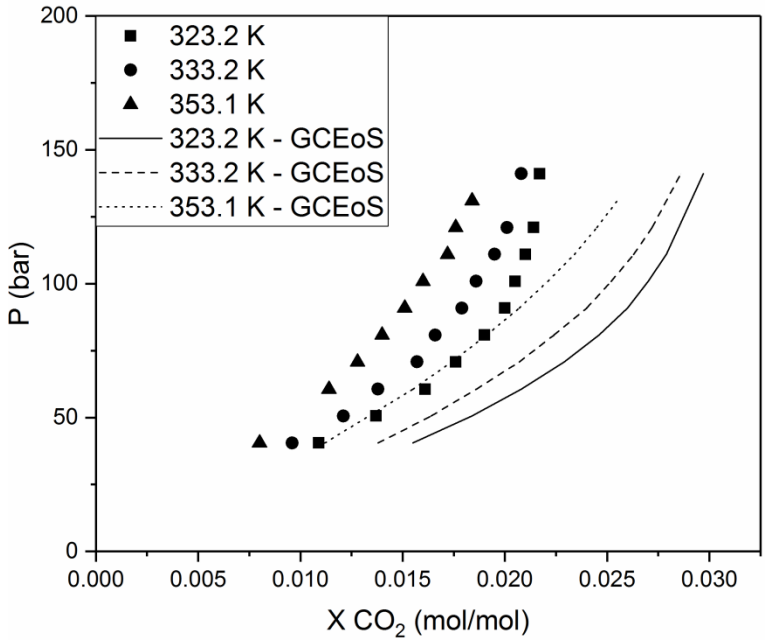

Figure 20 - Comparison between experimental data [68] and GC-EoS model (parameters from [65]) for the system H_2O-CO_2.

Table 15 - Interaction parameters used for the system H_2O-CO_2 (this work).

i	j	k_{ij}^{*}	k_{ij}'	α_{ij}	α_{ji}
H_2O	CO_2	0.7988	0.2318	-0.4249	0.3521

The results are shown in fig. 21 and a comparison with some experimental data is provided in table 16.

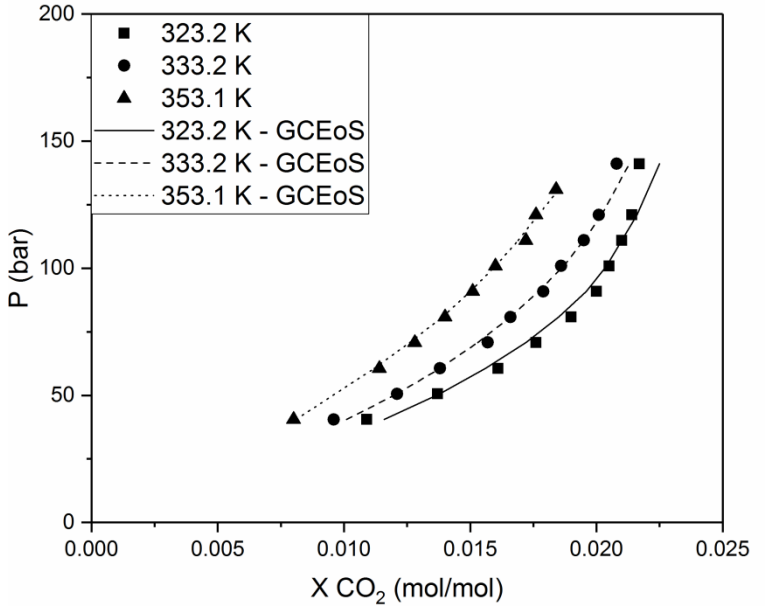

Figure 21 - Comparison between experimental data [68] and GC-EoS model (parameters from this work) for the system H_2O-CO_2.

The results obtained from the model were satisfactory.

The relative errors were in fact quite modest, and it should be taken into account that only a very small amount of CO_2 dissolves in water. A minimal variation shows a bigger error, but when considering fig. 20 it can be appreciated that the error is not reducing the quality of the model. Therefore the obtained parameters were used for the modelling of the ternary system Witepsol W31-H_2O-CO_2.

Table 16 - Comparison between experimental data and prediction from the GC-EoS for the system H_2O-CO_2 (xCO_2 in mol%).

T (K)	P (bar)	xCO_2, lit.	xCO_2, GCEOS	Rel. Err.
323.20	40.50	1.09%	1.16%	6.42%
323.20	141.10	2.17%	2.25%	3.69%
333.20	40.50	0.96%	1.01%	5.21%
333.20	141.10	2.08%	2.13%	2.40%
353.10	40.50	0.80%	0.81%	1.25%
353.10	131.00	1.84%	1.85%	0.54%

5.5 - Phase equilibria of the ternary system Witepsol W31-CO_2-H_2O

Obtaining experimentally the ternary phase equilibria of the system under study is very complicated. However, the knowledge of the binary systems shown in the previous paragraph should suffice to permit the prediction of the ternary system with the GC-EoS. In table 17 the interaction parameters not collected before in tables 12 and 15 are reported. These data were collected from [65]. Unfortunately the binary interaction parameters for the functional group TG and H_2O are not available. The parameters shown for TG-H_2O are an assumption.

Table 17 - Interaction parameters not shown in tables 12 and 15.

i	j	k_{ij}^{*}	k_{ij}'	α_{ij}	α_{ji}	Literature
CH_3	H_2O	0.560	0.00	0.495	0.495	[65]
CH_2	H_2O	0.560	0.00	0.495	0.495	[65]
TG	H_2O	1.00	0.00	0.00	0.00	This work

Fig. 22 shows the ternary diagram for the system Witepsol W31-CO_2-H_2O in molar base. A better understanding of the system is provided by fig. 23, which shows the same system but in mass base. The system has a very large three-phase area, due to immiscibility between H_2O and Witepsol W31, and the low solubility of CO_2 in H_2O and W31 in CO_2. The two-phases area V-L_1, that can be visualised in molar base, is almost completely disappearing when the mass base is considered. Another clear difference between the ternary diagram in mol/mol and in mass/mass is how large the area of the 2-phase equilibrium L_1-L_2 appears to be. This is due to the difference in molecular weight (MW) between W31 and CO_2. The pseudo-component used to model W31 has a MW of

667.05 g/mol, while CO_2 MW is 44.01 g/mol, more than 10 times lower. Therefore a large percentage in mol of CO_2 does not necessarily mean a large quantity in mass. This is the reason why L_1 has been identified as the phase in which W31 is most present in mass-base, even if when reading table 19 (in mol/mol %) it seems CO_2 is the prevalent compound. By looking at the tie-lines it can be observed that the solubility of CO_2 in W31 is higher than in H_2O. This is in agreement with the binary phase equilibria.

Table 18 - Composition of the equilibrium points of the ternary system Witepsol W31-CO_2-H_2O (mol/mol %)

V			**L_1**			**L_2**		
CO_2	**W31**	**H_2O**	**CO_2**	**W31**	**H_2O**	**CO_2**	**W31**	**H_2O**
Not present			1.00	95.42	3.58	0.01	0.00	99.99
			10.84	85.84	3.32	0.13	0.00	99.87
			20.03	76.90	3.07	0.25	0.00	99.75
			30.01	67.18	2.81	0.41	0.00	99.59
			40.02	57.43	2.55	0.60	0.00	99.40
			50.09	47.62	2.29	0.82	0.00	99.18
			60.77	37.21	2.02	1.10	0.00	98.90
100	0.00	0.00	70.89	29.11	0	Not present		
98.88	0.00	1.12	69.91	28.59	1.80	1.38	0.00	98.62

Table 19 - Composition of the equilibrium points of the ternary system Witepsol W31-CO_2-H_2O (mass/mass %)

V			**L_1**			**L_2**		
CO_2	**W31**	**H_2O**	**CO_2**	**W31**	**H_2O**	**CO_2**	**W31**	**H_2O**
Not present			0.07	99.83	0.10	0.03	0.00	99.97
			0.83	99.07	0.10	0.31	0.00	99.69
			1.69	98.21	0.11	0.62	0.00	99.38
			2.86	97.03	0.11	1.00	0.00	99.00
			4.39	95.49	0.11	1.45	0.00	98.55
			6.48	93.40	0.12	1.98	0.00	98.02
			9.71	90.15	0.13	2.65	0.00	97.35
100	0.00	0.00	13.84	86.16	0.00	Not present		
99.54	0.00	0.46	13.82	86.03	0.15	3.30	0.00	96.70

5.6 - Conclusions

The GC-EoS proved to be a reliable thermodynamic model for the prediction of systems involving high molecular weight compounds, like triglycerides, and supercritical fluids, i.e. CO_2. The possibility to use it for a mixture of triglycerides is of great importance, especially in processes where natural oils/lipids are used. In those cases the composition of the compound is not easily known, but modelling with a pseudo-component can be of great help to predict and model similar systems.

5.7 - Acknowledgments

The author would like to thank Prof. Ángel Martín of the University of Valladolid for the help, the teaching and the support on the modelling shown during the exchange period in Valladolid. Without him part of this work would have not been possible.

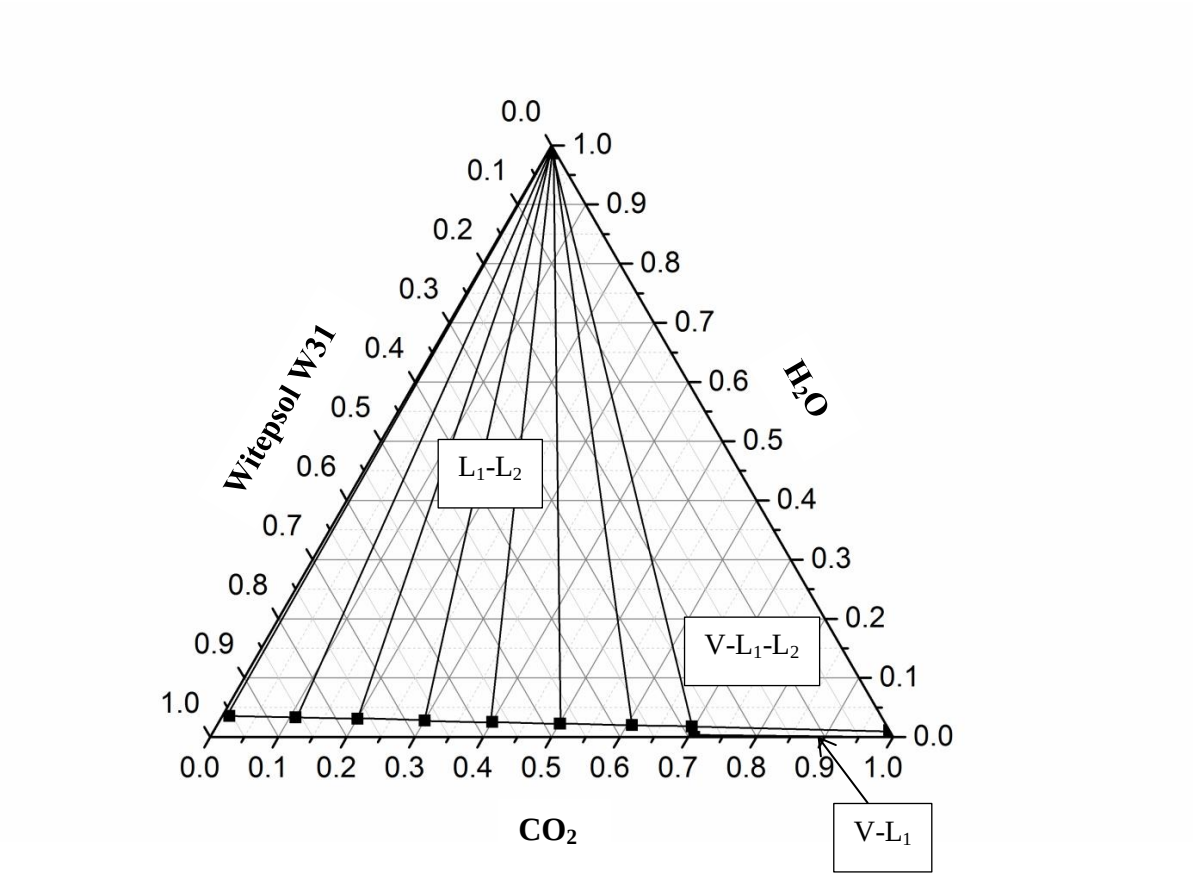

Figure 22 - Ternary diagram for the system Witepsol W31-CO_2-H_2O (compositions in mol/mol) at 80 °C and 80 bar. V represents the phase where CO_2 is prevalent, L_1 the one where Witepsol W31 is prevalent and L_2 the one where H_2O is prevalent.

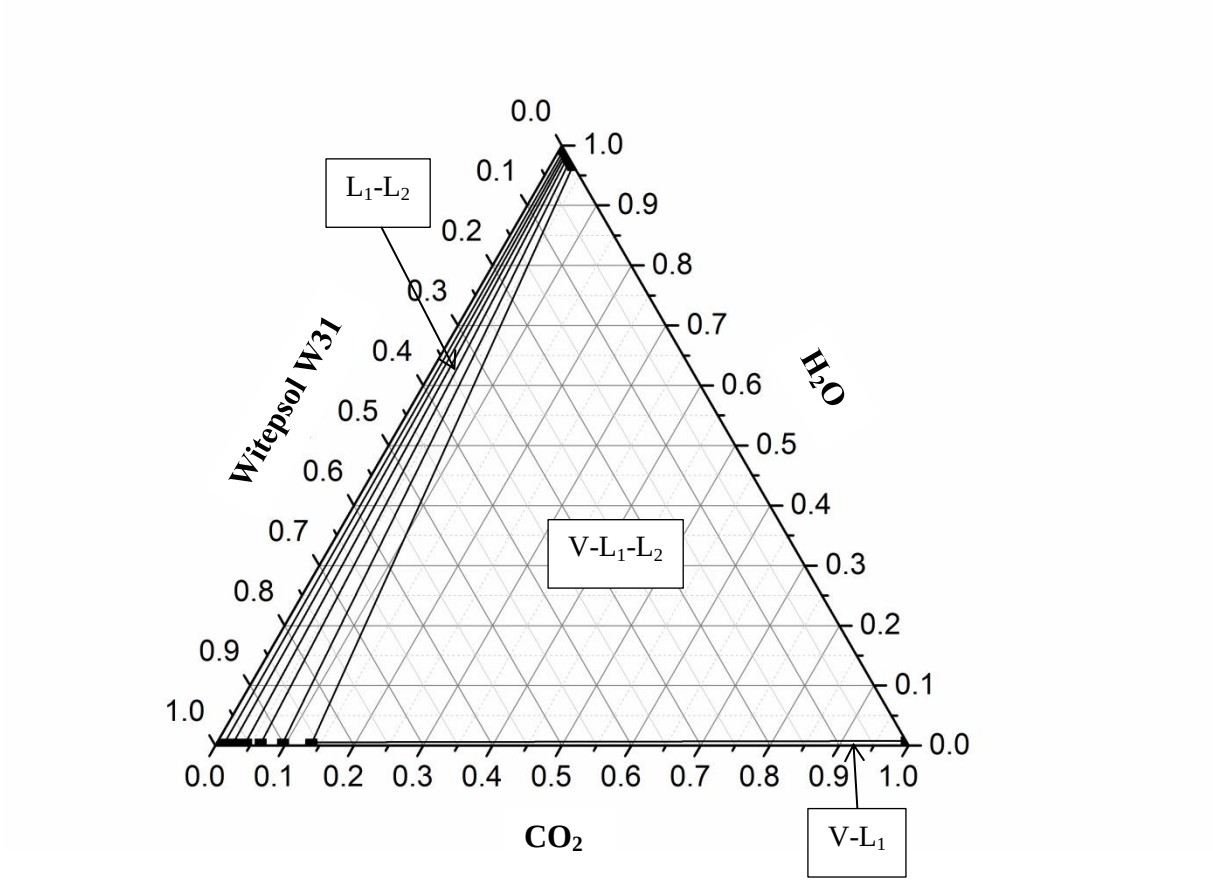

Figure 23 - Ternary diagram for the system Witepsol W31-CO_2-H_2O (compositions in mass/mass). at 80 °C and 80 bar. V represents the gas phase, L_1 the liquid phase due to Witepsol W31 and L_2 the liquid phase due to H_2O.

6 Capsules from Melt Dispersion Technique

Preliminary studies on the effect of the emulsifier on the encapsulation efficiency and release patterns were performed on capsules generated via a double emulsion technique called melt dispersion technique (MDT) [4,54,55]. These tests aimed to have an insight on how differently the emulsifiers would act in the system under study.

Span 65, Span 80, Tween 80 and PGPR were tested at two different concentrations with respect to the Witepsol W31, precisely 1 and 5 w/w%. All tests were repeated at least three times.

In this chapter the encapsulation efficiency is discussed. Further information regarding the characterization of the capsules, like PSD or morphology, can be found on [69] and [70].

6.1 - Encapsulation Efficiency

To calculate the encapsulation efficiency (EE) of NaCl the conductivity of salt in water was measured as described in section 4.4.5. This was done by using two different methods: one by measuring the conductivity in the external water after the preparation and the washing water (indicated as “From external water”), the other by melting 0.3 g of washed capsules in 30 g of distilled water and measuring the conductivity in the water after filtering the capsules (indicated as “By melting”).

The results are shown in fig. 24 and 25. In general, it can be observed that the encapsulation efficiencies are quite comparable between the two methods, which was a sign of the reliability of the tests.

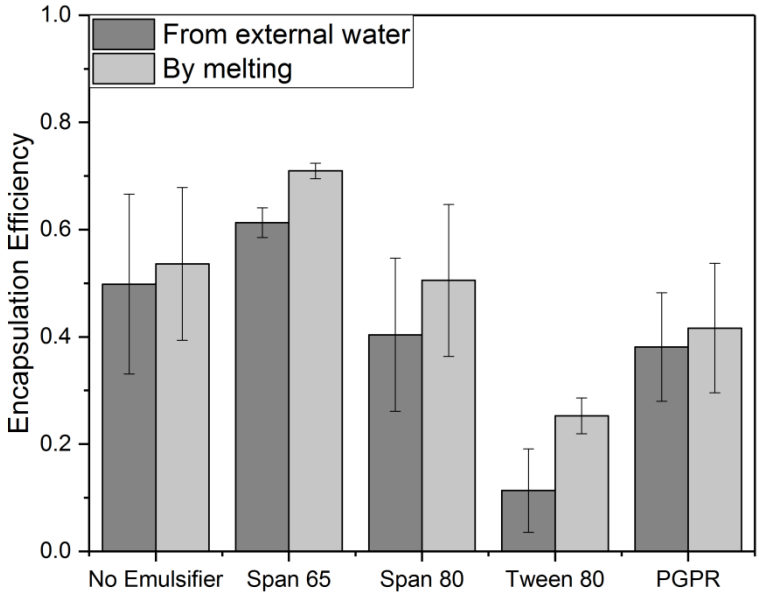

Figure 24 - Encapsulation efficiency (1% of emulsifier).

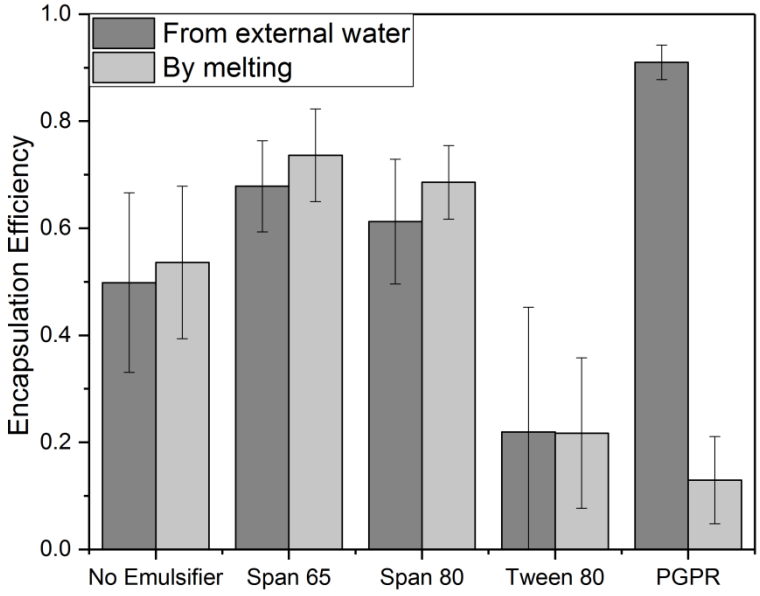

Figure 25 - Encapsulation Efficiency (5% emulsifier).

Figure 24 shows the EE of the produced capsules by adding 1% w/w of emulsifier to the shell material. The experiments show that at such concentration the presence of an emulsifier do not improve the EE when making a comparison with capsules prepared without emulsifier. The EE is either similar, e.g. Span 65, or it is reduced, like in the other cases studied. Tween 80 behaviour will be explained at the end of this section.

When the amount of emulsifier is increased from 1% to 5% (figure 25) the EE increases as well. Tween 80 shows also here a different behaviour, due to its hydrophilic nature. In particular in the case of PGPR increasing the percentage of emulsifier has a positive effect on the morphology of the capsules that show a complete closed surface at higher concentration, while holes are present at lower concentration [69].

The results show that the EE from the different methods are consistent with each other, except in the case of PGPR 5%. This is very obvious when observing figure 25.
The discrepancy could be due to the PGPR increasing the conductivity of the water (affecting mostly the EE "from external water") or to the fact that melting the capsules was not enough to release the NaCl (affecting the EE "by melting"). To prove the cause of the difference in EE two different tests were performed.
The first hypothesis was tested by measuring the conductivity of a 9 w/w% NaCl solution in distilled water with and without emulsifier. The results are collected in table 20. It can be easily observed that the difference in the conductivity in presence of an emulsifier is minimal. Therefore the results of the EE "from external water" are correct.
To check the second hypothesis, capsules with the different emulsifiers were prepared, but rather than using just a NaCl solution as core material, eYFP was added. The capsules obtained were analysed with **f**ast **re**laxation **i**maging (FreI), which combines fluorescence microscopy and temperature jumps [53,71]. A more clear insight will be given in section 6.2. From the images obtained it could be seen that there is almost no release of core substances by melting the capsule containing 5% of PGPR (as shown in fig. 25). This

explains the poor EE that is obtained “by melting”, since just a little of the NaCl contained in the capsule is released in the water. Therefore the results of the EE “by melting” are also correctly measured. Nevertheless the right EE results are the one measured “from external water” because it is not possible to release the complete NaCl solution from molten PGPR capsules.

With the method used to generate microcapsules, Witepsol W31 showed to be a good shell material just by itself. Adding a lipophilic emulsifier enhances the encapsulation efficiency, especially when the concentration of emulsifier is higher. On the other hand, the use of a hydrophilic emulsifier, like Tween 80, leads to a significant drop in the encapsulation efficiency. This is due to the nature of the emulsifier which favours the formation of an O/W emulsion, with the majority of NaCl solution present in the external water phase. Comparing the lipophilic emulsifier, Span 65 is slightly better than Span 80. The difference probably stems from the chemical structure of the emulsifier. Span 65 is in fact better solvated in Witepsol due to the three lipophilic side chains forming an interface with higher stability against breakage and leaking during the formation of the W/O/W emulsion.

PGPR proved to be the best emulsifiers among those investigated here. Moreover, when the capsules are molten the obtained emulsion is very stable, as observed also by Wolf [72]. A possible explanation is provided by Moglia et al. [51]. The Span family presents -OH groups in the polar head, while PGPR in the hydrophobic tail. These -OH groups act as hydrogen donors and the hydrogen bonding could interact with the lipid phase. If the polar head interact with the lipid phase the emulsifier loses his potential as a stabilizer. On the other hand if the –OH group strengthen the bond between the lipophilic tail and the lipid phase, as PGPR does, the stabilization at the water/oil interface is improved.

Table 20 - Conductivity of emulsifiers in NaCl solutions

Emulsifier	**Concentration (w/w)**	**Conductivity (mS/cm)**	**T (°C)**	**Conductivity at 25 °C (mS/cm)**
None	-	131.8	26.0	129.1
Span 65	1%	145.9	30.5	129.0
Span 65	5%	146.4	30.6	129.2
Span 80	1%	131.6	26.1	128.6
Span 80	5%	134.6	26.0	131.7
Tween 80	1%	134.3	27.0	128.6
Tween 80	5%	132.8	27.2	126.6
PGPR	1%	132.9	26.4	129.0
PGPR	5%	134.7	26.8	129.6

6.2 - Investigation with fluorescent protein

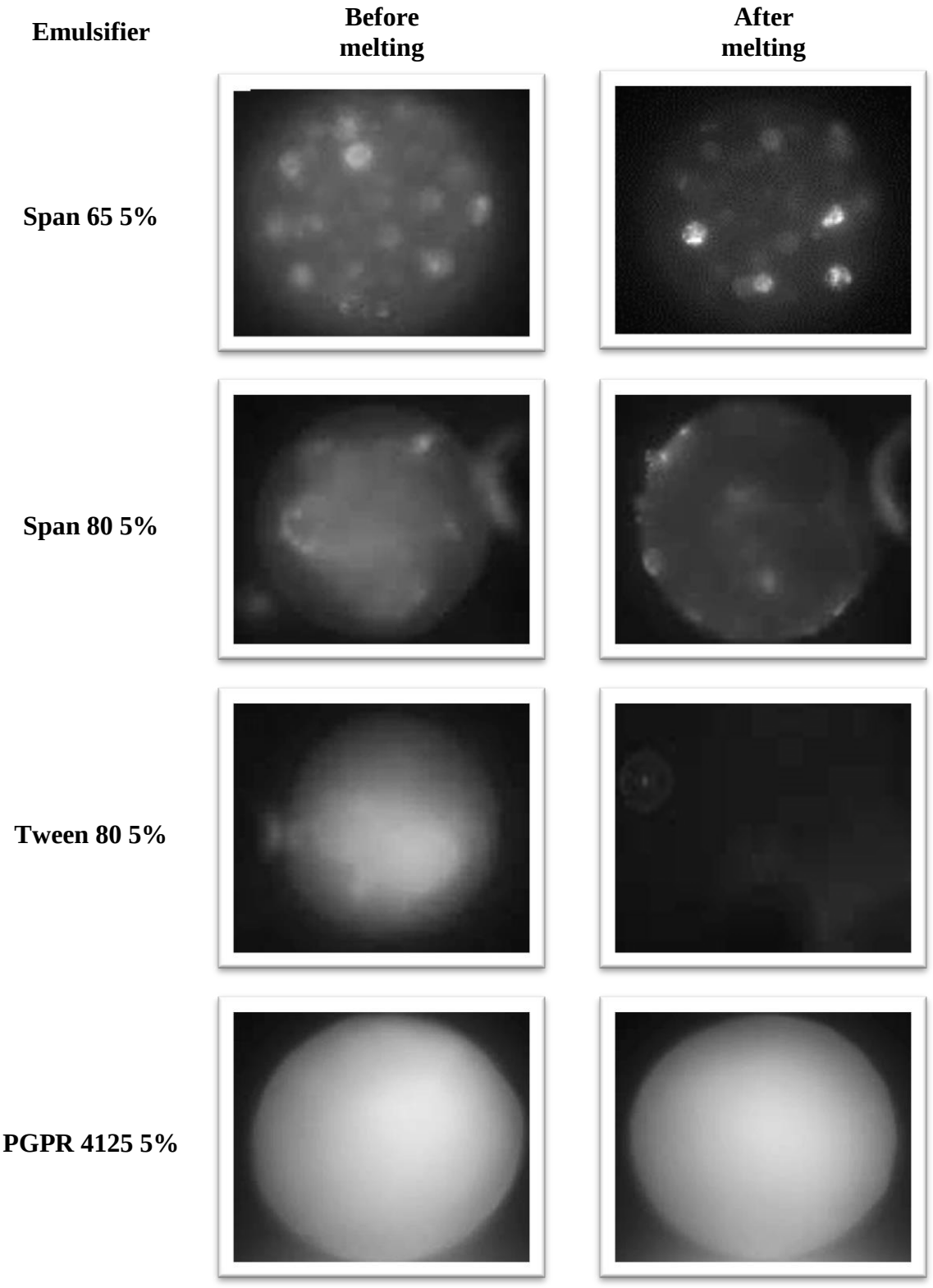

Figure 26 - Examples of fluorescence in capsules containing eYFP and NaCl solution with different emulsifiers.

Capsules were produced following the procedure described in the Method section, although this time the core material was a solution of eYFP and NaCl solution. The addition of eYFP enabled to observe both the melting of the capsules and what happens to them in the presence of different emulsifiers. On the left side of figure 26 it is possible to observe the capsules before melting. The light grey-white areas indicate the presence of eYFP. As expected by the results shown in the previous section, lipophilic emulsifiers have more light grey-white area when compared to Tween 80, a hydrophilic emulsifier. On the right side, the pictures of the capsules after melting and resolidification can be examined. Span 65 reduces the quantity of eYFP entrapped, shown by the reduction in light grey-white areas. PGPR do not show appreciable differences. The capsules with Tween 80 "after melting" disappear.

As mentioned before, PGPR is the only emulsifier that shows only a slight change in the fluorescence over time, indicating a very limited release.

These tests showed how the emulsifier affects the release when the capsules are molten. In general it is observed that, when reaching the melting temperature of the shell material, the capsule liquefies and the core material is released. The only exceptions are capsules prepared with PGPR at 5% and Tween 80.

In the latter case, not only there is a burst release but also the capsules look like they "exploded" (fig. 26), completely disappearing as a spherical capsule. The presence of Tween 80 favours O/W emulsions and when the capsule is molten the core substance is released and the Tween 80 leads to small droplets of oil in water. The picture taken after the following cooling perfectly captures this situation: the fluorescence is not focused in one area anymore and the microscope does not detect it, therefore the area is almost complete black. Looking carefully on the top right angle, it is possible to observe one of the smaller droplets containing the fluorescent protein, soon to be dissolved in the surrounding medium.

The capsules containing 5% PGPR are on the opposite spectrum. They show a very good stability even after melting, with limited signs of release. Jiahong was suggesting that the presence of NaCl in the internal water phase generates a flux of water from the external phase to the inside of the capsules, resulting in an increase in water droplet size and therefore an increase in the volume fraction of water [73]. For capsules containing PGPR 5%, the concentration of the emulsifier could be high enough to be in excess in the fat phase, protecting adequately the water droplets [73]. Pawlik et al. [74] showed also that the presence of NaCl increases the stability of W/O emulsions prepared with PGPR, however the molar concentration of the NaCl solution used in this work is higher than the one in their work.

6.3 - Release

In figures 27-28 the release of NaCl from the capsules is shown. It is reported as the ratio between the NaCl released after a certain amount of time and the NaCl released "by melting". The only exception, as explained in section 6-1, is in the case of PGPR 5% where the NaCl released after a certain amount of time is divided by the encapsulated NaCl as calculated in eq. 11 (method "from external water").

The mass fraction of the emulsifier affects the release. A lower amount does not prove to be better than the pure shell material. However certain emulsifiers can offer a better protection from release in higher amounts. Tween 80, even by having the least amount of NaCl in the capsules, shows the fastest release. Its more hydrophilic nature helps the release of the aqueous core solution. On the other hand when a lipophilic emulsifier, e.g. Span 80, is present the release is hindered, in comparison to the use of a hydrophilic emulsifier. Span 65 and Span 80 speed up the release compared to the capsules without an emulsifier. Once more, the nature of these emulsifiers and the presence of –OH groups weaken the stabilization caused by the emulsifiers. Instead, for the same reasons explained regarding the encapsulation efficiency, the capsules containing PGPR have the slowest release over time.

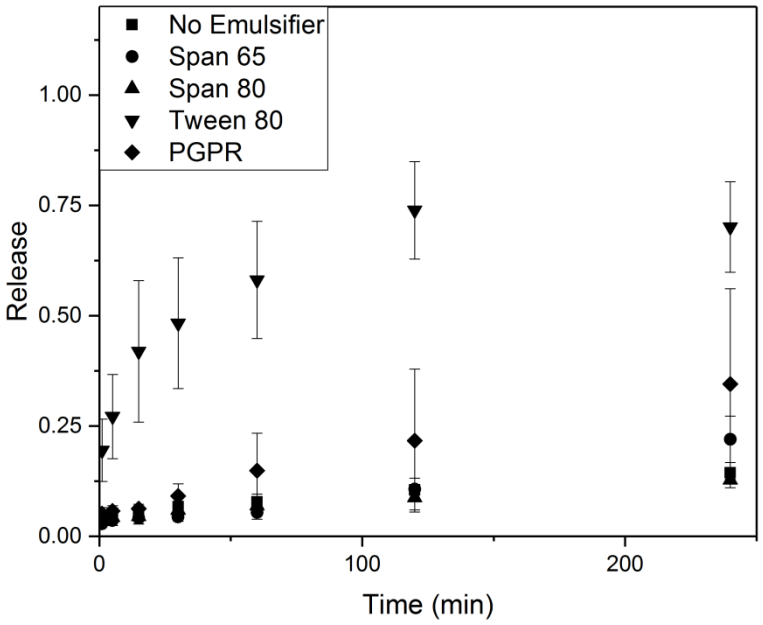

Figure 27 - Release of NaCl from capsules (1% emulsifier).

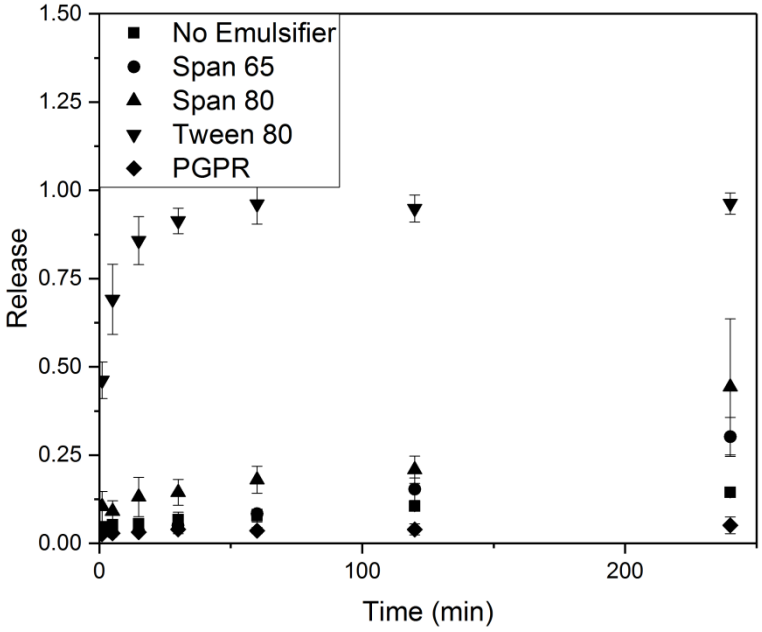

Figure 28 - Release of NaCl from capsules (5% emulsifier).

6.4 - Acknowledgments

The author would like to thank M. Sc. Rebecca Scholz, colleague at the VTP department, and Dr. Tobias Vöpel of the department of Physical Chemistry II, Ruhr-Universität Bochum, for the discussions, the analysis of the data and the experiments with the thermal microscopy combined with laser-induced heating and fluorescence imaging.

7 Capsules from PGSS

The preliminary tests performed with the melt dispersion technique proved that the addition of emulsifiers in the shell material has a positive effect on the encapsulation process. The only exception between the emulsifier taken in consideration was Tween 80, which was then excluded for the generation of capsules via the PGSS process.

In this chapter the word “particles” refer to powder which is composed only of the shell material, therefore Witepsol W31. The word “capsules” will refer instead to powder which is obtained by combination of shell and core material.

7.1 - Particles production

The study of the PGSS process for the generation of capsules with the addition of emulsifiers started with a series of test to assess the effect of the process conditions on the shell material. Therefore, before spraying emulsions, the PGSS process was employed with pure Witepsol W31 alone. The parameters taken in consideration are temperature and pressure before the expansion, GPR (**G**as to **P**roduct **R**atio), temperature in the spray tower and nozzle size. All these parameters are not independent and are influencing each other. For example, the GPR depends on the nozzle size and pressure due to the plant layout.

Table 21 - List of experiments performed by spraying pure Witepsol W31

Experiment number	Nozzle size [mm]	T pre-exp. [°C]	P pre-exp. [MPa]	T spray tower [°C]	GPR
1	0.5	53.3	8.0	17.7	1.9
2	0.5	52.5	8.1	23.8	2.0
3	0.5	52.9	8.0	21.2	1.7
4	0.5	53.1	8.3	19.7	1.6
5	0.83	52.8	8.0	5.9	7.9
6	0.34	52.4	8.3	25.5	1.0
7	0.34	62.5	8.4	27.0	1.1
8	0.34	51.7	10.3	19.2	1.6
9	0.34	61.7	10.3	24.1	1.5
10	0.5	72.9	8.2	25.9	2.4
11	0.5	62.7	8.2	23.4	2.6
12	0.34	62.5	8.5	26.9	1.0
13	0.34	72.7	10.0	26.9	1.4
14	0.34	72.4	8.1	29.1	0.9
15	0.5	61.0	5.1	28.0	1.4

Via these tests the effect of process parameters on bulk density, PSD and particle morphology was studied. The general trends were in agreement with previous studies on the PGSS process [11–13,17,18].

The repeatability of the tests was checked with experiments 1 to 4. Experiments 4, 5 and 6 were used to observe the differences in morphology. The study of the PSD and the bulk density was based on all the experiments.

7.1.1 - Repeatability

Experiments 1 to 4 were performed to test the repeatability of the experiments performed in the PGSS plant. The conditions were kept constant for all these experiments, with minor deviations in the temperature and pressure pre-expansion, and therefore GPR.

Table 22 - Characteristic of tests 1 to 4

Experiment number	Bulk density [kg/m^3]	D_{10} [µm]	D_{50} [µm]	D_{90} [µm]	Span
1	64.5 ± 0.4	1.1	7.4	22.2	2.9
2	74.6 ± 2.1	1.0	9.2	21.4	2.2
3	59.6 ± 0.4	0.9	7.7	17.7	2.2
4	67.8 ± 2.3	1.0	8.7	21.1	2.3

The bulk density, the PSD and the morphology of the produced particles were analysed. Table 22 collects the bulk density measurements results, as well as the major information on the PSD. In figure 29 the complete PSD is shown.

It can be observed that the particles obtained by performing the tests at the same conditions have similar PSD and bulk density. This proves that the experiments are repeatable; therefore the results obtained are accurate.

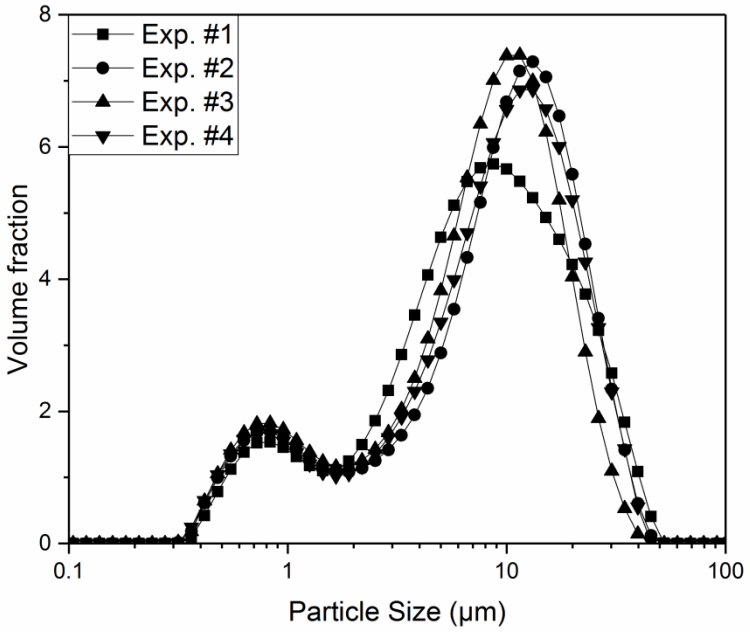

Figure 29 - PSD of repeatability test experiments

In Figure 30 some of the SEM images of the particles of the repeatability experiments are shown. They are all pretty similar: some completely round particles surrounded by smaller attached particles, with a closed or open structure, resembling a sponge.

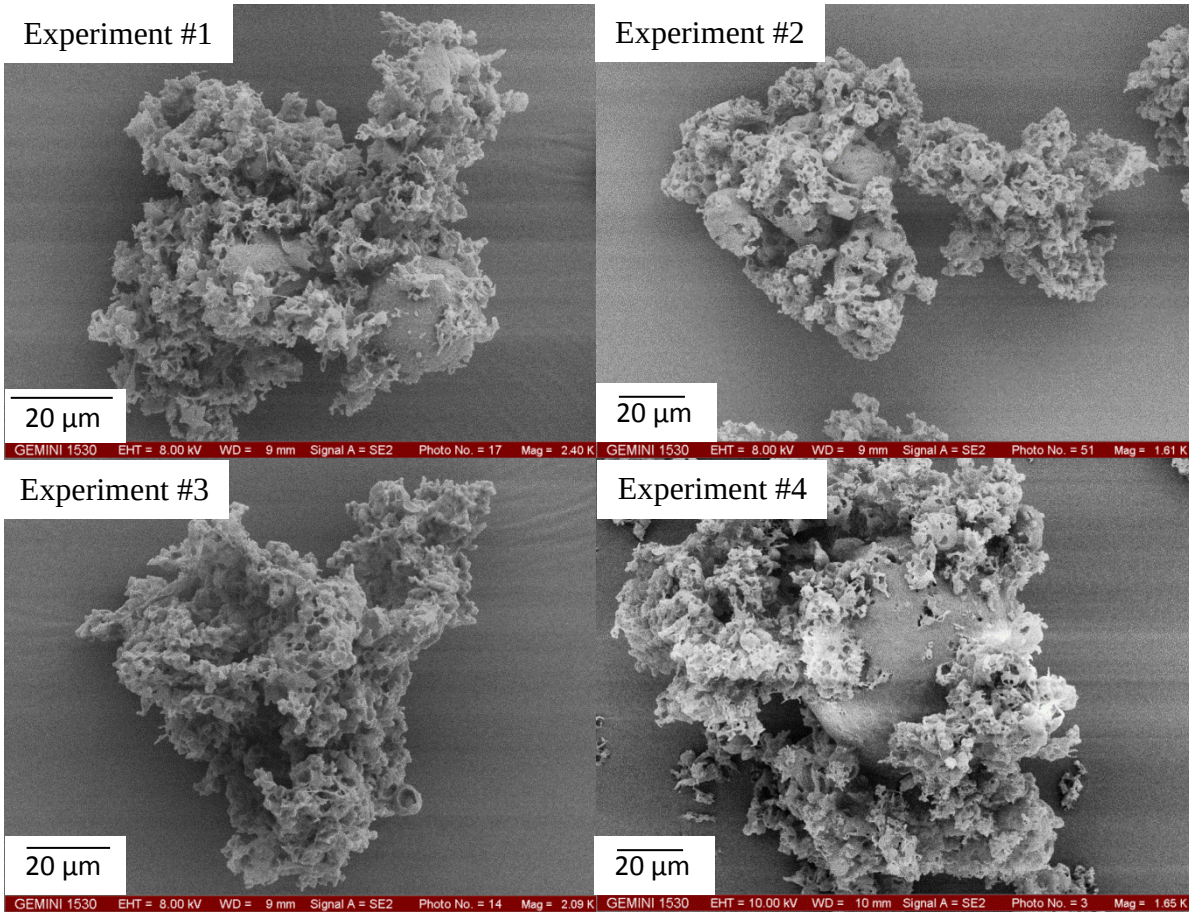

Figure 30 - Morphology of the particles of experiments 1 to 4

7.1.2 - Effect on bulk density

Figures 31 and 32 show the effect of the GPR and the temperature in the spray tower, respectively, on the bulk density. It can be observed that there is a trend: the higher the GPR the lower the bulk density. The opposite is instead true for the spray tower temperature. In this case the higher the temperature, the higher is the bulk density.

The effect of the two parameters is similar. This happens because the two parameters are strictly correlated: more CO_2 lowers the temperature in the spray tower because the cooling power provided by the expansion is higher. The dashed line represents a limit to the formation of the particles as experimentally observed. The line corresponds to the condition of the experiment where not only powder was obtained but sheets of solidified Witepsol at the inner walls of the spray tower were found at the end of the experiment as well. This happened because there was not enough CO_2 to solidify the droplets after the nozzle.

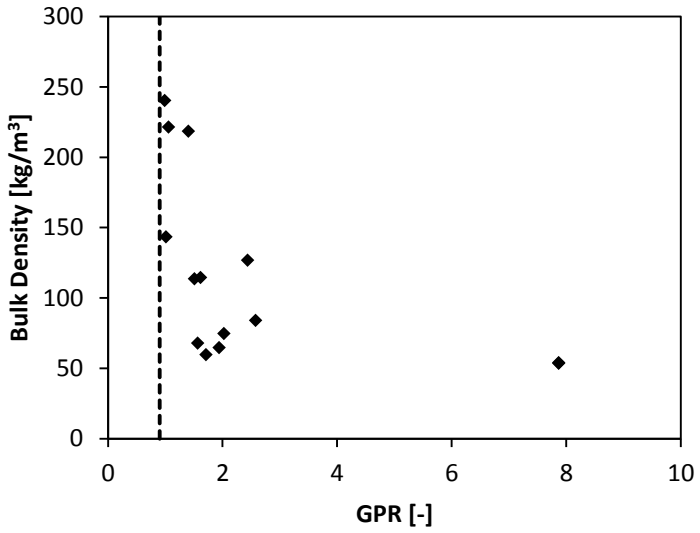

Figure 31 - Effect of GPR on bulk density

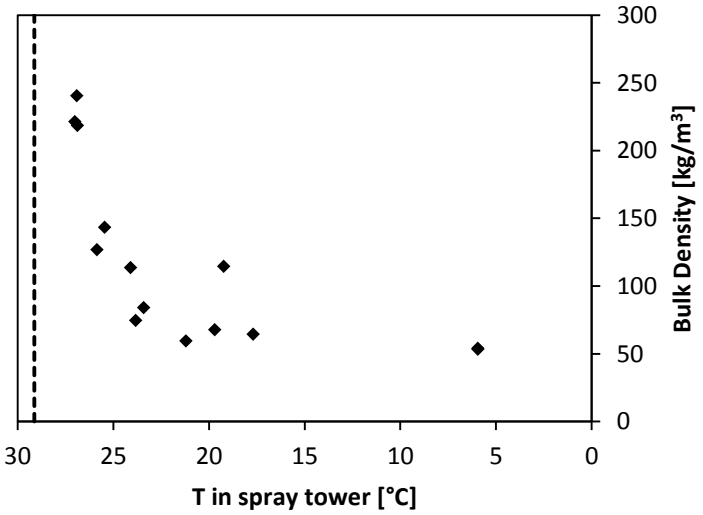

Figure 32 - Effect of the temperature in the spray tower on the bulk density

It is possible to combine the GPR and T in the spray tower in a single parameter, the power ratio. This is the ratio between the cooling power of the CO_2 and the required power to cool down the Witepsol W31 to the spray tower temperature.

The calculation of the powers and the ratio are as follows:

$$\dot{Q}_{CO_2} = \dot{m}_{CO_2}\left(h_{T'',p''} - h_{T',p'}\right) \tag{43}$$

$$\dot{Q}_{W31} = \dot{m}_{W31}\left(\lambda + c_{p,W31} * \left(T'' - T'\right)\right) \tag{44}$$

$$\text{Power ratio} = \left|\frac{\dot{Q}_{CO_2}}{\dot{Q}_{W31}}\right| \tag{45}$$

where $\dot{Q}_{CO_2}$ and $\dot{Q}_{W31}$ are the power [kJ/s] of the CO_2 and the W31, respectively, between the conditions before the nozzle (T' [K] and p' [MPa]) and in the spray tower (T" and p"); h is the enthalpy [kJ/kg] at the specified temperature and pressure; $\dot{m}_{CO_2}$ and $\dot{m}_{W31}$ are the mass flows [kg/s]; λ is the latent heat of solidification of W31 (138 kJ/kg) and $c_{p,W31}$ is the heat capacity averaged between the operating conditions (for W31 2.2 kJ/kg K). Heat of mixing is not considered, but as shown by Weidner this energy is very small compared to latent heat [75].

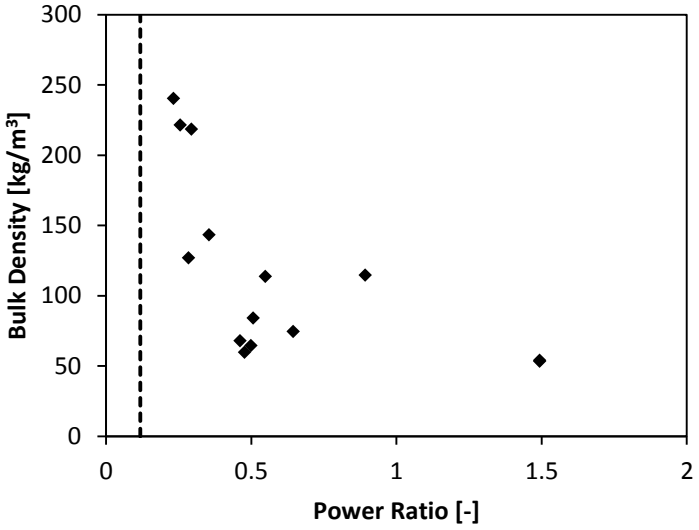

Figure 33 - Bulk density vs Power Ratio

When the Power ratio is plotted versus the bulk density, the diagram (figure 33) shows the same trend as figures 31 and 32. It is interesting to notice that to obtain particles via PGSS it is not required to provide the total amount of cooling that the shell material would require (ratio =1) but a smaller amount is sufficient. This was also observed by other authors [13,17].

At the same time, it is important to consider that the energy balance is not closed in any of the experiments, when assuming adiabatic conditions. For a complete solidification the extra energy is taken by the environment. It happens when ratio < 1 and only if the temperature in the spray tower is higher than the ambient temperature. This condition was satisfied by any experiment whose ratio value was lower than 1.

7.1.3 - Effect on particle size distribution

The **P**article **S**ize **D**istribution (PSD) is affected by the operating conditions. The parameter which affects the PSD the most is the GPR. This can be easily noticed in figure 34. When the GRP is the lowest, the PSD has the most variability, with higher value for the D_{90}. This is due to the low amount of CO_2, which favours the agglomeration of the particles during the solidification phase. This is resulting in bigger particles as detected by the Mastersizer. An exception is experiment 11, which has a high GPR but

still present a high D_{90}. Nevertheless the D_{50} in this case is in the same range as the experiments with a lower span.

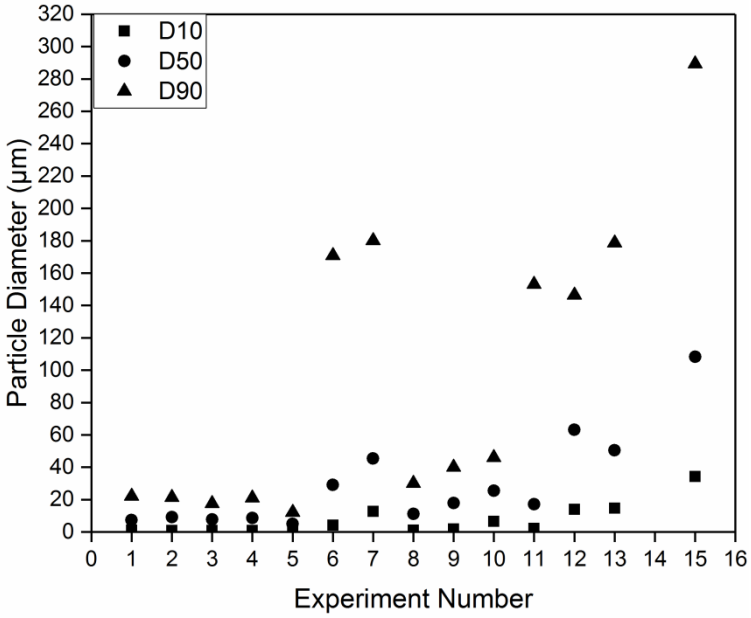

Figure 34 - Particle size of the Witepsol W31 particles

7.1.4 - Effect on morphology

The effect of the GPR is not only limited to bulk density and to particle size. It affects also the morphology of the particles as shown in fig. 35. Table 23 shows the data of the experiments visualised in fig. 35.

Table 23 - Effect of nozzle size and GPR on the powder obtained via PGSS for pure Witepsol W31

Nozzle size [mm]	**T pre-exp. [°C]**	**P pre-exp. [MPa]**	**T spray tower [°C]**	**GPR**	**Bulk density [kg/m^3]**	**D_{50} [µm]**
0.83	53	8.3	6	7.9	53.4 ± 1	7.5
0.5	53	8.0	20	1.6	67.8 ± 2.31	14
0.34	52	8.3	25	1	143.34 ± 4.37	39

The particles were produced at the same operating conditions but the GPR was modified by changing the nozzle size. The higher the diameter of the nozzle boring, the higher is the GPR. As it can be seen the higher the GPR the less spherical the particles are. This happens because a great excess of CO_2 cools down the droplets after the nozzle much faster, solidifying the particles of W31 before they have enough time to reach a spherical shape. This also influences the particle size and the bulk density, which in general decrease the less spherical the particles are.

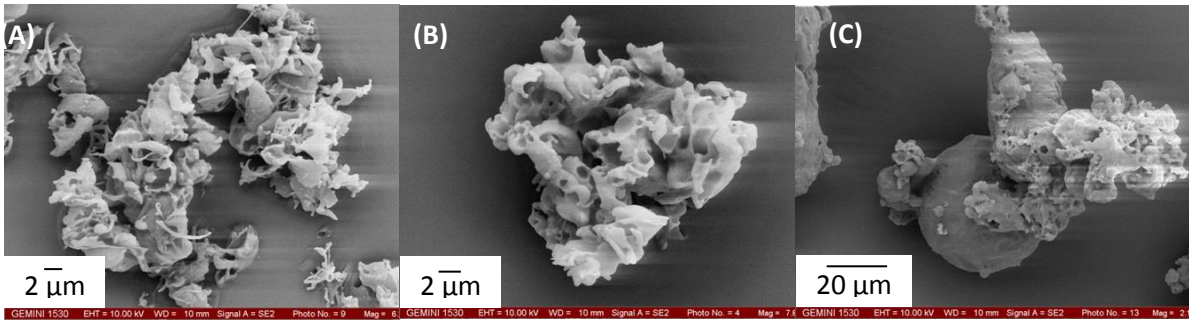

Figure 35 - Morphology of the particles obtained by spraying at the conditions indicated in table 23. (A) Nozzle size 0.83 mm; (B) Nozzle size 0.5 mm; (C) Nozzle size 0.34 mm

7.2 - Capsules production

Seven experiments have been carried out for the capsules production. The spraying conditions have been kept constant for all the experiments (T = 60 °C, P = 5 MPa, nozzle size = 0.5 mm). The temperature was chosen in order to guarantee homogeneity in the experiments. Span 65 has a melting point of 60 °C, therefore a lower temperature could have negatively affected its properties as an emulsifier. By working at this temperature the solidification of the emulsion between its preparation and the insert in the tank of the PGGS plant is also avoided. It was not possible to utilize a smaller nozzle due to blockage when spraying. By using the nozzle with an inner diameter of 0.5 mm the pressure for the capsules production was chosen as 5 MPa, in order to obtain composites as spherical as possible, due to the interaction between GPR/pressure and the morphology of the W31 particles.

Emulsions of different composition have been sprayed and the composition and the spraying conditions can be found in table 24. The amount of core solution and the type of the emulsifier were studied. The mass fraction of the emulsifier was kept constant at 5 % (respect to W31), because of the results of the preliminary studies performed with the MDT.

Table 24 - Capsules production experiments conditions

I.D.	**W31**	**Emulsifier**		**NaCl solution**	**T**	**p**	**GPR**	**$T_{spray\ tower}$**
	Wt. %	**Type**	**Wt. %**	**Wt. %**	**°C**	**bar**	**-**	**°C**
C1	86	SPAN 65	4	10	61.2	51.6	1.3	23.5
C2	86	SPAN 80	4	10	61	51.7	1.4	23.3
C3	86	PGPR	4	10	60.7	52	1.3	23.3
C4	76	SPAN 65	4	20	60.8	51	1.3	21.7
C5	76	SPAN 80	4	20	62.7	52.4	1.5	21.4
C6	76	PGPR	4	20	60.9	52.3	1.2	22.5
C7	80	-	-	20	61.0	51.2	1.5	21.9

The operating conditions have been the same for all the experiments and this reflects on the capsules characteristics. The bulk density and the PSD are not very different between all the experiments (table 25). The bulk density ranges between 140 and 180 kg/m^3 while the D_{50} ranges between 24 and 38 µm. It can also be concluded that the emulsifiers do not have an influence on these capsules characteristics

Table 25 - Characteristics of the produced capsules

I.D.	Bulk Density	D_{10}	D_{50}	D_{90}
	kg/m^3	µm	µm	µm
C1	165.3 ± 4.7	16.19	34.53	169.51
C2	181.1 ± 7.3	12.81	36.42	172.87
C3	178.4 ± 4.5	13.55	37.52	177.13
C4	141.1 ± 2.6	5.44	24.58	170.56
C5	156.3 ± 8.3	2.14	23.49	50.70
C6	164.5 ± 4.2	13.31	35.03	181.43
C7	159.2 ± 2.5	5.68	24.59	45.12

If the characteristics of the capsules do not seem to be influenced by the emulsifier, this does not hold true regarding the morphologies of the capsules surface (fig. 36, 37). In particular the presence of Span 80 (A and C) increases the roughness of the surface, showing the presence of veins. Span 65 instead increases the presence of pinholes (B and D). PGPR 4125 appears to have no effect (E and G), having a surface similar to the capsules produced without an emulsifier (F) or similar to the particles generated at the same operating conditions by spraying only W31 (H).

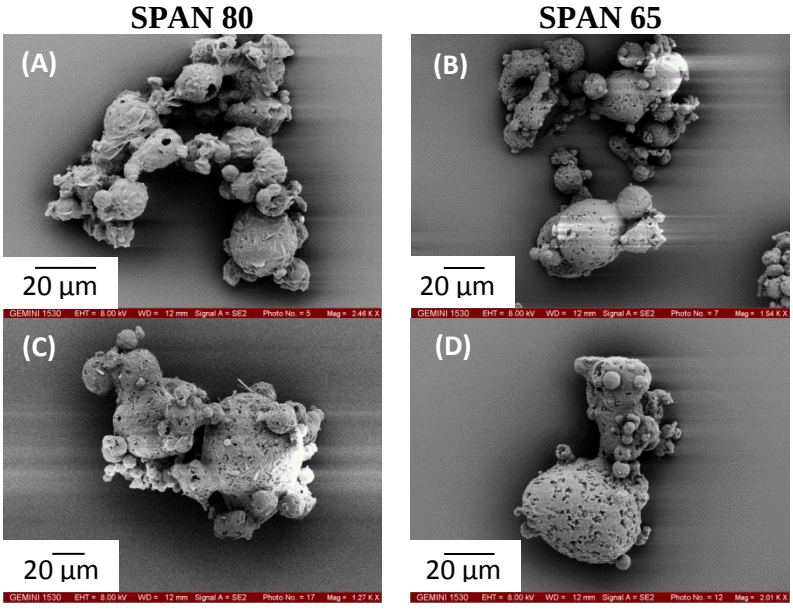

Figure 36 - SEM images. (A), (B) from emulsion 80/20; (C), (D) from emulsion 90/10

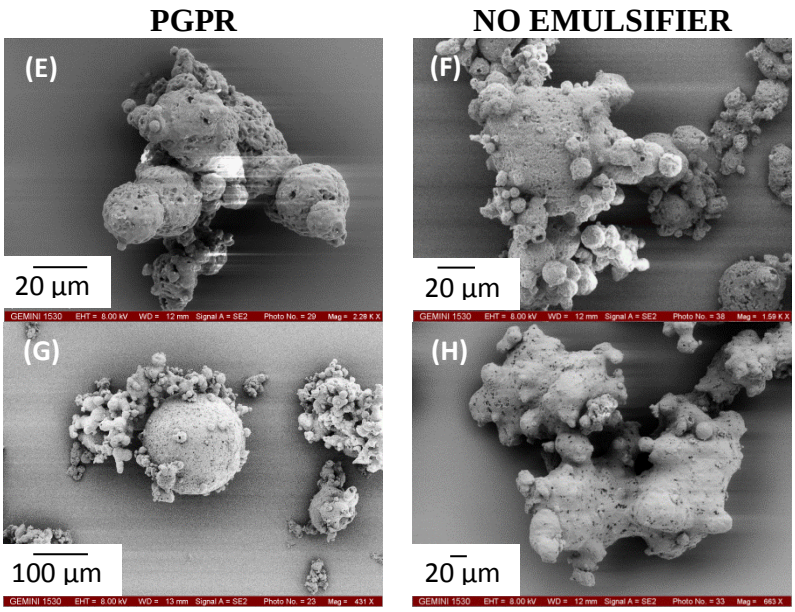

Figure 37 - SEM images. (E), (F) from emulsion 80/20; (G) from emulsion 90/10; (H) pure W31

7.2.1 - NaCl encapsulation and release

The NaCl encapsulation was evaluated with two methods, one by melting the capsules, the second by washing them [76]. In the first case the totality of the NaCl from the capsules that dissolves into the water is measured; in the second only the superficial NaCl is dissolved in water. Therefore to obtain the encapsulation efficiency (EE) the amount measured has to be subtracted from the total amount of NaCl. The results are shown in fig. 38 and 39.

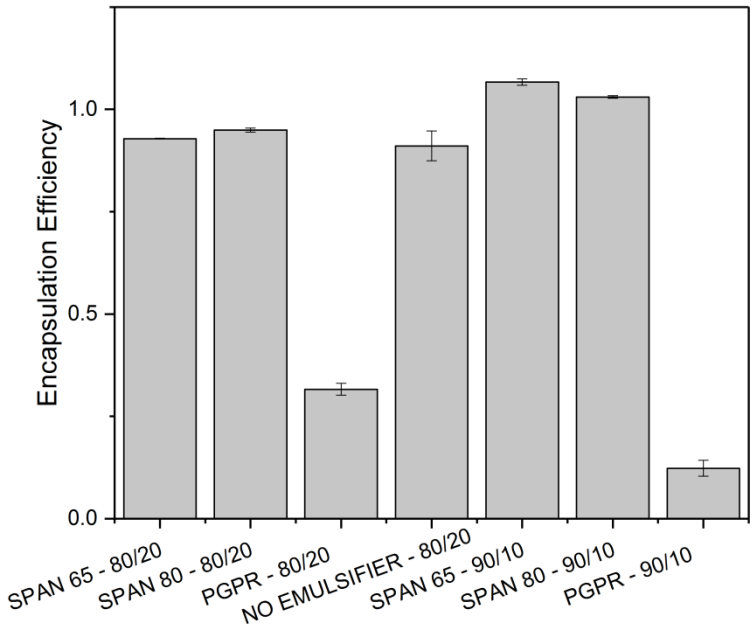

Figure 38 - Encapsulation efficiency by melting

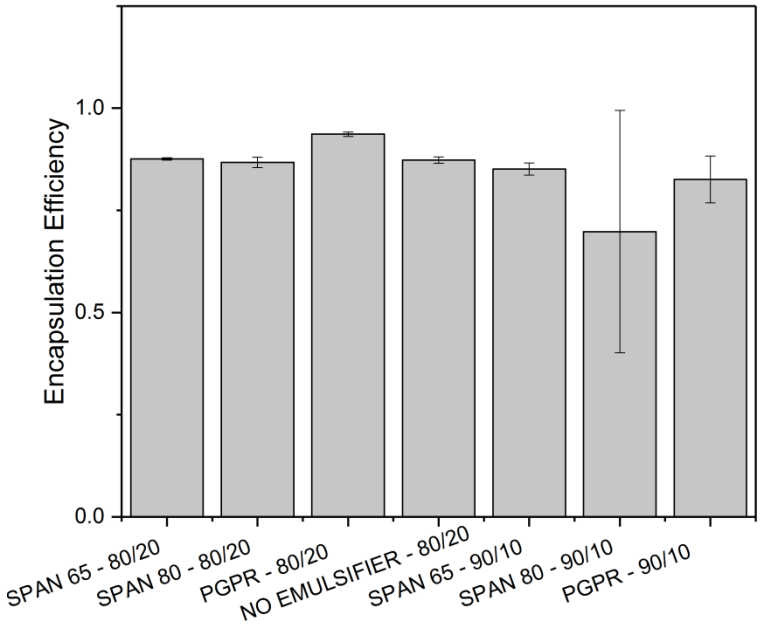

Figure 39 - Encapsulation efficiency by washing

Both methods show that most of the NaCl is encapsulated, with some of it being present on the surface of the capsules; this is why the EE by washing is generally lower than the EE by melting. The capsules containing PGPR show again an unusual behaviour, as observed with the MDT experiments; when molten they release just a small portion of the encapsulated NaCl (fig. 38). PGPR is the better emulsifier among the ones studied and when the capsules are molten the obtained emulsion is very stable (as observed also by Wolf [72]). The possible explanation comes from the observation of Moglia et al. [51] as previously stated: the -OH groups act as hydrogen donors and when present in the lipophilic tail, as in the case of PGPR, they increase the stabilization at the water/oil interface.

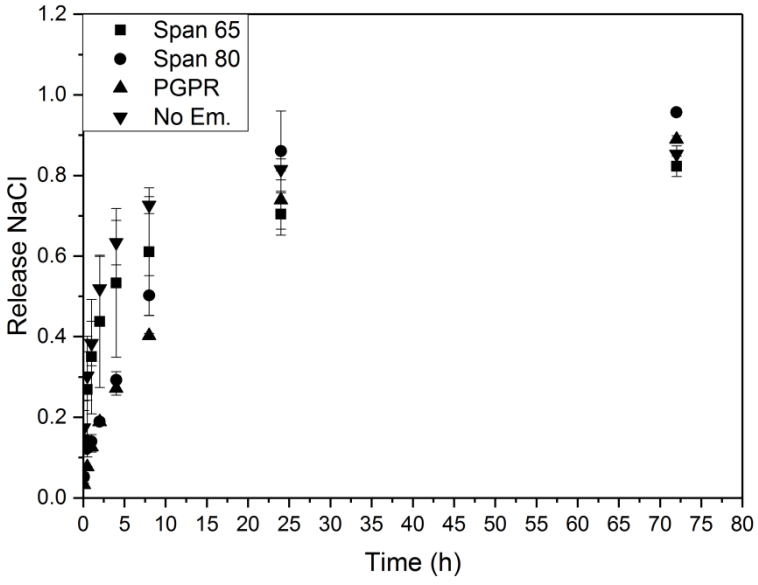

Figure 40 - Release of NaCl in water. Capsules from emulsion W/O 20/80

Regarding the release of NaCl in water (fig. 40) no observable difference is present between the different capsules; therefore no clear effect of the emulsifier can be deducted. The Span family has a faster release, but this could be due to an increased presence of pinholes rather than an effect of the emulsifier. The release of the NaCl from the capsules containing PGPR is faster than the one observed by the capsules produced via a double emulsion technique. The difference in behaviour can be associated to the difference in particle size. The particles obtained via PGSS are one order of magnitude smaller, therefore the release is faster. Another reason lies with the fact that the capsules obtained via PGSS present pinholes; therefore water can easily pass through it, while, when the capsules were produced via MDT they were completely closed, therefore the release was slower. When the capsules containing PGPR are molten the pinholes get closed, and this explains why the EE of PGPR when melting is very low. The fact that the NaCl released is close to 100% in respect to the total NaCl sprayed is an ulterior confirmation of the high encapsulation of NaCl.

7.2.2 - Water loading efficiency

While the NaCl encapsulation is almost complete, the water content of the capsules is always lower (fig 41). The results from the moisture analyser and the Karl Fischer Titration clearly show this.

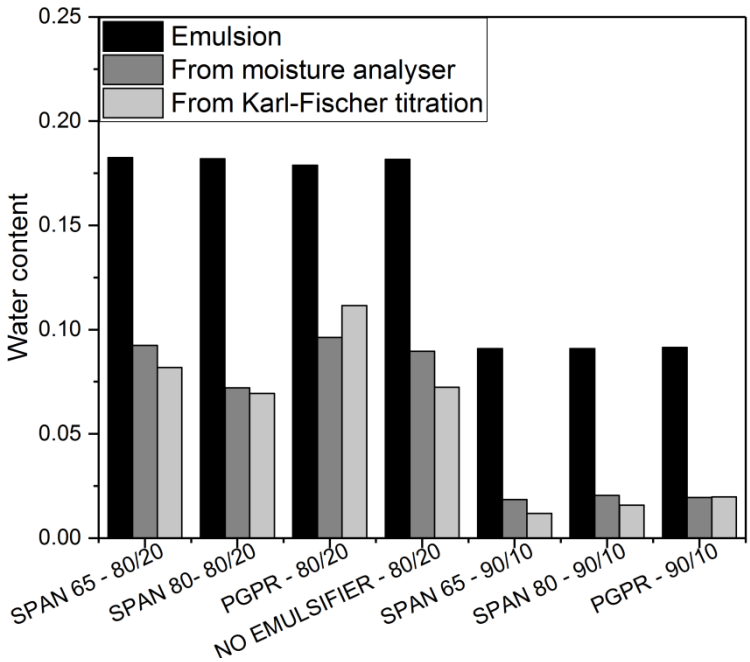

Figure 41 - Water content from this work

It can be observed that the water entrapped in the capsules is always lower than the total water present in the emulsion. It can also be observed that the higher the water content of the emulsion, the higher is the loading efficiency. This is in agreement with the observations of Hanu [17] working with palm fat and Ilieva [18] working with tristearin, but no clear answer was provided to explain this behaviour. In order to find a possible justification to this phenomenon the characteristics of the capsules and the powder of pure

W31 obtained at the same spraying conditions have been compared (fig 42, 43). It can be seen that the particle size distribution and the bulk density of the powder generated from pure W31 are much higher than those generated from the emulsions, even if the experiments were performed at the same operating conditions. A justification could be the fact that in all these cases the cooling provided by CO_2 is not enough by itself, but when emulsions are sprayed the water can provide the missing energy required by evaporating. The lower cooling energy provided by CO_2 alone favours aggregation of the droplets during spraying, which explains why the bulk density and the PSD show higher values in the case of W31 alone.

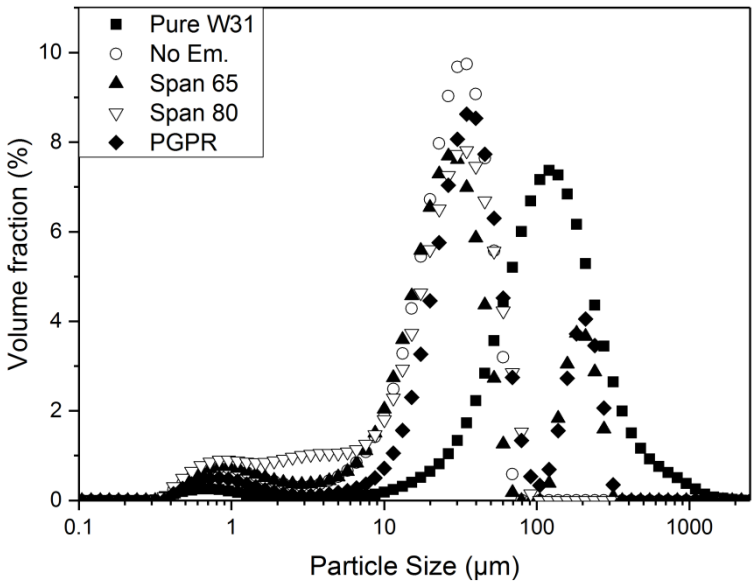

Figure 42 - Comparison between the PSD of pure W31 and emulsion W/O 20/80 sprayed at the same operating conditions

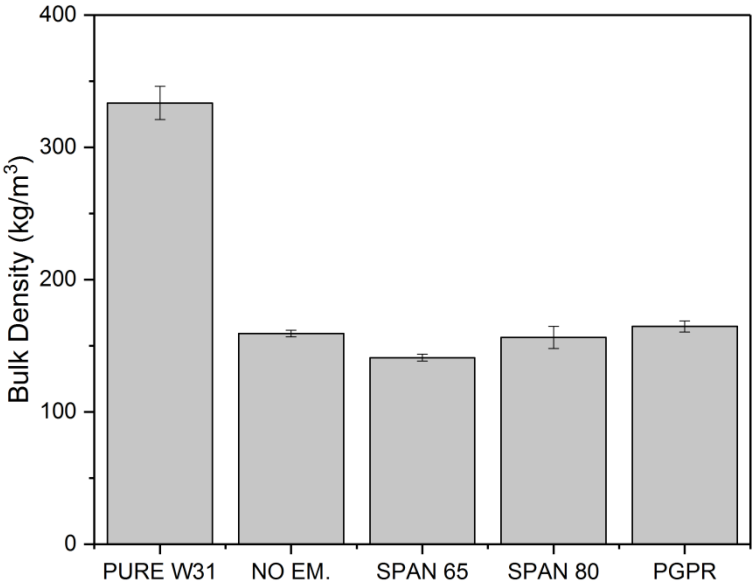

Figure 43 - Comparison between the bulk density of pure W31 and emulsion W/O 20/80 sprayed at the same operating conditions

To prove whether this was the case an energy and mass balance has been applied on the spray tower. To simplify the system under investigation it was assumed that the spray tower is completely isolated from the external environment, i.e. no heat exchange can take place at the walls of the spray tower. This is justified by the presence of heat insulation around the spray tower.

It is possible to calculate and predict how much water would be lost, knowing the spraying conditions (GPR, p, T) and the temperature in the spray tower. At first the energy that CO_2 can provide and that the emulsion requires from the conditions before the nozzle to those after expansion have to be calculated applying the following equations:

$$\mathrm{Q_{CO_2}} = \dot{\mathrm{m}}_{\mathrm{CO_2}}\left(\mathrm{h_{T,p,}}_{CO_2} - \mathrm{h_{T',p',}}_{CO_2}\right) \tag{46}$$

$$\dot{\mathrm{Q}}_{em} = \dot{\mathrm{m}}_{W31}\left[\lambda_{W31} + c_{p,W31}\left(T' - \mathrm{T''}\right)\right] + \dot{\mathrm{m}}_{H_2O}\left(\mathrm{h_{T',p',}}_{H_2O} - \mathrm{h_{T,p,}}_{H_2O}\right) \tag{47}$$

where $\dot{\mathrm{Q}}_{\mathrm{CO_2}}$ is the power that CO_2 can provide by expanding from the condition before the nozzle (T', P') and after (T", p"), $\dot{\mathrm{m}}_{\mathrm{CO_2}}$ is the mass flow of CO_2, h is the enthalpy, $\dot{\mathrm{Q}}_{em}$ is the power required by the emulsion to go from the condition before the nozzle to those after, $\dot{\mathrm{m}}_{W31}$ is the mass flow of W31, λ_{W31} is the enthalpy of fusion of W31, $c_{p,W31}$ is the specific heat capacity of W31, $\dot{\mathrm{m}}_{H_2O}$ is the mass flow of H_2O.

It is then possible to calculate the difference in power and if CO_2 provides insufficient power it is possible to calculate the mass of water that evaporates to provide the missing energy, and from there it is possible to estimate the water content of the capsules with the following equations:

$$\Delta\dot{Q} = \dot{\mathrm{Q}}_{\mathrm{CO_2}} - \dot{\mathrm{Q}}_{em} \tag{48}$$

$$\dot{m}_{H_2O,ev} = \frac{|\Delta\dot{W}|}{\lambda_{H_2O,T''}} \text{ if } \Delta\dot{Q} < 0 \tag{49}$$

$$\dot{m}_{H_2O,caps} = \dot{\mathrm{m}}_{H_2O} - \dot{m}_{H_2O,ev} \tag{50}$$

$$x_{H_2O,caps} = \frac{\dot{m}_{H_2O,caps}}{\dot{m}_{H_2O,caps} + \dot{\mathrm{m}}_{W31}} \tag{51}$$

where $\Delta\dot{Q}$ is the difference in power between CO_2 and the emulsion, $\dot{m}_{H_2O,ev}$ is the mass flow of evaporated water, $\lambda_{H_2O,T''}$ is the enthalpy of evaporation of water at T", $x_{H_2O,caps}$ is the mass fraction of H_2O in the capsules.

The results of this calculations applied to the experiments can be seen in table 26. The predicted results are close to the results of the experiments.

Table 26 - Moisture content calculated vs moisture measured in the capsules

	Moisture content		
I.D.	**Calculated**	**Thermobalance**	**Karl-Fischer**
C1	11.12%	7.21%	6.94%
C2	11.33%	9.24%	8.18%
C3	1.19%	1.86%	1.19%
C4	1.28%	2.05%	1.58%
C5	1.38%	1.95%	1.98%
C6	10.98%	9.63%	11.16%
C7	11.05%	8.96%	7.23%

The same method to calculate the water content was applied to the experiments found on Ilieva [18] and Hanu [17] (fig. 44, 45). The numbers of the experiments correspond to the number indicated in the respective work. The method provided results in good agreement with their experimental observations. The reason why the loading efficiency decreases when decreasing the water content in the sprayed emulsion is well explained. At the same spraying conditions the ratio of cooling required by the fat and the one provided by CO_2 is constant. The missing energy is provided by evaporating water and it is constant too. Therefore, in percentage, more water evaporates when less is present in the emulsion, leading to lower encapsulation efficiencies.

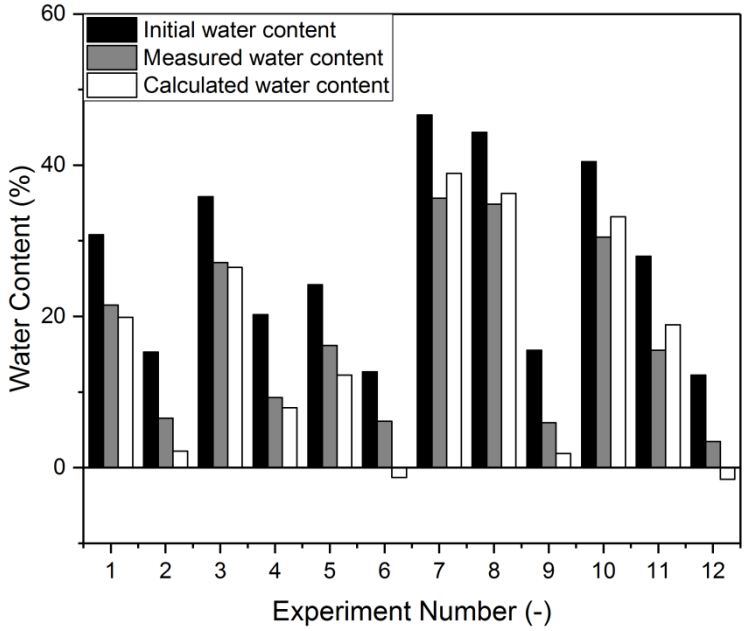

Figure 44 - Water content from Ilieva [18]

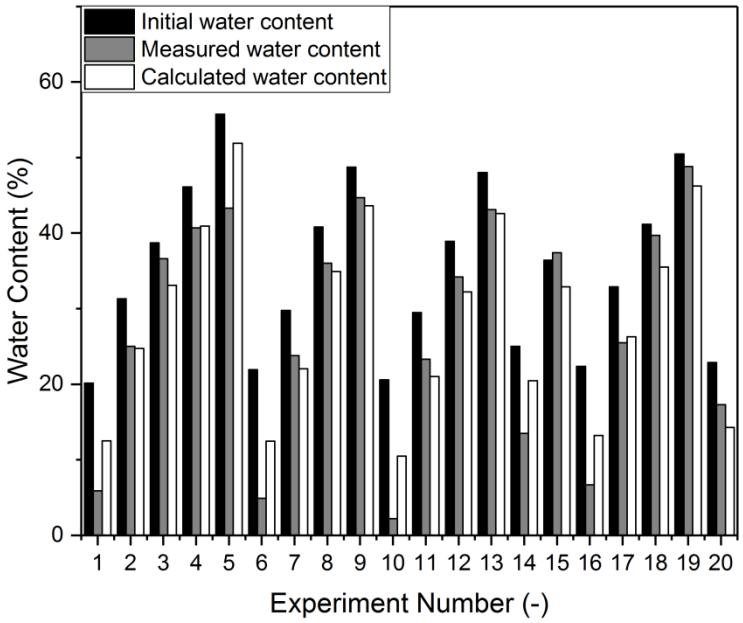

Figure 45 - Water content from Hanu [17]

The method can be improved by knowing the heat exchange with the external environment, which has not been possible to be implemented in this work due to missing information, like ambient temperature or the mass flow taken out by the filter which could bring in air from the outside to the spray tower.

The method shown previously to calculate and predict the water content in the capsules, knowing the initial water content of the emulsion and the spraying conditions, can also be used to evaluate the loading efficiency. The results are shown in fig. 46. The line "prediction" refers to spraying an emulsion of Witepsol W31 and water at average spraying conditions similar to those of the experiments. Therefore the only changing parameter is the mass fraction of water in the emulsion, while the other parameters are kept constant. In particular the temperature before spraying is 60 °C, the pressure before spraying is 50 bar, the GPR is 1.3 and the temperature in the spray tower is 22 °C.

As fig. 46 shows, the calculated values follow the same trend as the experiments, an asymptotic curve closely reaching 100% LE with increasing water content in the emulsion. The LE increases with the initial water content because, at the same spraying conditions, the amount of water that has to evaporate in order to close the energy balance equation is always the same. If the water present in the system is higher, the loss in percentage is lower; therefore higher loading efficiencies can be obtained.

Other possibilities of water loss, like solubilized water in the CO_2 cannot explain this behaviour by themselves. Moreover the maximum amount of solubilized water in CO_2 at the considered spraying conditions is very low, around 0.0055 mol/mol [68].

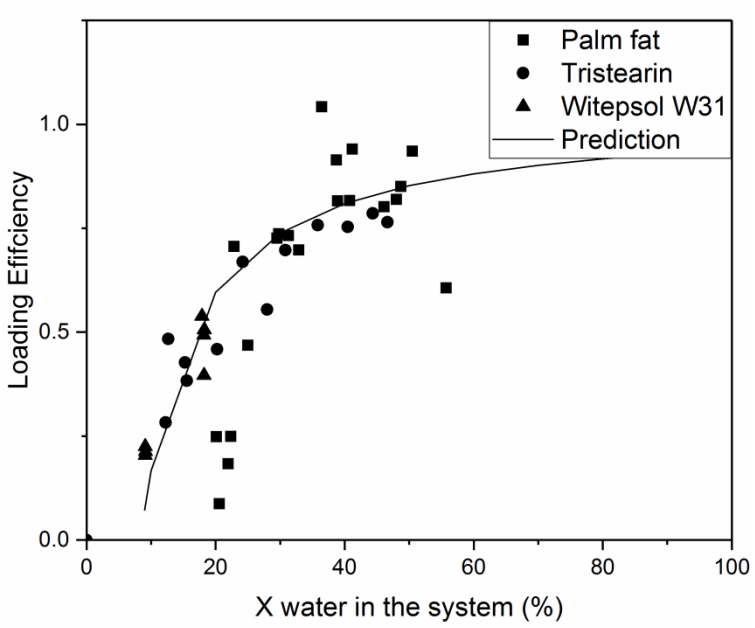

Figure 46 - Mass fraction of water in the emulsion before spraying vs encapsulation efficiency (palm fat = Hanu; tristearin = Ilieva)

7.2.3 - Improving the water loading efficiency

Having identified the possible reason for the loss of water in the PGSS process, four more experiments have been performed to prove experimentally that an increase in CO_2 cooling power has a positive effect on the water loading of the composites. The spraying conditions are summarized in table 27. The core material was distilled water and not a NaCl solution because the focus of these tests was only on the water loading efficiency. The only emulsifier tested was PGPR 4125.

Table 27 - Conditions for experiment C8 to C11.
[a] GPR refers to the ratio of CO_2 and emulsion before the nozzle, the extra CO_2 is not included

I.D.	**W31**	**Emulsifier**		**H_2O**	**T**	**p**	**GPR[a]**	**Extra CO_2**	**$T_{spray\ tower}$**
	Wt. %	**Type**	**Wt. %**	**Wt. %**	**°C**	**bar**	**-**	**kg/min**	**°C**
C8	81	PGPR	4	15	62.0	99.0	3.7	-	16.0
C9	81	PGPR	4	15	61.7	98.3	3.3	-	16.2
C10	81	PGPR	4	15	60.8	52.0	1.1	0.25	18.8
C11	82	PGPR	4	14	61.0	50.3	1.1	0.10	19.4

Two tests were performed at higher pre-expansion pressure than the previous experiments (C8 and C9). The increase in pressure resulted in a higher CO_2 mass flow, due to the layout of the plant, and therefore in an increase in GPR. The other two experiments were conducted at the same pre-expansion condition (60 °C, 50 bar) but an extra source of CO_2 was added directly in the spray tower. This was achieved by connecting a bottle of CO_2 to the spray tower. The bottle was positioned on a scale to monitor the mass flow of the CO_2. The CO_2 contained in the bottle was at room temperature and at 50 bar. The mass

flow of the extra CO_2 was 0.25 kg/min and 0.1 kg/min, respectively for experiment C10 and C11.

The results on the water content are collected in table 28.

Table 28 - Comparison between moisture content of emulsion, calculated and measured by Karl Fischer titration

	Moisture content		
I.D.	**Emulsion**	**Calculated**	**Karl-Fischer**
C8	15.44%	14.73%	11.18%
C9	14.72%	13.62%	10.19%
C10	15.39%	13.24%	11.59%
C11	13.93%	7.84%	8.58%

It can be observed that the water content measured via Karl-Fischer titration is higher than the previous test, even if the mass fraction of H_2O in the emulsion is lower than experiments C1, C2, C6 and C7. This seems to be in contradiction with the previous observation made in this work and [17,18], where higher loading efficiencies were obtained by increasing the water content of the emulsion (figure 45). The explanation is that an increase in CO_2 cooling power due to higher GPR or by adding an extra source directly in the spray tower has a beneficial effect on the water loading. This could be easily predicted by looking at Eq. 48 and 49. The only way to decrease $|\Delta\dot{Q}|$ is by increasing $\dot{Q}_{CO_2}$, since it is the only component on which it is possible to act. As extra proof, it is interesting to note that in experiment C10 and C11 the different mass flow from the bottle of CO_2 affects the water content of the composites, resulting in a lower value in experiment C11, where the mass flow was lower, therefore lower $\dot{Q}_{CO_2}$.

Nevertheless intervening in such way has its effect not only on the water loading but also on the other characteristics of the composites. Table 29 collects the bulk density of the obtained composites and fig. 47 shows the morphology of the produced microcomposites.

The bulk density is lower in the experiments where the pressure was increased. This is in agreement with what was observed in the experiment with pure W31 and as demonstrated by various authors who worked with the PGSS process [11–13,17,18,26]. The extra source of CO_2 does not affect the bulk density as drastically, having values in line with the experiments performed at the same conditions but without an extra source of CO_2.

Table 29 - Bulk density of the experiments C8-C11

Experiment I.D.	**Bulk density (kg/m3)**	**Standard deviation (kg/m3)**
C8	74.1	3.9
C9	68.7	0.6
C10	145.7	1.1
C11	155.1	5.1

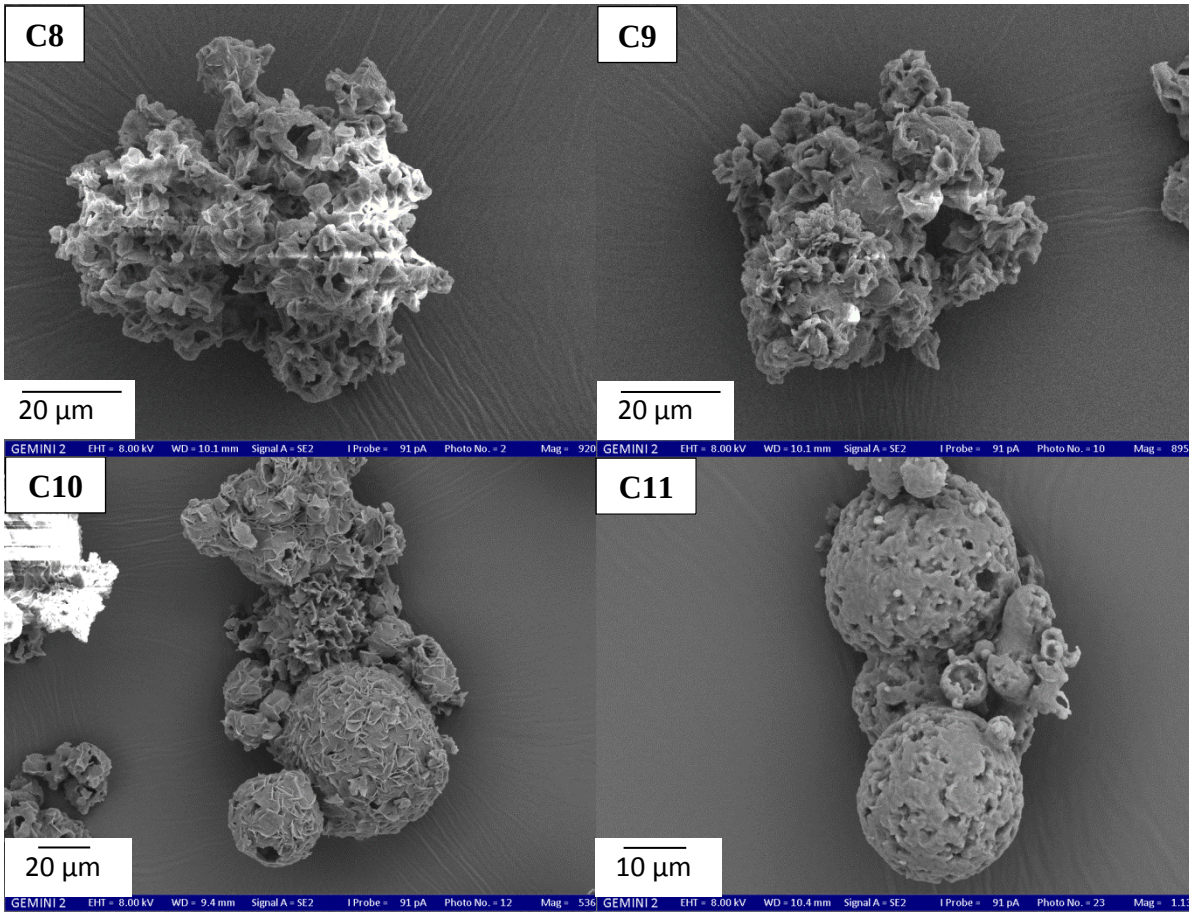

Figure 47 - Morphology of experiments C8-C11

The changes in spraying conditions are also affecting the morphology of the obtained composites. When the pre-expansion pressure is 100 bar, the capsules are less spherical. The cooling is faster due to the higher amount of CO_2 and the lower temperatures in the spray tower, which leads to a fast solidification of the liquid droplets in non-spherical form. The extra source of CO_2 does not seem to interfere in any meaningful way with the solidification of the fat, a sign that the particle shape is not as affected by the quantity of CO_2. This is visible when comparing experiment C8 and C9 with experiment C10, where the same amount of CO_2 is introduced in the spray tower, but in different ways. The particles do not assume the same shape but the water content is similar (figure 47).

7.2.4 - Sensitivity analysis on water loading efficiency of various parameters

By applying the eq. 46 to 51 it is possible to study the effect of different parameters on the water loading efficiency. The parameters taken in consideration are water content of the emulsion (fig. 46), pre-expansion temperature, pre-expansion pressure, temperature in the spray tower and GPR.

The appointed baseline conditions are similar to the one chosen for the experimental tests and only one parameter is changed per sensitivity analysis. When they are not changed, the parameters have the values collected in table 30.

Table 30 - Baseline conditions

Parameter	Value	Unit
Emulsion water content	20	Mass %
Pre-expansion temperature	60	°C
Pre-expansion pressure	50	bar
Temperature in the spray tower	22	°C
GPR	1.3	-

The first parameter taken in consideration is the temperature before spraying. The temperature has been changed between 40 and 130 °C while all the others parameters were left untouched. The results are collected in fig. 48. An increase in spraying temperature results in a decrease of water content in the capsules and therefore of loading efficiency. Higher difference in T between pre and post expansion means higher energy required to cool down and solidify the emulsion. Moreover particular attention has to be paid to the CO_2. At the conditions taken in consideration, from a pre-expansion T of 70 °C and forward, the enthalpy of CO_2 after expansion is lower than before expansion. This results in the CO_2 having a negative impact in the encapsulation of water, because in order to reduce its enthalpy has to release energy and the water balances the system by evaporating even more.

In fig. 49 the effect of the pre-expansion pressure in regard to the capsules water content and the loading efficiency is shown. The pressure has been changed between 40 and 130 bar while all the others parameters correspond to the baseline condition. By increasing the pre-expansion pressure the energy that the emulsion has to release in order to cool down and solidify slightly increases but the energy that the CO_2 can absorb vastly increments. It can be easily seen in a TS diagram for CO_2 that the enthalpy of CO_2 at spray tower conditions is much higher than at pre-expansion conditions, therefore it can take more of the energy released during the production of the capsules and less water has to evaporate. Increasing the pre-expansion P has a positive impact on the final water content of the capsules and therefore on the loading efficiency. This was also shown in experiment C8 and C9, but in the experiments an increase in pressure also brings to an increase in GPR and it was not possible to evaluate the effect of each individually.

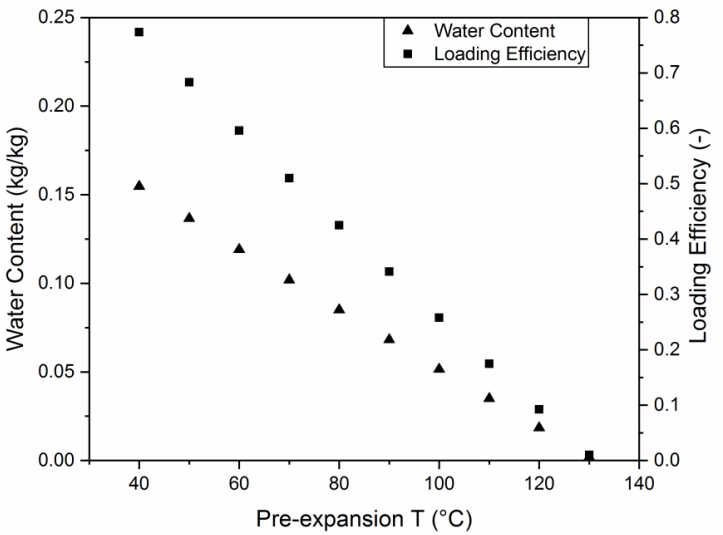

Figure 48 - Effect of the pre-expansion T on capsules water content and loading efficiency

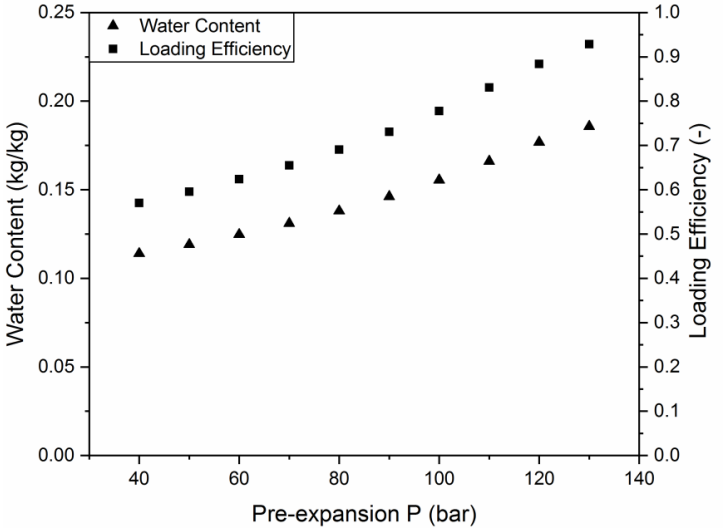

Figure 49 - Effect of the pre-expansion P on capsules water content and loading efficiency

The GPR was varied between 0.1 and 15 (figure 50). As expected from the previously performed experiments, increasing the GPR increases the capsules water content and the loading efficiency. The Δh of CO_2 is constant because it depends on the pressure and temperature before and after the expansion, but by increasing the amount of CO_2 it increases also the power that can be taken up. Of course, this is only valid when the Δh of CO_2 is positive. If it was negative, meaning that the enthalpy of CO_2 in the spray tower was lower than the enthalpy of CO_2 before the nozzle, an increase of mass flow of CO_2 would be detrimental to the final water content of the capsules.

At last the effect of the spray tower temperature is studied. The temperature was varied from 14 to 32 °C. The effect is slightly beneficial as it can be seen in fig. 51.

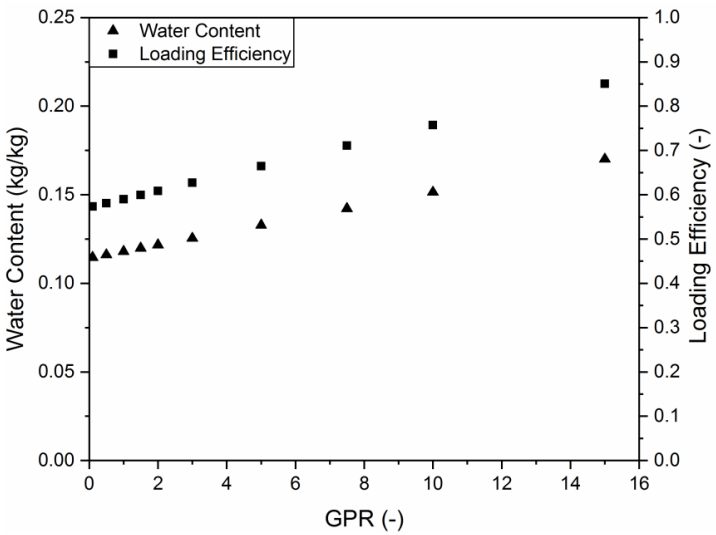

Figure 50 - Effect of the GPR on capsules water content and loading efficiency

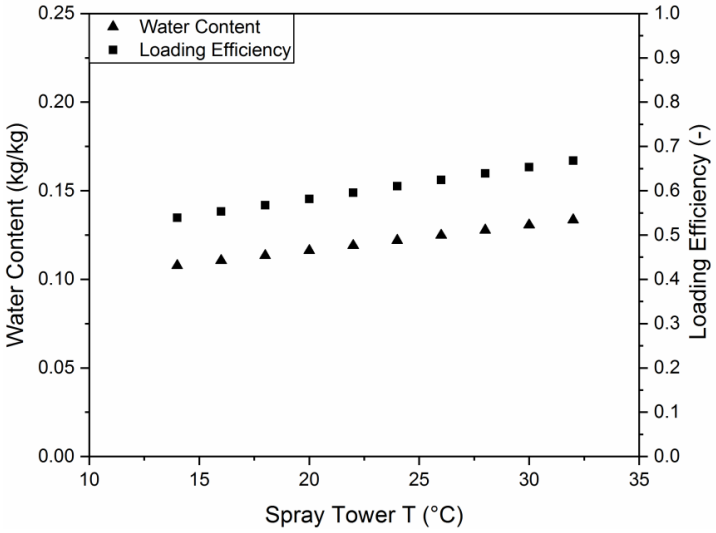

Figure 51 - Effect of the spray tower T on capsules water content and loading efficiency

An increase of spray tower T means a decrease of the energy necessary to cool down and solidify and this is why the water content and the loading efficiency are slightly improved. Practically it is necessary to pay attention on how high the T in the spray tower is. It has to be lower than the solidification point of the shell material. Moreover higher spray tower T can be detrimental to the formation of single capsules, because with less driving force the solidification takes longer and there is the risk to not obtain full formed capsules while the droplets are falling to the bottom of the spray tower. If the droplets are still partially liquid when reaching the bottom it increases the chances of agglomeration, reducing the number of capsules and increasing the chances to obtain non-spherical capsules [11].

In conclusion these analyses confirm what was experimentally observed: increasing GPR and/or the pressure has a beneficial impact on the loading efficiency and the water content of the capsules. The eq. 46 to 51 can be used as a preliminary tool to identify the appropriate range of spraying conditions in order to achieve certain moisture content.

8 Economic evaluation

An economic evaluation of a PGSS plant for the production of W/O microcomposites has been performed to study the economic feasibility of such a plant. The knowledge acquired from this works and previous works [13,17,18] has been used to achieve this objective.
A plant for the production of 10 t/day of capsules has been taken into consideration. It has been assumed that the yield is 100%, as first estimation. This value is not far away from reality; the work of Münüklü [13] showed that a yield of 98% is easily achieved.

8.1 - Method for economic evaluation

The method firstly introduced by Douglas [19] for the economic evaluation of chemical plants was employed to make an economic evaluation of a PGSS plant for the production of W/O microcomposites.
This method uses a hierarchical approach. At first a simple evaluation of the mass streams is performed. Subsequently the various operational units of the plant have been identified. It has been chosen that the storage of the raw materials and of the finished products is Out Side Battery Limits (OSBL) while only the plant is In Side Battery Limits (ISBL). This distinction is necessary for the subsequent sizing and evaluation of the cost of the equipment necessary to run a PGSS plant.

8.2 - Design conditions

The design of the plant has been developed around the spray tower, which is the equipment around which the mass flow of CO_2 has to be evaluated. The idea behind this choice is that, in order to have a 100% L.E., enough CO_2 has to be provided to completely solidify the capsules and reach the desired spray tower temperature. The pre-expansions conditions have been chosen as 40 °C, in order to guarantee molten W31, and 80 bar, an average pressure value amid the operating conditions of a PGSS plant for the production of W/O composites. The conditions inside the spray tower have been assumed at 25 °C, room temperature, and atmospheric pressure.
By knowing the operating conditions before and after the expansion and the mass flow of the W31 and H_2O it is possible to calculate the required amount of CO_2 by solving eq. 46 in respect to the mass flow of CO_2, aiming for an isenthalpic process.
For the design conditions taken in consideration the mass flow of CO_2 is around 62 kg/h, which correspond to a GPR of 1.5.
Once the mass flows are identified it is possible to proceed to the evaluation of the equipment and perform the economical evaluation.

8.3 - Process flow diagram

The PGSS plant chosen for the economic evaluation is a continuous PGSS plant with mixing of the core and shell material in a static mixer positioned before the spray tower. CO_2 is admixed at the static mixer as well. This setup was chosen because it is the one that requires less equipment compared to the other option of premixing the shell and the core material and forming an emulsion. Comparing the results, no real benefit, in terms of L.E., is obtained by using a premixed emulsion over a static mixer as the comparison of the results of the experiments of this work and Hanu and Ilieva's has demonstrated [17,18].

The process flow diagram (PFD) of the plant is shown in figure 52.

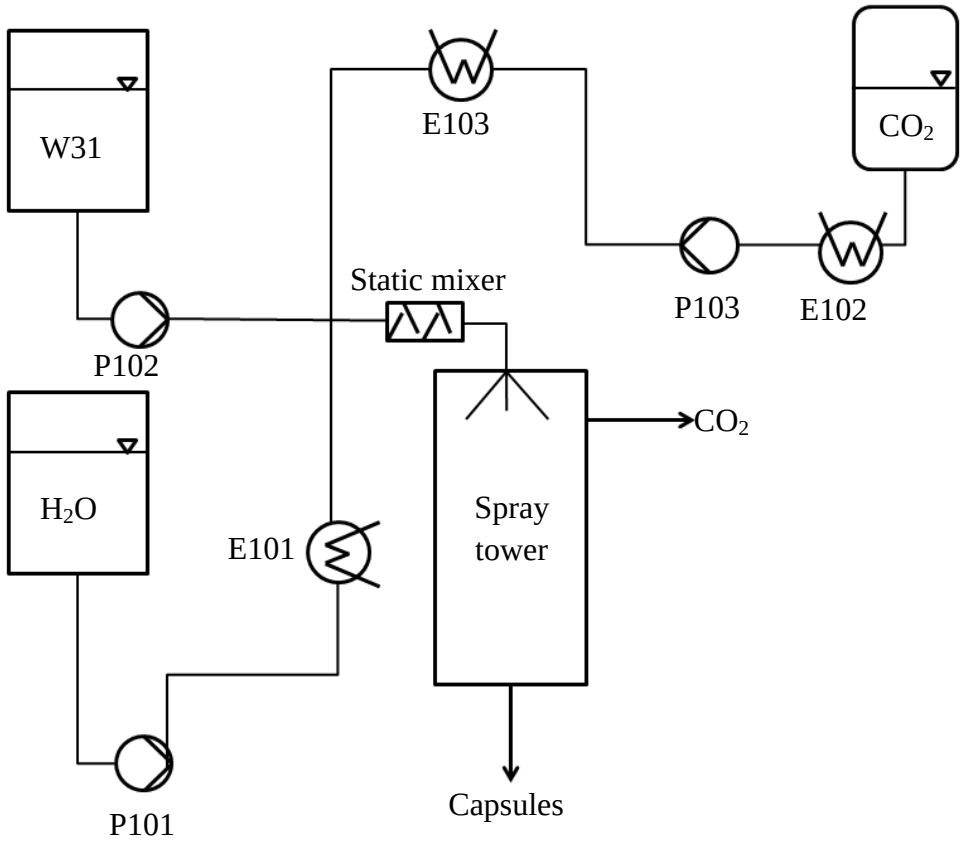

Figure 52 - PFD of the plant for the economical evaluation

8.3.1 - Water side

Water is assumed to come out of a tank at a temperature of 15 °C and atmospheric pressure. It has to be pressurized and heated up at the operating conditions of the plant. A reciprocating pump (P101) is used to reach the pressure of 80 bar and subsequently it

enters a shell-and-tube heat exchanger (E101) to reach the desired temperature of 40 °C. The heat exchange medium chosen is Marlotherm SH (Sasol, Germany).

8.3.2 - W31 side

Molten Witepsol W31 is assumed to come from a heated tank at the operating temperature. It is only required to reach the operating pressure. This is achieved by a reciprocating pump (P102).

8.3.3 - CO_2 side

Liquid CO_2 is taken by a tank kept at a constant temperature of 15 °C. The equilibrium pressure inside the tank at this temperature is 51 bar. It is sub-cooled to 0 °C in a shell and tube heat exchanger (E102) where Kryo 51 (Lauda, Germany) is used as cooling medium. Sub-cooling is necessary to prevent cavitation in the subsequent pump used to reach the desired pressure. The chosen pump is of the reciprocating type (P103).The pressurized CO_2 enters another shell and tube heat exchanger (E103) to reach the operating temperature of the system.

8.3.4 - Mixing and expansion

The three streams of the materials enter in a static mixer where an emulsion is formed [18,77] and CO_2 dissolves in the shell material. The mixed stream is expanded in an expansion vessel (6.9 m^3) where the composites are recovered. CO_2 is sent to a filter to remove the smaller particles (OSBL) and released in the atmosphere.

8.4 - Equipment design and sizing

The equipment design and sizing was based on the stream conditions firstly identified once the PFD was established.

For the pumps the power that they should provide was calculated by an energy balance between the stream conditions in and out. It was assumed an isentropic efficiency of 0.7 for safety reasons.

For the sizing of the heat exchangers the method proposed by Sinnot [78] was employed. The power to be provided for heating the stream (or removing in case of cooling) is calculated by an energy balance of the stream in and out. Once it is known, it is possible to calculate the heat transfer area required (A) from:

$$\dot{Q} = UA\Delta T_{ln} \tag{50}$$

where $\dot{Q}$ is the power (W), A is the heat transfer area (m^2) and U is the overall heat transfer coefficient (J/s K m^2). U is at first determined by qualified guessing. The sizing of the heat exchanger is chosen (length of pipes, length of shell, number of passes, etc…) to have the same area as calculated. The overall heat transfer coefficient is calculated by

the transfer coefficient on each side (shell and pipes) and if the value obtained is close to the guessed U the heat exchanger is sized. If not the value of U is changed and the sizing continues iteratively.

Table 31 - Design and sizing of the required equipment for the plant

ID	ITEM	Conditions (Design) P (bar)	T(°C)	TYPE	SIZE
P101	Water pump	1 to 80	15	Reciprocating Pump	Power = 0.26KW
P102	W31 pump	1 to 80	40	Reciprocating Pump	Power = 1.1 KW
P103	CO_2 pump	51 to 80	10	Reciprocating Pump	Power = 1.5 KW
E101	Heater H_2O	80	15 to 40	Shell and Tube Double pass	A = 0.17 m^2 L = 1.5 m Duty = 3.6 KW # pipes = 6
E102	Cooler CO_2	51	15 to 0	Shell and Tube Double pass	A = 0.74 m2 L = 1 m Duty = 13.7 KW # pipes = 40
E103	Heater CO_2	80	0 to 40	Shell and Tube Double pass	A = 1.94 m^2 L = 1 m Duty = 65.3 KW # pipes = 104
Spray Tower	Spray Tower	1	25	Cylinder	V = 0.69 m^3 L = 3.24 m Ø = 1.62 m

8.5 - Economic evaluation

An estimation of the total capital investment and of the added production costs per ton of capsules produced was performed following the methods suggested in Douglas [19] and Peters et al. [79].

The chosen method for the estimation of the total capital investment was the one based on the percentage of delivered-equipment cost. This method requires estimating the cost of the equipment of the plant and then the total capital investment is calculated as percentage from the delivered-equipment cost. The total capital investment is the sum of the direct costs, the indirect costs and the working capital. In table 32 the components that are part of these costs and the percentage relative to the delivered-equipment costs are tabulated.

The type of plant chosen was the “fluid processing plant” because even if the plant deals with both fluids (from the pumping to the spray tower) and solids (capsules produced inside the spray tower), the “fluid processing plant” has the highest multipliers, therefore no costs is underestimated in this evaluation [79].

Table 32 - Components of total capital investment and their relative percentage of delivered-equipment [79]

	PERCENTAGE OF DELIVERED-EQUIPMENT COST FOR		
	Solid Processing plant	***Solid-Fluid Processing plant***	***Fluid Processing plant***
Direct Costs			
Purchased equipment delivered	100	100	100
Purchased equipment installation	45	39	47
Instrumentation and controls (installed)	18	26	36
Piping (installed)	16	31	68
Electrical Systems (installed)	10	10	11
Building (including services)	25	29	18
Yard improvements	15	12	10
Service facilities	40	55	70
Total direct plant cost	269	302	360
Indirect Costs			
Engineering and Supervision	33	32	33
Construction expenses	39	34	41
Legal expenses	4	4	4
Contractor's fee	17	19	22
Contingency	35	37	44
Total indirect plant cost	128	126	144
Fixed-capital investment	397	428	504
Working capital (around 15% of total capital investment)	70	75	89
Total Capital investment	467	503	593

8.5.1 - Estimation of the delivered-equipment cost

The cost of the equipment was evaluated from the data present in Peters et al. [79]. In the book all the equipment costs, as of the year of publication or edition, are collected in figures where the purchased cost of the equipment depends on a characteristic of the

equipment. For example for a pump the cost depends on the capacity required, for a heat exchanger on the surface area. Depending on the type or the material different lines are present in these graphs.

The present cost can be calculated from the following equation:

$$Present\ cost = original\ cost \left(\frac{CEPCI_{present\ time}}{CEPCI_{reference\ time}}\right) \cdot CF_p \quad (52)$$

where CF_p refers to a correction factor due to the pressure range of the equipment. CEPCI is an acronym for Chemical Engineering Plant Cost Index. It is been first introduced in 1963 and it is used to update the costs to the present knowing the cost in a certain past period of time.

Table 33 - CEPCI used in this work

Year	**CEPCI**	**Reference**
2002	390.4	[79]
2016	541.7	[80]

In table 34 the estimated cost of the equipment taken in consideration for the plant is shown. Due to the low pressure required (80 bar) the cost of the pump is limited. If this goes up to 250/300 bar the price would increase around 10 times.

Table 34 - Cost estimation of the delivered-equipment

ID	**ITEM**	**Estimated cost (k€)**
P101	Water pump	5.5
P102	W31 pump	5.5
P103	CO_2 pump	7.0
E101	Heater H_2O	1.5
E102	Cooler CO_2	3.6
E103	Heater CO_2	6.4
Static Mixer	Static Mixer	10.0
Spray Tower	Spray Tower	9.2

8.5.2 - Estimation of the total capital investment

The fixed capital investment is twice the sum of the total direct and indirect plant costs because it has been considered that the plant is constructed anew at an undeveloped site, which brings to an increase of 100% compared to the construction of an equivalent plant in a pre-existing plant [79]. The start-up cost was estimated with 9% of the total capital investment.

8.5.3 - Estimation of the total production cost

The total production cost is defined as the sum of the manufacturing cost and the general expenses [19,79]. For the purpose of this work the general expenses has not been considered, because they are a percentage of the sale revenues which are beyond the purpose of this work.

The manufacturing cost can be calculated by the sum of three components:

- Direct production cost;
- Fixed charges;
- Plant overhead cost.

Table 35 - Breakdown of the total capital investment parameters

Direct Costs	**(k€)**
Purchased equipment delivered	48.7
Purchased-Equipment installation	22.9
Instrumentatiuon and controls (installed)	17.5
Piping (installed)	33.1
Electrical Systems (installed)	5.4
Building (including services)	8.8
Yard improvements	4.9
Service facilities	34.1
Total direct plant cost	175.3
Indirect Costs	
Engineering and Supervision	16.1
Construction expenses	20.0
Legal expenses	1.9
Contractor's fee	10.7
Contingency	21.4
Total indirect plant cost	70.1
Fixed-capital investment	490.8
Start-up Cost	5.4
Working capital (15% of total capital investment)	86.7
Total Capital investment	582.9

The direct production cost includes the cost of raw materials, operating labour, supervision, patents and royalties and in general everything connected directly to the production. This includes the utilities. For simplicity the utilities are calculated only as electricity. This is a method suggested by Douglas [19] to make it easier to evaluate them. Therefore the cost of utilities like Marlotherm or Cryo 51 are considered as the equivalent value by using thermodynamics, i.e the cost of the mass flow of Marlotherm in a heat-exchanger is compared to the cost of the electricity to provide the same power as Marlotherm. In order to not underestimate the cost of the utilities the power necessary for the heat exchangers has been multiplied by a safety factor of 1.5.

Fixed charges includes the capital charges, calculated as the fixed capital investment divided by the economic plant life assumed as 12 years [13], the local taxes, and the insurance. The last two components can be calculated as a percentage of the fixed capital investment. The percentage value for local taxes and insurance in this work has been assumed as 2 % and 1 % respectively [79]. The plant overhead cost include the general plant upkeep and overhead, payroll overhead, packaging, medical services, safety and protection, restaurants, recreation and more and can be calculated as about 50 - 70 % of the cost of operating labour, supervision and maintenance or 5 - 15 % of total product cost [79]. In this work it has been chosen to consider them as 60 % of the cost of operating labour, supervision and maintenance. The operating labour was evaluated by using the diagram of operating labour for chemical process industries (fig. 53) from which it is possible to correlate the plant capacity to the employee-hour per day per processing step (E.H.). For the plant in consideration three processing steps were identified (pumping, heating, powderisation). The average wage per hour was assumed to be of 15 €/h. By knowing this information the operating labour (O.L.) was calculated as:

$$O.L. = E.H. * days\ per\ year * process\ steps \tag{53}$$

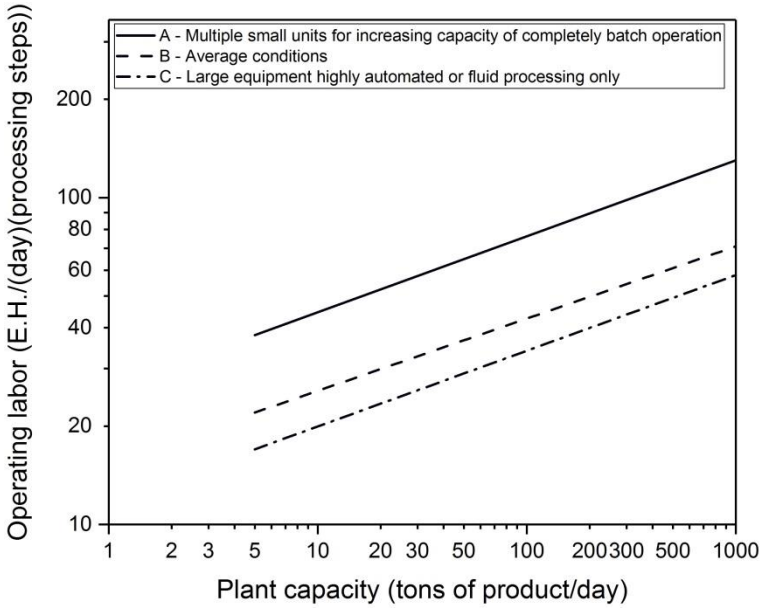

Figure 53 - Operating labour requirements for chemical process industries. Modified from [79]

In table 36 the breakdown of the total production cost and the added unit cost is tabulated.

The total added cost for the capsules production is then 1.63 €/kg.

Table 36 - Breakdown of the cost for the estimation of total product cost and total added cost per unit

Item	Annual cost (k€)
Direct production cost	
W31 + H_2O	12006
CO_2	3308
Utilities	29
Maintenance and repairs	34
Operating supplies	5
Patents & royalties	676
Operating labor	378
Supervision	57
Laboratory charges	57
Fixed charges	
Capital charges	49
Local taxes	10
Insurance	5
Plant overhead	281
Total product cost	16893
Total added cost per unit	1.63 €/kg

8.6 - Sensitivity analysis

A sensitivity analysis was performed to evaluate the total added cost for increasing production, up to 100 ton/day. The equipment, and therefore the total direct plant cost, was scaled up by applying the six-tenth rule, which states that as the size increases the cost increase by a factor of six-tenth according to equation 54 [81].

$$\frac{cost_1}{cost_2} = \left(\frac{size_1}{size_2}\right)^{0.6} \tag{54}$$

Total indirect cost, working capital and start-up cost increase proportionally in percentage respect to the total capital investment. Raw materials and utilities cost increase proportionally to the production rate, i.e. it doubles when the production rate is of 20 ton/day. Maintenance and repair, operating supplies, patents and royalties and laboratory charges increase proportionally, in percentage, with the direct production cost. Operating labour is recalculated by changing the employee-hour per day per processing step, accordingly to the production rate. The cost for the supervision is kept constant. The capital charges, local taxes and insurance were calculated as usual.

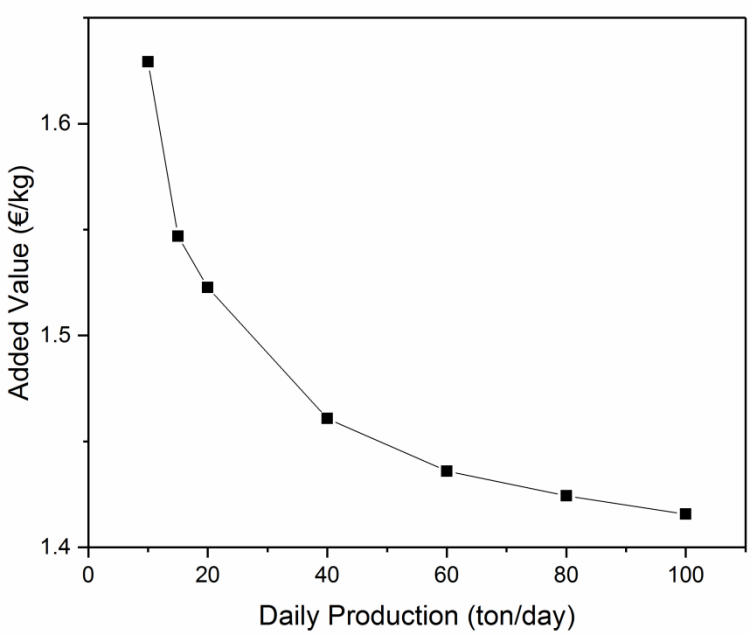

Figure 54 - Sensitivity analysis per production rate

In fig. 54 the total added cost value is plotted versus the daily production. It can be observed that the cost decreases by increasing the production rate.

8.7 - Improving the process

The term that most influences the added cost value is the cost of CO_2. It is possible to reduce the quantity consumed per day by recycling part of it. After the expansion the CO_2 is filtered to remove the smallest particles that it could take away with it, compressed and cooled down. It is then pumped and heated at the operating conditions, mixed with fresh CO_2, necessary to guarantee the correct GPR, and the process goes as usual.

The recovery of CO_2 results in an increase in capital investment due to the presence of new equipment, namely a compressor, heat exchangers and a vessel where to store the CO_2 to be recycled. The external CO_2 is mixed with the liquid CO_2 coming from this vessel after being compressed to the same pressure as the fresh CO_2. The mixed streams of CO_2 are then compressed to the operative pressure and heated to the desired temperature, so the CO_2 line is similar to the line with no recycle.

For the purpose of economical evaluation it was assumed that 90% of CO_2 was recycled.

The plant is shown in figure 55. A two stage compressor with a cooler is necessary to bring the recycled CO_2 from 1 bar, pressure after expansion, to 20 bar. It is then cooled and condensed. Due to the high quantity of condensation enthalpy, two separate heat exchangers are present, one for cooling down the recycled CO_2 and one for the condensation. CO_2 is then stored in a vessel from which the necessary amount is pumped to mix with fresh CO_2 and the cycle starts over.

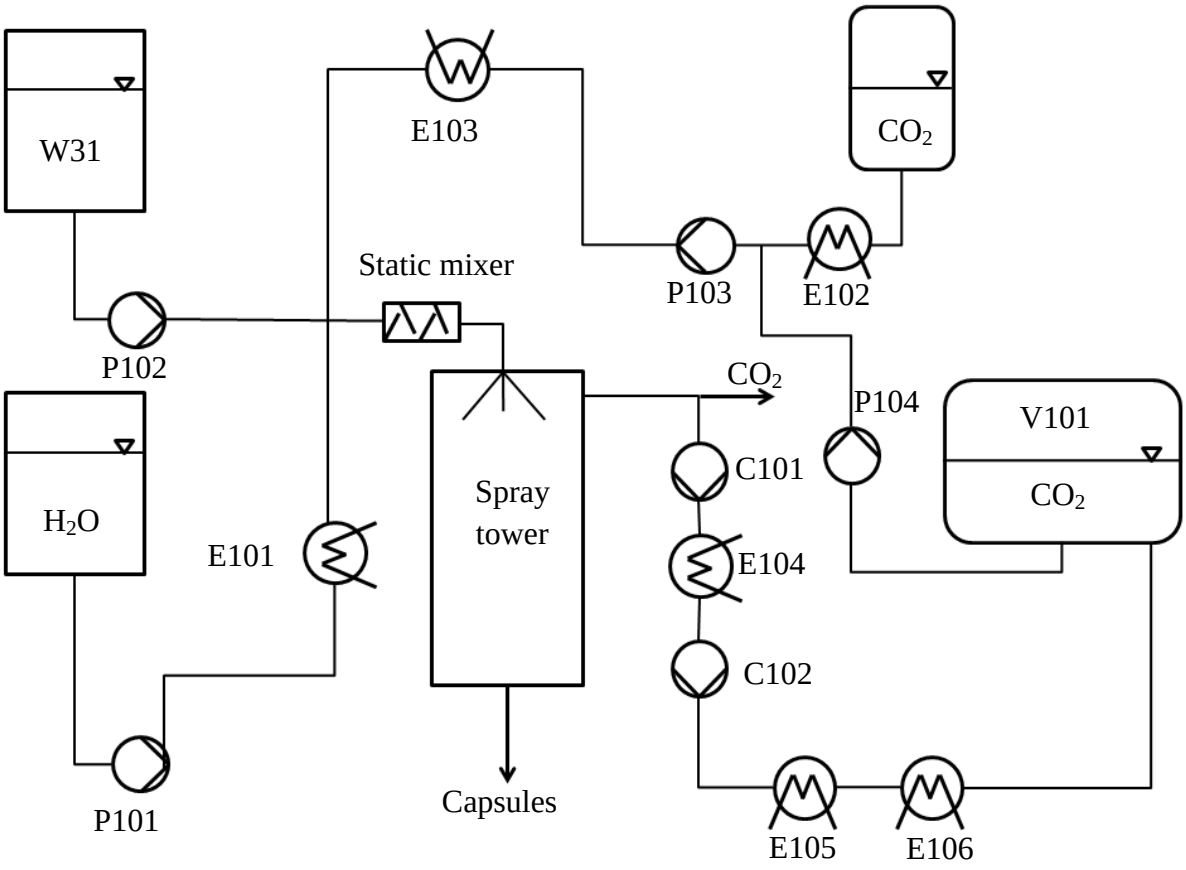

Figure 55 - PFD of the plant for the economical evaluation with recycle

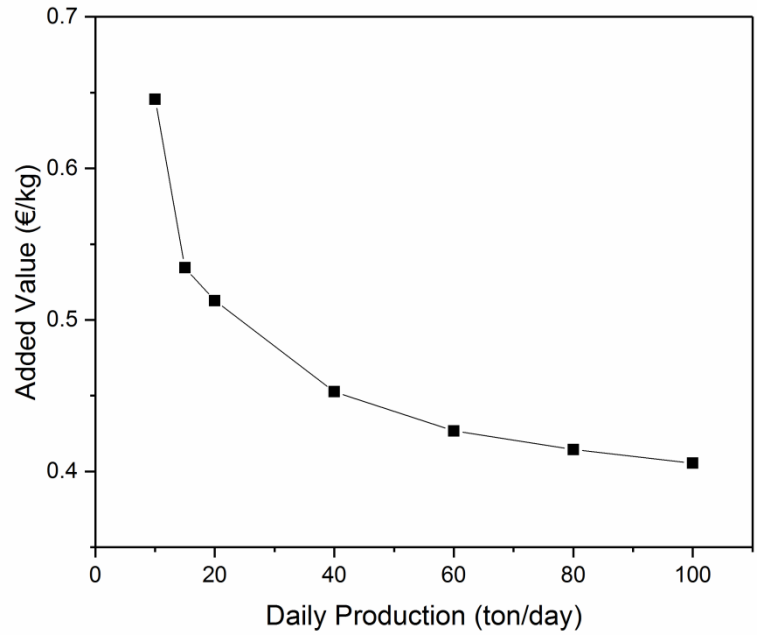

Figure 56 - Sensitivity analysis for a PGSS plant with 90% recycle of CO_2

The equipment sizing and the breakdown for the total capital investment and the added value cost are collected in annex D. The sensitivity analysis is shown in figure 56.

It can be observed how the added value cost decreases in comparison to a plant with no recycle even if a mayor increase in the total capital investment is necessary. By recycling, the cost of CO_2 is reduced by 10 times and since CO_2 was the cost with the most influence on the added unit cost this is of great inflence.

The added unit cost ranges from 0.65 €/kg for a production of 10 ton/say to 0.41 €/kg for a production of 100 ton/day.

Refining the plant for the production of capsules by including a cyclone and filters to make sure that no capsule enters the recycle stream of CO_2, the purchased equipment delivered cost is increased of around 20 k€ (compared to table 58 in Annex D), which brings the total capital investment in the order of 1.1 M€.

This does not affect the total added cost per unit, which slightly increases from 0.65 €/kg to 0.66 €/kg. By increasing the production this effect is practically nullified: for a production of 100 ton/day the added unit cost is still 0.41 €/kg.

9 Conclusions and outlooks

Microencapsulation is a technology useful to increase the shelf life, to improve stability and to control the release of the encapsulated active compounds. In addition, powderous composites are easy to handle and to add for specific application. Various types of active compounds can be encapsulated, including aromas, vitamins and proteins.
Different encapsulation techniques are available. In the last decades particular attention has been paid to supercritical fluids and high pressure processes. In particular, supercritical or compressed CO_2 has been proven as a promising alternative to the various solvents usually employed in encapsulation techniques, with the advantage of being a GRAS (**G**enerally **R**ecognized **A**s **S**afe) component and helping in producing solvent–free capsules.

In this work the **P**articles from **G**as **S**aturated **S**olutions (PGSS) has been employed to manufacture water-filled capsules.
Over the last years, PGSS has been successfully used for the micronisation of various substances, as well as for the generation of capsules, with tailor-made characteristics, such as particle size or morphology.

The goal of the present work was to produce water-filled capsules and to improve the overall state of knowledge on the encapsulation process. Previous studies demonstrated the generation of water-filled capsules but little was known about the loading efficiency and the process.

In order to provide an answer to this question, a system composed by Witepsol W31, H_2O, NaCl and CO_2 was studied. Witepsol W31 is a lipid with melting point of 35-37 °C which is composed by a mixture of mainly triglycerides, diglycerides and monoglycerides. A solution of 9% w/w NaCl in H_2O was chosen as core material. It allowed studying both the loading efficiency of H_2O, i.e. the percentage of the sprayed H_2O present in the capsules, and the encapsulation efficiency of NaCl, i.e. the percentage of sprayed NaCl encapsulated in the capsules. NaCl was chosen mainly as a tracer, but it might be of relevance in food industry in an encapsulated form. In addition, emulsifiers were studied.

Before the encapsulation process, the phase equilibrium of W31 and CO_2 was studied. The measurements took place in a high pressure viewing cell with variable volume. A static-analytical method was employed. The parameters were modified from 50 to 80 °C and from 50 to 150 bar, corresponding to the required range for the system under study. As typical for lipids, the solubility of one component into the other increased by increasing the pressure and decreased by increasing temperature. The solubility of CO_2 into W31 is very high, while only a small quantity of W31 is solubilized in CO_2. The phase equilibria were modelled with the Group Contribution Equation of State (GCEoS), firstly introduced by Skjold-Jørgensen in 1984. The modelling was successful, despite the

use of a substance like Witepsol W31, which is a mixture, not a pure substance. GCEoS can be easily applied to a variety of substances and in case of lipids or mixture of lipids it works very well. It did not require any parametrization, but the definition of the properties of each substance under study, e.g. molecular weight, critical diameter and critical temperature. When not available in literature or when dealing with mixture of lipids, the parameters were obtained by use of graphs after having defined a pseudo-component to describe the lipid mixture. The use of GCEoS is recommended as a primary choice for modelling such systems. The GCEoS was also applied for studying the phase equilibria of the W31-CO_2-H_2O system. It confirmed that the amount of H_2O that would be lost due to solubilisation into CO_2 would be minimal.

Before spraying with the PGSS process, a study on the effect of the emulsifiers on both encapsulation efficiency and release patterns had been performed. The experiments utilized the melt dispersion technique (MDT), which required the generation of a double emulsion to form capsules. Span 65, Span 80, Tween 80 and PGPR 4125 were selected as emulsifiers, at a 1% or 5% w/w concentration with respect to the shell material. The hydrophilic emulsifier (Tween 80) confirmed to be the worst for encapsulating. The best encapsulation efficiency was obtained with PGPR 4125 at 5% w/w concentration. The possible explanation is provided by Moglia et al. [51]: the -OH groups act as hydrogen donors and when present in the lipophilic tail, as in the case of PGPR, they increase the stabilization at the water/oil interface. Since it is not possible to know a priori which emulsifier is ideal in a system, the aforementioned tests are crucial. PGPR 4125 was also the emulsifier which provided the slowest release of NaCl over time. This was confirmed when an enhanced yellow fluorescent protein was added into the capsules and they were analysed with a microscopy technique combined with high speed image acquisition and laser induced heating.

The PGSS process was firstly employed to generate powder of pure Witepsol W31, since no information was available on it. A total of 15 experiments were carried out modifying the temperature from 50 to 80 °C and the pressure from 50 to 100 bar. Three different sized nozzles were also studied. As in the case of the phase equilibria measurements Witepsol W31 behaved as a normal lipid when undergoing spraying with high pressure CO_2, i.e. lower bulk density and smaller particle sizes at higher GPR (gas to product ratio). As noted in previous works, the experimental amount of CO_2 could be inferior to the calculated one from mass and energy balances in order to obtain powder. In this work the ratio between the power provided by the CO_2 and the one required to solidify the sprayed Witepsol W31 was calculated and correlated to the bulk density. The lower the ratio the higher is the bulk density of the powder, which also means more spherical and bigger particles.

A total of seven experiments were carried out for the capsule generation. An emulsion of W31, NaCl solution and the chosen emulsifier for the test were sprayed with CO_2. The spraying conditions were the same for all experiments: 60 °C and 50 bar. The core solution content of the emulsion varied between 10 and 20%. Span 65, Span 80 and PGPR 4125 were tested at a concentration of 5 % w/w in respect to the shell material. The

encapsulation efficiency of NaCl reached almost 100% in all the experiments. No differences were observed in the release patterns. This was probably due to the presence of holes and tunnels in the capsules. In fact, when melting the capsules, those produced with PGPR 4125 showed the same behavior observed with the MDT, i.e. very slow release over time of NaCl.

Instead, the loading efficiency of H_2O was always greatly inferior to 100%; up to a maximum of 58% in the case of an initial moisture content of 18% and PGPR 4125 as emulsifier. It was observed that the lower is the moisture content of the emulsion the lower is the loading efficiency. The reason lies in the power ratio, studied previously in the pure Witepsol W31 spraying experiments. Since CO_2 is not able to provide sufficient cooling, i.e. absorb enough energy for the complete solidification of the shell material, the missing energy is taken by water which evaporates and therefore cannot be found in the capsules. This is also notable when considering the quantity of H_2O lost in the experiments. Since all the experiments are performed under similar condition, the quantity of H_2O lost is almost the same in all the experiments. Therefore, when the emulsion contains less water, more water is lost in percentage. By applying the same line of reasoning in previous works it was possible to compare and generalize the results. To further prove the consistency of these results four experiments were performed. In two of them the pressure was raised to 100 bar, in the other two an extra source of CO_2 was inserted in the spray tower. In all these cases the loading efficiency was higher than in the previous experiments, reaching 70 %.

A conceptual design for a PGSS plant for the encapsulation of H_2O has been presented. For a plant that recycle 90% of the CO_2 the capital investment can go up to 1.1 M€. Recycling CO_2 is important in order to reduce the cost per unit, since CO_2 had the highest impact on the final cost of the product. Increasing the production makes the process overall more economically, even if in view of an increase of total capital investment. By increasing the production ten times, the total capital investment is almost quintupled but the added cost per unit is almost halved.

Further work is required to achieve a better encapsulation process. With this work it has been proved that the use of an emulsifier is not always detrimental as suggested by previous works, but it can increase the encapsulation efficiency. The use of different emulsifiers can also provide different release patterns, so they can be used to tune the capsules for specific uses. Any fat will require proper study on each individual emulsifier, because there is no rule to identify the perfect emulsifier for each application.

Regarding encapsulating water, this may require more consideration on what the scope is. Encapsulating water per se is not complicated, but even fat shells will lose water over time, because all fats have a low solubility for water, therefore water is able to transfer through the fat membrane. More over any fault in the membrane, such as holes or tunnels, may offer water leakage. If it is possible to store the capsules in a close vessel this should not be a problem, but in an open one the capsules dry. If the capsules can be applied directly from the container for their application, for example controlled moisture release

to provoke reaction at defined times, then encapsulating water can be taken in consideration.

Another application could be the encapsulation of water soluble substances. By starting with an emulsion and then generating capsules with the PGSS process it is possible to obtain solid lipid particles containing the chosen material. By tuning the amount of CO_2 and the operating conditions it would also be possible to remove most of the water.

References

[1] K.G.H. Desai, H. Jin Park, Recent Developments in Microencapsulation of Food Ingredients, Drying Technology 23 (2005) 1361–1394.

[2] M.-H. Lee, S.-G. Oh, S.-K. Moon, S.-Y. Bae, Preparation of Silica Particles Encapsulating Retinol Using O/W/O Multiple Emulsions, Journal of Colloid and Interface Science 240 (2001) 83–89.

[3] A. Silva-Cunha, J.L. Grossiord, F. Puisieux, M. Seiller, W/O/W multiple emulsions of insulin containing a protease inhibitor and an absorption enhancer, International Journal of Pharmaceutics 158 (1997) 79–89.

[4] M. Mellema, W.A.J. van Benthum, B. Boer, J. von Harras, A. Visser, Wax encapsulation of water-soluble compounds for application in foods, Journal of Microencapsulation 23 (2006) 729–740.

[5] D.A. Campos, A.R. Madureira, A.M. Gomes, B. Sarmento, M.M. Pintado, Optimization of the production of solid Witepsol nanoparticles loaded with rosmarinic acid, Colloids and surfaces. B, Biointerfaces 115 (2014) 109–117.

[6] M. Amid, Y. Manap, N.K. Zohdi, Microencapsulation of purified amylase enzyme from pitaya (Hylocereus polyrhizus) peel in Arabic gum-chitosan using freeze drying, Molecules (Basel, Switzerland) 19 (2014) 3731–3743.

[7] N. Mongenot, S. Charrier, P. Chalier, Effect of Ultrasound Emulsification on Cheese Aroma Encapsulation by Carbohydrates, J. Agric. Food Chem. 48 (2000) 861–867.

[8] Wilson, N. and Shah, N.P., Microencapsualtion of vitamins, ASEAN Food journal 14 (2007) 1–14.

[9] S. D. Braun N. F. Olson, Encapsulation of proteins and peptides in milkfat: encapsulation efficiency and temperature and freezing stabilities, Journal of Microencapsulation 3 (1986) 115–126.

[10] A. Martín, M.J. Cocero, Micronization processes with supercritical fluids, Advanced drug delivery reviews 60 (2008) 339–350.

[11] T. Wendt, Herstellung flüssigkeitshaltiger pulverförmiger Komposite durch ein Hochdrucksprühverfahren für Anwendungen im Lebensmittelbereich, Bochum, 2006.

[12] S. Pörschke, Ein Beitrag zur Herstellung pulverförmiger Biowachse und mögliche Anwendungen, Bochum, 2014.

[13] P. Münüklü, Particle Formation of Ductile Materials using the PGSS Technology with Supercritical Carbon Dioxide. Doctoral Dissertation, Delft, 2005.

[14] Z. Knez, E. Weidner, Particles formation and particle design using supercritical fluids, Current Opinion in Solid State and Materials Science 7 (2003) 353–361.

[15] S. Skjold-Jørgensen, Group Contribution Equation of State (GC-EOS): A Predictive Method for Phase Equilibrium Computations over Wide Ranges of Temperatures and Pressures up to 30 MPa, Industrial & Engineering Chemistry Research 27 (1988) 110–118.

[16] S. Skjold-Jørgensen, Gas Solubility Calculations II. Application of a new Group-Contribution Equation of State, Fluid Phase Equilibria 16 (1984) 317–351.

[17] L.G. Hanu, Manufacturing and Characterization of Water Filled Microcomposites Obtained by the PGSS Process, Bochum, 2010.
[18] P. Ilieva, On the Influence of Carbon Dioxide on the Spray Formation, Emulsification and Encapsulation in the PGSS Process. Dissertation, Bochum, 2016.
[19] J.M. Douglas, Conceptual Design of Chemical Processes, New York, 1988.
[20] H.N. Yow, A.F. Routh, Formation of liquid core–polymer shell microcapsules, Soft Matter 2 (2006) 940–949.
[21] S.K. Ghosh, Functional Coatings: by Polymer Microencapsulation, 2016.
[22] N.J. Zuidam (Ed.), Encapsulation Technologies for Active Food Ingredients and Food Processing, Springer Science+Business Media LLC, New York, NY, 2010.
[23] A. Madene, M. Jacquot, J. Scher, S. Desobry, Flavour encapsulation and controlled release - a review, Int J Food Sci Tech 41 (2006) 1–21.
[24] L.G. Hanu, P. Alessi, A. Kilzer, S. Kareth, Manufacturing and characterization of water filled micro-composites, The Journal of Supercritical Fluids 66 (2012) 274–281.
[25] M.J. Cocero, Á. Martín, F. Mattea, S. Varona, Encapsulation and co-precipitation processes with supercritical fluids, The Journal of Supercritical Fluids 47 (2009) 546–555.
[26] Y. Hakuta, H. Hayashi, K. Arai, Fine particle formation using supercritical fluids, Current Opinion in Solid State and Materials Science 7 (2003) 341–351.
[27] P.G. Debenedetti, J.W. Tom, X. Kwauk, S.-D. Yeo, Rapid expansion of supercritical solutions (ress), Fluid Phase Equilibria 82 (1993) 311–321.
[28] M. Türk, P. Hils, B. Helfgen, K. Schaber, H.-J. Martin, M.A. Wahl, Micronization of pharmaceutical substances by the Rapid Expansion of Supercritical Solutions (RESS), The Journal of Supercritical Fluids 22 (2002) 75–84.
[29] J.-H. Kim, T.E. Paxton, D.L. Tomasko, Microencapsulation of Naproxen Using Rapid Expansion of Supercritical Solutions, Biotechnol. Prog. 12 (1996) 650–661.
[30] J. Jung, M. Perrut, Particle design using supercritical fluids, The Journal of Supercritical Fluids 20 (2001) 179–219.
[31] Y. Wang, Y. Wang, J. Yang, R. Pfeffer, R. Dave, B. Michniak, The application of a supercritical antisolvent process for sustained drug delivery, Powder Technology 164 (2006) 94–102.
[32] Y. Wang, R.N. Dave, R. Pfeffer, Polymer coating/encapsulation of nanoparticles using a supercritical anti-solvent process, The Journal of Supercritical Fluids 28 (2004) 85–99.
[33] M. Perrut, J. Jung, F. Leboeuf, Method for obtaining particles from at least a water soluble product, US2004110871 (2004).
[34] G. Lévai, Á. Martín, A. Moro, A.A. Matias, V.S.S. Gonçalves, M.R. Bronze, C.M.M. Duarte, S. Rodríguez-Rojo, M.J. Cocero, Production of encapsulated quercetin particles using supercritical fluid technologies, Powder Technology 317 (2017) 142–153.
[35] E. Weidner, M. Petermann, Z. Knez, Multifunctional composites by high-pressure spray processes, Current Opinion in Solid State and Materials Science 7 (2003) 385–390.

[36] M. Rodrigues, N. Peiriço, H. Matos, E. Gomes de Azevedo, M.R. Lobato, A.J. Almeida, Microcomposites theophylline/hydrogenated palm oil from a PGSS process for controlled drug delivery systems, The Journal of Supercritical Fluids 29 (2004) 175–184.
[37] M. Fraile, ÿ. Martín, D. Deodato, S. Rodriguez-Rojo, I.D. Nogueira, A.L. Simplício, M.J. Cocero, C.M.M. Duarte, Production of new hybrid systems for drug delivery by PGSS (Particles from Gas Saturated Solutions) process, The Journal of Supercritical Fluids 81 (2013) 226–235.
[38] S. Varona, S. Kareth, Á. Martín, M.J. Cocero, Formulation of lavandin essential oil with biopolymers by PGSS for application as biocide in ecological agriculture, The Journal of Supercritical Fluids 54 (2010) 369–377.
[39] H.-J. Butt, K. Graf, M. Kappl, Physics and chemistry of interfaces, Wiley-VCH, Weinheim, 2003.
[40] D.W.S. Wong, Mechanism and Theory in Food Chemistry, Second Edition, 2nd ed., Springer International Publishing, Cham, 2018.
[41] G.L. Hasenhuettl, R.W. Hartel (Eds.), Food emulsifiers and Their Applications, 2nd ed., Springer Science+Business Media LLC, New York, NY, 2008.
[42] W.C. Griffin, Classification of surface-active agents by "HLB", Journal of Cosmetic Science 1 (1949) 311–326.
[43] W.C. Griffin, Calculation of HLB values of non-ionic surfactants, Journal of Cosmetic Science 5 (1954) 249–256.
[44] J.T. Davies (Ed.), a quantitative kinetic theory of emulsion type. I. physical chemistry of the emulsifying agent, Butterworths, 1957.
[45] IOI Oleo Gmbh, Witepsol, https://www.ioioleo.de/de-wAssets/docs/english/pharma/Witepsol.pdf, 2018.
[46] R.H. Perry, D.W. Green, Perry's chemical engineers' handbook, 8th ed., McGraw-Hill Professional; London McGraw-Hill [distributor], New York, 2008.
[47] M.R. Rietberg, D. Rousseau, L. Duizer, Sensory evaluation of sodium chloride-containing water-in-oil emulsions, Journal of agricultural and food chemistry 60 (2012) 4005–4011.
[48] Sigma Aldrich GmbH, Span 65, https://www.sigmaaldrich.com/catalog/product/sigma/85547?lang=de&region=DE, 2018.
[49] R. Dinarvand, S.H. Moghadam, A. Sheikhi, F. Atyabi, Effect of surfactant HLB and different formulation variables on the properties of poly-D,L-lactide microspheres of naltrexone prepared by double emulsion technique, Journal of Microencapsulation 22 (2005) 139–151.
[50] Sigma Aldrich GmbH, Span 80, https://www.sigmaaldrich.com/catalog/product/sigma/s6760?lang=de&region=DE (accessed 23.03.2018).
[51] R.S. Moglia, J.L. Holm, N.A. Sears, C.J. Wilson, D.M. Harrison, E. Cosgriff-Hernandez, Injectable polyHIPEs as high-porosity bone grafts, Biomacromolecules 12 (2011) 3621–3628.
[52] W. Wagner, FLUIDCAL, Ruhr-Universität Bochum, Bochum, 2018.

[53] T. Vöpel, R. Scholz, L. Davico, M. Gross, S. Büning, S. Kareth, E. Weidner, S. Ebbinghaus, Infrared laser triggered release of bioactive compounds from single hard shell microcapsules, Chemical communications (Cambridge, England) 51 (2015) 6913–6916.
[54] R. Bodmeier, J. Wang, H. Bhagwatwar, Process and formulation variables in the preparation of wax microparticles by a melt dispersion technique. II. W/O/W multiple emulsion technique for water-soluble drugs, Journal of Microencapsulation 9 (1992) 99–107.
[55] J. Milanovic, S. Levic, V. Manojlovic, V. Nedovic, B. Bugarski, Carnauba wax microparticles produced by melt dispersion technique, Chemical Papers 65 (2011) 65.
[56] L. Davico, Scholz, R., Vöpel, T., S. Kareth, E. Weidner (Eds.), Effect of Emulsifiers in hard Fat Microcapsules Generated From an Emulsion, 2016.
[57] L. Wollenweber, Investigation of Polymorphic transition of Lipid Particles obtained with PGSS Process for Pharamaceutical Applications, in: 15th European Meeting on Supercritical Fluids, Germany, 2016.
[58] ISO 13320 Particle size analysis - Laser diffraction methods, 2009.
[59] N. Roß, Herstellung von Hartfettkompositen unter Geringem Energieeintrag durch Metallische Mikrosiebe. Master thesis, Bochum, 2015.
[60] DIN EN 543 Bestimmung der Schüttdichte von Pulver- und Granulatklebstoffen.
[61] I. Minkoff, Applications of the scanning electron microscope in materials science, Journal of material science 2 (1967) 388–394.
[62] Metrohm AG, 870 KF Titrino plus Manual.
[63] S. Espinosa, T. Fornari, S.B. Bottini, E.A. Brignole, Phase equilibria in mixtures of fatty oils and derivatives with near critical fluids using the GC-EOS model, The Journal of Supercritical Fluids 23 (2002) 91–102.
[64] T. Fornari, D. Tenllado, C. Torres, G. Reglero, Supercritical Phase Equilibria Modeling of Glyceride Mixtures and Carbon Dioxide Using the Group Contribution EoS, Journal of Thermodynamics 2011 (2011) 1–9.
[65] T. Fornari, Revision and summary of the group contribution equation of state parameter table, Fluid Phase Equilibria 262 (2007) 187–209.
[66] S.B. Bottini, T. Fornari, E.A. Brignole, Phase equilibrium modelling of triglycerides with near critical solvents, Fluid Phase Equilibria 158-160 (1999) 211–218.
[67] M. Cismondi, J. Mollerup, E.A. Brignole, M.S. Zabaloy, Modeling the high-pressure phase equilibria of carbon dioxide–triglyceride systems, Fluid Phase Equilibria 281 (2009) 40–48.
[68] A. Bamberger, G. Sieder, G. Maurer, High-pressure (vapor+liquid) equilibrium in binary mixtures of (carbon dioxide+water or acetic acid) at temperatures from 313 to 353 K, The Journal of Supercritical Fluids 17 (2000) 97–110.
[69] R. Scholz, L. Davico, V. Jakobi, S. Kareth, A. Rosenhahn, E. Weidner, Verkapselungseffizienz und Freisetzungsverhalten fettbasierter Mikrokapseln mit lipophilen Emulgatoren, Chemie Ingenieur Technik 90 (2018) 562–567.
[70] R. Scholz, Herstellung und Charakterisierung von freisetzungsverzögerten Kapseln aus Wasser-in-Öl-in-Wasser Emulsionen. Doctoral dissertation, Bochum, 2018.

[71] S. Ebbinghaus, A. Dhar, J.D. McDonald, M. Gruebele, Protein folding stability and dynamics imaged in a living cell, Nature methods 7 (2010) 319–323.
[72] F. Wolf, K. Koehler, H.P. Schuchmann, Stabilization of Water Droplets in Oil with PGPR for Use in Oral and Dermal Applications, J Food Process Eng 36 (2013) 276–283.
[73] S. Jiahong, Formation and stability of food-grade water-in-oil-in-water emulsions. Doctoral Dissertation, Palmerston North, New Zealand, 2008.
[74] A. Pawlik, P.W. Cox, I.T. Norton, Food grade duplex emulsions designed and stabilised with different osmotic pressures, Journal of Colloid and Interface Science 352 (2010) 59–67.
[75] E. Weidner, Manufacturing of powder by spraying of gas containing solutions. Habilitation, Erlangen, 1996.
[76] H.C.F. Carneiro, R.V. Tonon, C.R.F. Grosso, M.D. Hubinger, Encapsulation efficiency and oxidative stability of flaxseed oil microencapsulated by spray drying using different combinations of wall materials, Journal of Food Engineering 115 (2013) 443–451.
[77] S. Marcos, M. Meinecke, A. Kilzer, M. Petermann, Study of L–L water-in-oil dispersions generated in SMX-Plus static mixers with dissolved CO 2 under high pressure, The Journal of Supercritical Fluids 132 (2018) 24–32.
[78] R.K. Sinnot, Coulson & Richardson's Chemical Engineering Design, 4th ed., Elsevier Butterworth - Heinemann, Oxford, 2005.
[79] M.S. Peters, K.D. Timmerhaus, Plant Design and Economics for Chemical Engineers, Mc Graw Hill, New York, 2002.
[80] ww.chemengonline.com, CEPCI.
[81] McGraw-Hill Dictionary of Scientific & Technical Terms, https://encyclopedia2.thefreedictionary.com/six-tenths+factor (accessed 30.04.2018).

Annex A - Phase equilibria measurements

Table 37 - Experimental data for calculation of Witepsol W31 solubility in CO_2

	p	t	t_a	p_a	m_{empty}	m_{sample}	$m_{degassed}$	V_{before}	V_{after}	wt-% CO_2
	bar	°C	°C	Torr	g	g	g	m^3	m^3	%
1	50	50	21.1	738.0	65.250	65.276	65.255	0.226051	0.226376	99.2
2	50	50	21.1	738.0	65.243	65.270	65.249	0.226375	0.226612	98.7
3	50	50	22.5	753.0	66.411	66.429	66.412	0.248221	0.248422	99.7
4	50	50	22.5	753.0	64.766	64.787	64.768	0.248422	0.248660	99.5
5	50	50	22.5	753.0	63.655	63.680	63.657	0.248660	0.248899	99.5
6	50	65	21.6	749.6	66.694	66.721	66.694	0.229390	0.229682	99.9
7	50	65	21.6	749.6	65.686	65.714	65.686	0.229682	0.229901	100.0
8	50	65	21.6	749.6	65.393	65.418	65.394	0.229901	0.230017	99.8
9	50	80	21.2	743.7	64.436	64.462	64.436	0.227558	0.228010	100.0
10	50	80	21.2	743.7	67.339	67.364	67.338	0.228008	0.228141	100.2
11	50	80	21.2	743.7	65.337	65.364	65.337	0.228141	0.228350	100.0
12	100	50	22.1	751.0	66.002	66.023	66.002	0.232380	0.232866	100.0
13	100	50	22.1	751.0	65.033	65.056	65.034	0.232866	0.233420	99.9
14	100	50	22.1	751.0	66.787	66.809	66.788	0.233420	0.234007	99.9
15	100	65	23.9	747.1	66.184	66.202	66.183	0.236280	0.236705	100.1
16	100	65	23.9	747.1	63.755	63.778	63.757	0.236705	0.237186	99.8
17	100	65	23.9	747.1	66.447	66.466	66.447	0.237186	0.237690	100.0
18	100	80	24.2	743.8	66.376	66.393	66.377	0.240619	0.241046	99.8
19	100	80	24.2	743.8	65.306	65.331	65.308	0.241046	0.241430	99.7
20	100	80	24.2	743.8	67.163	67.180	67.165	0.241430	0.241954	99.8
21	150	50	23.1	750.1	66.939	66.963	66.940	0.250587	0.250835	99.7
22	150	50	23.1	750.1	64.781	64.798	64.780	0.250835	0.251211	100.2
23	150	50	23.1	750.1	65.531	65.552	65.532	0.251211	0.251529	99.8
24	150	65	24.8	756.1	64.549	64.573	64.551	0.255157	0.255488	99.6
25	150	65	24.8	756.1	64.644	64.669	64.646	0.255488	0.255789	99.6
26	150	65	24.8	756.1	66.829	66.855	66.831	0.255789	0.256190	99.7
27	150	80	22.8	746.3	66.904	66.928	66.910	0.245739	0.246060	98.9
28	150	80	22.8	746.3	66.109	66.134	66.112	0.246060	0.246466	99.7
29	150	80	22.8	746.3	65.324	65.348	65.327	0.246466	0.246797	99.6

Table 38 - Experimental data for calculation of CO_2 solubility in Witepsol W31

	p	t	t_a	p_a	m_{empty}	m_{sample}	$m_{degassed}$	V_{before}	V_{after}	wt-% CO_2
	bar	**°C**	**°C**	**Torr**	**g**	**g**	**g**	**m3**	**m3**	**%**
1	50	50	21.1	738	65.263	68.146	68.116	0.22538	0.225449	5.1
2	50	50	21.1	738	64.410	66.672	66.645	0.225449	0.22558	10.5
3	50	50	21.1	738	66.296	68.208	68.181	0.22558	0.225715	12.4
4	50	50	22.5	753	66.614	70.199	70.168	0.247499	0.247753	12.1
5	50	50	22.5	753	64.870	68.766	68.736	0.247753	0.248026	11.9
6	50	50	22.5	753	62.839	65.747	65.719	0.248026	0.248221	11.7
7	50	65	21.6	749.6	66.054	69.477	69.446	0.228828	0.22909	13.0
8	50	65	21.6	749.6	64.903	68.054	67.917	0.22909	0.229188	9.4
9	50	65	21.6	749.6	67.400	71.245	71.218	0.229188	0.22939	9.3
10	50	80	21.2	743.7	66.458	69.175	69.145	0.227141	0.227238	7.1
11	50	80	21.2	743.7	65.731	68.723	68.691	0.227238	0.227359	7.8
12	50	80	21.2	743.7	67.745	71.974	71.942	0.227359	0.227558	8.5
13	100	50	22.1	751	67.315	69.230	69.196	0.231633	0.231983	26.2
14	100	50	22.1	751	64.105	65.375	65.346	0.231983	0.232187	24.3
15	100	50	22.1	751	65.017	66.163	66.136	0.232187	0.23238	25.2
16	100	65	23.9	747.1	67.271	68.915	68.886	0.235447	0.235668	20.8
17	100	65	23.9	747.1	65.598	68.194	68.162	0.235668	0.236028	20.9
18	100	65	23.9	747.1	64.946	66.928	66.898	0.236028	0.23628	19.7
19	100	80	24.2	743.8	64.969	66.857	66.832	0.239883	0.240078	16.7
20	100	80	24.2	743.8	64.574	66.792	66.762	0.240078	0.2403	16.3
21	100	80	24.2	743.8	64.238	67.175	67.145	0.2403	0.240619	17.0
22	150	50	23.1	750.1	63.827	65.325	65.289	0.249741	0.25004	28.2
23	150	50	23.1	750.1	63.426	64.586	64.551	0.25004	0.250309	31.6
24	150	50	23.1	750.1	66.413	67.521	67.485	0.250309	0.250587	33.4
25	150	65	24.8	756.1	66.485	67.489	67.463	0.254494	0.25468	27.0
26	150	65	24.8	756.1	65.627	66.775	66.748	0.25468	0.254901	27.5
27	150	65	24.8	756.1	65.030	66.396	66.369	0.254901	0.255157	26.8
28	150	80	22.8	746.3	65.863	66.863	66.837	0.245101	0.245235	21.5
29	150	80	22.8	746.3	63.771	64.571	64.547	0.245235	0.24535	22.8
30	150	80	22.8	746.3	65.073	67.280	67.252	0.24535	0.245739	25.0

Annex B - Melt Dispersion Technique experiments

Table 39 - EE from external water of the MDT experiments

	W31	Emulsifier		NaCl solution	Conc. NaCl solution	Filtered water	Conductivity at 25 °C	Washing water	Conductivity at 25° C	EE
	g		g	g	g_{NaCl}/g_{tot}	g	µS/cm	g	µS/cm	
E1	5.08	-	-	1.13	0.09	97.79	766.99	56.78	70.20	0.56
E2	5.02	-	-	1.11	0.09	96.21	628.55	56.78	74.97	0.62
E3	5.05	-	-	1.03	0.09	101.11	1,095.31	56.45	112.85	0.31
E4	5.00	SPAN 65	0.05	1.01	0.09	99.80	618.87	87.10	46.94	0.60
E5	5.02	SPAN 65	0.05	1.01	0.09	100.00	619.78	92.75	43.76	0.60
E6	5.03	SPAN 65	0.05	1.01	0.09	100.81	544.10	171.11	23.35	0.64
E7	5.01	SPAN 80	0.06	1.03	0.09	101.04	887.59	136.88	44.34	0.43
E8	5.01	SPAN 80	0.05	1.01	0.09	99.66	723.15	50.55	96.95	0.53
E9	5.01	SPAN 80	0.05	1.02	0.09	99.57	1,149.57	56.92	163.08	0.25
E10	5.00	TWEEN 80	0.05	1.01	0.09	98.99	1,217.87	111.76	102.44	0.18
E11	5.01	TWEEN 80	0.05	1.02	0.08	99.99	1,399.07	93.00	80.52	0.03

E12	5.05	TWEEN 80	0.06	1.02	0.10	100.60	1,408.91	93.63	145.57	0.13
E13	5.02	PGPR 4125	0.05	1.01	0.09	99.94	1,097.22	49.98	148.75	0.28
E14	5.00	PGPR 4125	0.05	1.00	0.09	99.28	776.73	57.41	102.13	0.49
E15	5.00	PGPR 4125	0.06	1.01	0.09	99.44	941.61	159.87	58.83	0.37
E16	5.02	SPAN 65	0.26	0.09	0.09	100.48	419.73	93.50	36.48	0.73
E17	5.39	SPAN 65	0.25	0.10	0.09	103.13	438.01	76.48	42.84	0.73
E18	5.12	SPAN 65	0.26	0.09	0.09	100.38	642.22	41.85	93.71	0.58
E19	5.09	SPAN 80	0.25	1.04	0.09	98.46	484.06	71.71	80.47	0.68
E20	5.31	SPAN 80	0.26	1.02	0.09	98.93	483.34	71.71	55.83	0.68
E21	5.14	SPAN 80	0.25	1.01	0.09	98.76	783.58	92.26	83.00	0.48
E22	5.02	TWEEN 80	0.26	1.05	0.09	96.70	674.24	122.12	719.89	0.13
E23	5.05	TWEEN 80	0.26	1.02	0.09	95.46	835.44	93.48	865.25	0.04
E24	5.00	TWEEN 80	0.25	1.03	0.09	96.76	657.11	83.80	244.88	0.48
E25	5.01	PGPR 4125	0.26	1.00	0.09	99.22	173.25	49.13	66.37	0.88
E26	5.01	PGPR 4125	0.25	1.01	0.09	98.34	62.26	58.89	14.10	0.96

E27	5.02	PGPR 4125	0.25	1.02	0.09	99.06	130.78	77.39	18.41	0.91
E28	5.01	PGPR 4125	0.26	1.12	0.09	97.28	130.94	52.53	41.41	0.92
E29	5.08	PGPR 4125	0.26	1.01	0.09	101.32	167.05	64.97	29.27	0.88

Table 40 - EE by melting of the MDT experiments

	Capsules	Water	Conductivity at 25 °C	EE
	g	g	µS/cm	
E1	0.29	27.13	264.62	0.61
E2	0.30	30.14	246.22	0.63
E3	0.33	30.11	150.65	0.37
E4	0.30	30.03	253.75	0.70
E5	0.30	30.05	252.04	0.70
E6	0.30	30.02	264.84	0.73
E7	0.30	30.66	207.51	0.56
E8	0.30	30.10	219.53	0.61
E9	0.30	30.04	125.81	0.34
E10	0.30	30.00	100.45	0.28
E11	0.30	30.16	79.22	0.24
E12	0.30	30.02	91.80	0.23
E13	0.30	30.06	99.81	0.28
E14	0.30	30.00	154.75	0.43
E15	0.30	30.02	193.82	0.52
E16	0.31	30.04	299.18	0.78
E17	0.31	30.08	281.74	0.79
E18	0.31	30.01	234.51	0.64
E19	0.32	29.86	279.67	0.72
E20	0.29	30.16	244.42	0.73
E21	0.31	30.11	224.40	0.61
E22	0.30	30.25	63.10	0.17
E23	0.30	30.14	40.17	0.11
E24	0.31	29.99	139.91	0.38
E25	0.30	30.01	38.48	0.11
E26	0.30	30.01	28.68	0.08
E27	0.30	30.01	38.48	0.09
E28	0.30	30.00	38.49	0.10
E29	0.30	30.00	96.04	0.27

Table 41 - Release for MDT experiments without emulsifier

	Time	Capsules	Water	Conductivity at 25 °C	Release	Release
	min	g	g	µS/cm	from external water	by melting
E1	1	0.30	30.02	10.68	4.34%	4.02%
	5	0.30	30.10	15.73	6.63%	6.14%
	15	0.30	30.11	16.18	6.79%	6.30%
	30	0.30	30.08	22.31	9.48%	8.78%
	60	0.29	30.00	22.76	9.99%	9.26%
	120	0.30	30.03	28.52	12.16%	11.27%
	240	0.30	30.14	37.00	16.01%	14.83%
E2	1	0.30	30.02	13.49	5.08%	5.04%
	5	0.30	29.73	12.98	4.80%	4.76%
	15	0.30	30.01	16.96	6.41%	6.36%
	30	0.31	30.00	18.50	6.86%	6.80%
	60	0.30	29.74	22.03	8.44%	8.38%
	120	0.30	30.02	28.55	11.19%	11.10%
	240	0.30	30.06	37.13	14.77%	14.66%
E3	1	0.31	30.02	6.82	5.01%	4.15%
	5	0.30	30.18	7.67	5.91%	4.89%
	15	0.34	30.20	6.82	4.63%	3.83%
	30	0.30	30.03	7.27	5.62%	4.65%
	60	0.30	30.03	8.98	7.10%	5.88%
	120	0.32	30.00	14.14	11.07%	9.16%
	240	0.31	30.02	20.27	16.73%	13.85%

Table 42 - Release from MDT experiments with Span 65 at 1%

	Time	Capsules	Water	Conductivity at 25 °C	Release	Release
	min	g	g	µS/cm	from external water	by melting
E4	1	0.30	29.99	8.24	3.41%	2.90%
	5	0.30	30.01	8.24	3.38%	2.87%
	15	0.30	30.00	10.47	4.42%	3.76%
	30	0.30	30.00	10.65	4.51%	3.83%
	60	0.30	29.03	12.97	5.42%	4.60%
	120	0.30	30.05	27.33	12.28%	10.43%
	240	0.30	30.00	61.10	28.02%	23.80%
E5	1	0.30	30.06	8.74	3.64%	3.11%
	5	0.30	30.04	11.02	4.73%	4.04%
	15	0.30	30.03	14.94	6.50%	5.54%
	30	0.30	30.06	14.76	6.47%	5.52%
	60	0.30	30.03	18.68	8.33%	7.11%
	120	0.30	30.03	34.44	15.60%	13.31%
	240	0.30	30.02	64.00	29.29%	25.00%
E6	1	0.31	30.11	7.72	2.81%	2.49%
	5	0.30	30.29	11.06	4.41%	3.91%
	15	0.31	30.34	9.24	3.48%	3.09%
	30	0.33	30.19	11.93	4.36%	3.87%
	60	0.31	30.17	12.71	5.03%	4.46%
	120	0.33	30.00	24.72	9.43%	8.38%
	240	0.31	30.03	43.71	17.93%	15.92%

Table 43 - Release from MDT experiments with Span 80 at 1%

	Time	**Capsules**	**Water**	**Conductivity at 25 °C**	**Release**	**Release**
	min	**g**	**g**	**µS/cm**	**from external water**	**by melting**
E7	1	0.30	30.03	8.74	4.88%	3.76%
	5	0.30	30.02	8.93	4.96%	3.82%
	15	0.30	30.21	9.34	5.27%	4.06%
	30	0.30	30.02	13.75	8.04%	6.19%
	60	0.30	29.09	13.51	7.68%	5.92%
	120	0.30	30.01	16.64	9.80%	7.54%
	240	0.30	30.02	26.04	15.74%	12.12%
E8	1	0.30	30.03	6.43	2.87%	2.50%
	5	0.30	30.05	7.04	3.18%	2.77%
	15	0.30	30.00	7.75	3.56%	3.10%
	30	0.30	30.01	9.97	4.73%	4.12%
	60	0.30	30.03	13.80	6.73%	5.86%
	120	0.30	30.01	15.89	7.82%	6.81%
	240	0.30	30.04	25.95	13.10%	11.41%
E9	1	0.30	30.13	7.70	7.53%	5.43%
	5	0.30	30.00	8.79	8.65%	6.25%
	15	0.30	30.06	8.91	8.84%	6.38%
	30	0.30	30.01	10.26	10.33%	7.46%
	60	0.30	30.00	12.31	12.65%	9.13%
	120	0.30	29.99	15.80	16.57%	11.96%
	240	0.30	29.99	19.34	20.44%	14.75%

Table 44 - Release from MDT experiments with Tween 80 1%

	Time	Capsules	Water	Conductivity at 25 °C	Release	Release
	min	g	g	µS/cm	from external water	by melting
E10	1	0.30	30.04	28.29	43.11%	27.54%
	5	0.30	30.04	38.62	59.33%	37.90%
	15	0.30	30.06	60.12	93.72%	59.86%
	30	0.29	30.19	63.20	102.31%	65.35%
	60	0.34	30.14	82.47	114.94%	73.42%
	120	0.30	30.00	79.78	123.79%	79.07%
	240	0.30	30.01	81.80	127.55%	81.47%
E11	1	0.30	30.02	13.99	145.19%	16.63%
	5	0.30	30.03	19.63	208.37%	23.87%
	15	0.30	30.07	29.82	322.71%	36.96%
	30	0.30	30.01	33.43	359.87%	41.22%
	60	0.30	30.09	39.76	434.51%	49.77%
	120	0.30	30.03	65.13	710.64%	81.40%
	240	0.30	30.06	53.67	588.17%	67.37%
E12	1	0.31	30.01	14.30	24.94%	14.35%
	5	0.30	30.01	18.90	34.27%	19.72%
	15	0.31	30.01	27.80	50.36%	28.98%
	30	0.30	30.01	35.90	66.71%	38.39%
	60	0.30	30.00	47.28	88.81%	51.11%
	120	0.30	30.03	56.87	106.36%	61.21%
	240	0.30	30.00	57.00	106.84%	61.49%

Table 45 - Release from MDT experiments with PGPR 4125 at 1%

	Time	Capsules	Water	Conductivity at 25 °C	Release	Release
	min	**g**	**g**	**µS/cm**	**from external water**	**by melting**
E13	1	0.30	30.03	7.64	6.57%	6.76%
	5	0.30	30.02	7.90	6.77%	6.96%
	15	0.30	30.21	8.24	7.18%	7.38%
	30	0.30	30.02	12.18	11.06%	11.38%
	60	0.30	29.09	12.77	11.33%	11.66%
	120	0.30	30.01	15.93	14.66%	15.08%
	240	0.30	30.02	24.82	23.47%	24.14%
E14	1	0.30	30.00	7.93	4.02%	4.50%
	5	0.30	30.10	9.78	5.11%	5.73%
	15	0.30	30.03	10.27	5.40%	6.06%
	30	0.30	30.00	10.37	5.46%	6.12%
	60	0.30	30.01	14.12	7.60%	8.52%
	120	0.30	30.34	16.00	8.78%	9.85%
	240	0.30	30.00	32.11	17.96%	20.14%
E15	1	0.30	30.01	8.75	5.75%	4.14%
	5	0.30	30.02	9.50	6.27%	4.52%
	15	0.30	30.00	11.15	7.54%	5.43%
	30	0.31	30.01	20.27	13.82%	9.96%
	60	0.30	30.00	46.90	34.04%	24.53%
	120	0.30	30.01	76.91	55.72%	40.16%
	240	0.30	30.01	112.25	82.31%	59.32%

Table 46 - Release for MDT experiments with Span 65 at 5%

	Time	Capsules	Water	Conductivity at 25 °C	Release	Release
	min	g	g	µS/cm	from external water	by melting
E16	1	0.31	30.30	9.29	3.03%	2.82%
	5	0.31	30.04	8.56	2.73%	2.54%
	15	0.31	29.77	9.67	3.10%	2.88%
	30	0.31	29.99	12.35	4.10%	3.81%
	60	0.30	30.10	22.99	8.13%	7.56%
	120	0.31	30.07	42.57	15.26%	14.20%
	240	0.31	30.16	84.88	30.94%	28.79%
E17	1	0.31	29.99	9.85	3.41%	3.16%
	5	0.31	30.19	9.55	3.31%	3.06%
	15	0.30	30.00	10.67	3.77%	3.49%
	30	0.20	30.00	12.51	6.82%	6.32%
	60	0.30	30.09	28.07	10.69%	9.91%
	120	0.31	30.14	54.15	20.41%	18.91%
	240	0.30	30.06	99.97	39.14%	36.27%
E18	1	0.30	30.00	11.21	5.06%	4.48%
	5	0.30	30.00	8.52	3.73%	3.30%
	15	0.30	30.02	9.46	4.21%	3.73%
	30	0.30	29.99	12.57	5.64%	4.99%
	60	0.30	30.01	18.21	8.56%	7.58%
	120	0.30	30.02	30.32	14.59%	12.91%
	240	0.30	30.01	59.95	28.79%	25.47%

Table 47 - Release from MDT experiments with Span 80 at 5%

	Time	**Capsules**	**Water**	**Conductivity at 25 °C**	**Release**	**Release**
	min	**g**	**g**	**µS/cm**	**from external water**	**by melting**
E19	1	0.20	30.08	24.01	13.76%	12.94%
	5	0.30	30.04	31.73	12.46%	11.72%
	15	0.30	30.13	29.13	11.44%	10.75%
	30	0.30	30.23	37.75	14.91%	14.02%
	60	0.30	30.14	45.04	18.13%	17.05%
	120	0.30	30.02	54.46	21.67%	20.38%
	240	0.30	30.02	153.87	62.15%	58.44%
E20	1	0.29	30.04	29.68	12.80%	11.95%
	5	0.31	30.04	20.96	8.44%	7.88%
	15	0.30	30.26	49.08	20.72%	19.35%
	30	0.30	30.04	45.22	19.06%	17.80%
	60	0.30	29.99	55.63	23.36%	21.81%
	120	0.20	30.05	41.25	25.97%	24.25%
	240	0.30	30.01	119.07	50.37%	47.04%
E21	1	0.31	29.90	13.51	7.24%	5.70%
	5	0.31	30.42	15.95	8.80%	6.93%
	15	0.21	30.04	13.57	10.95%	8.63%
	30	0.31	30.19	23.84	13.40%	10.56%
	60	0.20	30.03	21.15	17.95%	14.14%
	120	0.30	30.65	36.13	21.17%	16.68%
	240	0.30	30.11	52.19	30.24%	23.83%

Table 48 - Release from MDT experiments with Tween 80 at 5%

	Time	**Capsules**	**Water**	**Conductivity at 25 °C**	**Release**	**Release**
	min	**g**	**g**	**µS/cm**	**from external water**	**by melting**
E22	1	0.30	30.12	32.64	63.43%	50.91%
	5	0.30	30.22	50.58	99.46%	79.83%
	15	0.30	30.04	57.48	114.54%	91.94%
	30	0.31	30.07	62.05	118.91%	95.44%
	60	0.32	30.08	62.72	118.80%	95.36%
	120	0.31	28.11	62.68	112.84%	90.57%
	240	0.30	30.01	59.89	118.95%	95.48%
E23	1	0.30	30.52	16.91	105.84%	40.70%
	5	0.30	30.29	24.43	156.45%	60.16%
	15	0.30	30.23	31.86	204.09%	78.49%
	30	0.30	30.07	36.61	231.12%	88.88%
	60	0.30	30.45	36.46	236.21%	90.84%
	120	0.30	30.06	39.30	249.90%	96.10%
	240	0.30	30.20	38.03	243.72%	93.72%
E24	1	0.30	29.99	64.99	36.59%	46.98%
	5	0.30	30.02	93.41	52.54%	67.46%
	15	0.31	30.00	124.70	67.64%	86.83%
	30	0.30	30.00	123.46	69.83%	89.65%
	60	0.30	30.02	140.76	79.66%	102.27%
	120	0.30	30.00	135.29	76.27%	97.92%
	240	0.30	30.01	136.57	77.56%	99.57%

Table 49 - Release of MDT experiments with PGPR 4125 at 5%

	Time	Capsules	Water	Conductivity at 25 °C	Release	Release
	min	g	g	µS/cm	from external water	by melting
E25	1	0.30	30.04	8.05	2.26%	18.86%
	5	0.30	30.47	8.33	2.41%	20.08%
	15	0.30	30.00	9.04	2.57%	21.45%
	30	0.30	30.05	11.28	3.26%	27.24%
	60	0.30	30.05	9.06	2.55%	21.30%
	120	0.30	30.10	9.53	2.72%	22.69%
	240	0.30	30.16	11.15	3.27%	27.26%
E26	1	0.30	30.05	9.96	2.61%	32.51%
	5	0.30	30.09	10.09	2.64%	32.89%
	15	0.30	30.02	12.05	3.21%	39.89%
	30	0.30	30.00	14.66	3.95%	49.19%
	60	0.30	30.03	14.66	3.96%	49.27%
	120	0.30	30.01	17.70	4.83%	60.03%
	240	0.30	30.00	17.97	4.88%	60.77%
E27	1	0.29	34.02	8.78	2.47%	23.97%
	5	0.30	30.03	10.97	2.71%	26.29%
	15	0.30	30.01	10.51	2.58%	24.98%
	30	0.30	30.06	12.51	3.14%	30.43%
	60	0.30	30.01	11.76	2.94%	28.52%
	120	0.30	30.12	10.87	2.71%	26.27%
	240	0.30	30.06	15.49	3.94%	38.15%
E28	1	0.30	30.01	10.74	2.96%	26.11%
	5	0.30	30.02	12.35	3.45%	30.43%
	15	0.30	30.14	14.71	4.18%	36.85%
	30	0.30	30.03	20.69	5.99%	52.84%
	60	0.30	30.03	16.84	4.78%	42.17%
	120	0.30	30.03	21.60	6.26%	55.23%
	240	0.30	30.02	31.59	9.25%	81.60%
E29	1	0.30	30.00	9.16	2.64%	8.52%
	5	0.31	30.01	11.33	3.32%	10.72%
	15	0.31	30.17	11.33	3.33%	10.77%
	30	0.30	29.66	11.53	3.42%	11.05%
	60	0.30	30.00	12.69	3.87%	12.49%
	120	0.43	30.01	14.84	3.19%	10.31%
	240	0.36	30.02	16.82	4.35%	14.06%

Annex C - PGSS process experiments

In tables 50 and 51 “top” refers to capsules taken from the top of the bag in which they were collected during the spraying experiments, “bottom” to the capsules taken from the bottom of the bag. The experiments also prove that no real difference regarding the EE can be observed: the spraying process and the emulsion are similar from the beginning to the end of the PGSS experiment. Capsules containing PGPR show a poor release while molten, same as the MDT capsules.

Table 50 - EE of the PGSS capsules by melting

Experiment	**Capsules**	**Water**	**Conductivity at 25 °C**	**EE**
	g	**g**	**µS/cm**	
C1 - TOP	0.30	30.32	242.80	1.06
C1 -BOTTOM	0.30	30.06	248.24	1.07
C2 - TOP	0.31	26.01	279.63	1.03
C2 -BOTTOM	0.30	25.88	271.03	1.03
C3 - TOP	0.31	30.30	53.51	0.14
C3 -BOTTOM	0.30	30.03	44.81	0.10
C4 - TOP	0.30	30.15	451.72	0.93
C4 -BOTTOM	0.30	30.11	458.51	0.93
C5 - TOP	0.30	30.04	468.70	0.94
C5 -BOTTOM	0.30	30.07	471.34	0.95
C6 - TOP	0.31	29.95	163.42	0.30
C6 -BOTTOM	0.30	30.03	174.06	0.33
C7 - TOP	0.31	29.89	475.13	0.95
C7 -BOTTOM	0.30	30.01	432.52	0.87

Table 51 - EE of the PGSS capsules by washing

Experiment	Capsules	Water	Conductivity at 25 °C	EE
	g	g	µS/cm	
C1 - TOP	0.31	30.56	46.86	0.89
C1 -BOTTOM	0.31	30.06	42.89	0.91
C2 - TOP	0.30	30.47	115.34	0.55
C2 -BOTTOM	0.30	30.26	33.04	0.95
C3 - TOP	0.30	30.12	57.61	0.84
C3 -BOTTOM	0.30	30.57	40.85	0.91
C4 - TOP	0.30	29.98	69.51	0.90
C4 -BOTTOM	0.31	30.35	72.04	0.90
C5 - TOP	0.31	30.20	78.88	0.88
C5 -BOTTOM	0.30	30.72	69.41	0.90
C6 - TOP	0.31	30.36	44.24	0.95
C6 -BOTTOM	0.30	30.29	40.72	0.96
C7 - TOP	0.30	30.41	73.23	0.89
C7 -BOTTOM	0.31	30.95	68.44	0.90

Table 52 - Release of PGSS experiments C1 and C2

[1] due to the results of the EE by melting the entirety of the NaCl sprayed was considered as encapsulated

Experiment	Time	Capsules	Water	Conductivity at 25 °C	Release compared to total NaCl[1]
	min	g	g	µS/cm	
C1 - Sample 1	5	0.30	30.02	43.88	0.10
	30	0.30	30.49	64.72	0.20
	60	0.30	30.14	79.07	0.27
	120	0.30	30.05	96.57	0.36
	240	0.30	30.04	128.30	0.51
	480	0.30	30.03	159.97	0.67
	1466	0.30	30.12	193.40	0.83
	4320	0.31	29.63	184.00	0.76
C1 - Sample 2	5	0.30	30.05	44.08	0.10
	30	0.31	30.97	56.44	0.16
	60	0.30	30.28	65.92	0.21
	120	0.30	30.22	84.79	0.30
	240	0.31	30.01	110.02	0.41
	480	0.31	30.02	142.39	0.57
	1440	0.30	30.33	174.56	0.74
	4320	0.31	30.19	195.22	0.82
C2 - Sample 1	5	0.31	30.84	101.43	0.38
	30	0.31	30.41	115.13	0.44
	60	0.27	30.34	95.53	0.39
	120	0.31	30.04	119.70	0.45
	240	0.31	30.15	128.49	0.50
	480	0.32	30.17	166.42	0.66
	1440	0.31	30.33	198.75	0.84
	4320	0.30	30.34	228.78	0.99
C2 - Sample 2	5	0.30	30.35	26.58	0.02
	30	0.32	30.77	43.30	0.09
	60	0.32	30.62	47.31	0.11
	120	0.31	30.09	59.63	0.17
	240	0.31	30.22	92.93	0.33
	480	0.32	30.41	123.29	0.45
	1440	0.30	30.32	222.28	0.96
	4320	0.30	30.06	230.88	1.00

Table 53 - Release of PGSS experiments C3 and C4

[1] due to the results of the EE by melting the entirety of the NaCl sprayed was considered as encapsulated

Experiment	Time	Capsules	Water	Conductivity at 25 °C	Release compared to total NaCl[1]
	min	g	g	µS/cm	
C3 - Sample 1	5	0.31	30.56	42.75	0.09
	30	0.30	30.16	58.08	0.17
	60	0.30	30.01	45.70	0.11
	120	0.30	30.33	54.72	0.15
	240	0.31	30.87	63.27	0.20
	480	0.31	30.48	71.70	0.23
	1440	0.30	30.28	99.33	0.37
	4320	0.31	30.58	133.91	0.53
C3 - Sample 2	5	0.31	30.05	47.47	0.12
	30	0.30	30.12	57.08	0.17
	60	0.30	30.40	64.38	0.20
	120	0.30	30.05	70.26	0.23
	240	0.31	30.61	79.76	0.27
	480	0.30	30.20	88.24	0.31
	1440	0.30	30.75	107.99	0.42
	4320	0.30	30.10	129.24	0.52
C4 - Sample 1	5	0.31	30.08	63.01	0.08
	30	0.30	30.09	100.27	0.17
	60	0.31	30.09	137.43	0.24
	120	0.30	30.00	168.13	0.32
	240	0.31	30.00	208.31	0.40
	480	0.30	30.37	246.40	0.49
	1440	0.30	30.01	329.92	0.66
	4320	0.30	30.20	392.43	0.80
C4 - Sample 2	5	0.31	30.01	112.18	0.19
	30	0.31	30.00	190.21	0.36
	60	0.30	30.60	224.90	0.45
	120	0.31	30.61	278.54	0.55
	240	0.31	30.48	329.65	0.66
	480	0.30	30.05	353.75	0.72
	1440	0.31	30.08	374.78	0.74
	4320	0.30	30.20	408.92	0.84

Table 54 - Release of PGSS experiments C5 and C6

[1] due to the results of the EE by melting the entirety of the NaCl sprayed was considered as encapsulated

	Time	**Capsules**	**Water**	**Conductivity at 25 °C**	**Release compared to total NaCl[1]**
	min	**g**	**g**	**µS/cm**	
C5 - Sample 1	5	0.30	30.24	39.88	0.04
	30	0.31	29.95	70.54	0.10
	60	0.30	30.30	78.60	0.12
	120	0.31	30.14	107.73	0.18
	240	0.30	30.17	147.70	0.27
	480	0.30	30.59	233.51	0.46
	1440	0.30	30.45	383.77	0.79
	4320	0.31	30.03	479.65	0.96
C5 - Sample 2	5	0.31	30.42	46.65	0.05
	30	0.30	30.23	83.60	0.13
	60	0.31	30.01	91.11	0.14
	120	0.30	30.07	108.42	0.18
	240	0.30	30.60	159.20	0.30
	480	0.30	30.27	269.64	0.53
	1440	0.31	30.01	461.33	0.93
	4320	0.30	30.01	463.66	0.95
C6 - Sample 1	5	0.31	30.66	35.13	0.03
	30	0.30	30.12	54.12	0.07
	60	0.32	30.23	73.78	0.11
	120	0.32	30.39	105.53	0.17
	243	0.31	30.08	148.54	0.28
	480	0.28	30.75	182.40	0.39
	1440	0.31	30.61	328.97	0.69
	4320	0.30	30.38	415.38	0.88
C6 - Sample 2	5	0.30	30.77	32.17	0.02
	30	0.30	30.20	53.00	0.07
	60	0.30	30.77	78.00	0.13
	120	0.31	30.11	108.82	0.19
	240	0.31	30.03	137.46	0.25
	480	0.30	30.11	201.01	0.40
	1440	0.30	30.87	365.79	0.79
	4320	0.30	30.05	422.98	0.90

Table 55 - Release of PGSS experiments C5 and C6

[1] due to the results of the EE by melting the entirety of the NaCl sprayed was considered as encapsulated

Experiment	**Time**	**Capsules**	**Water**	**Conductivity at 25 °C**	**Release compared to total NaCl[1]**
	min	**g**	**g**	**µS/cm**	
C7 - Sample 1	5	0.30	31.04	74.96	0.12
	30	0.30	30.12	138.83	0.25
	60	0.30	30.41	211.73	0.42
	120	0.30	30.08	232.47	0.46
	240	0.30	30.14	293.98	0.59
	480	0.31	30.24	348.77	0.71
	1440	0.30	30.20	398.46	0.83
	4320	0.31	30.33	419.59	0.87
C7 - Sample 2	5	0.30	30.13	120.21	0.21
	30	0.31	30.70	176.07	0.34
	60	0.30	30.68	174.09	0.34
	120	0.30	30.11	284.22	0.57
	240	0.30	30.04	327.30	0.67
	480	0.30	30.12	358.93	0.74
	1440	0.30	30.91	376.13	0.80
	4320	0.30	30.15	404.87	0.84

Annex D - Economical evaluation of a plant with 90% recycle of CO_2

The equipment sizing, equipment cost and the breakdown for the total capital investment and the added value cost are collected in tables 56, 57, 58 and 59 respectively.

Table 56 - Equipment sizing

ID	ITEM	Conditions (Design) P (bar) T(°C)		TYPE	SIZE
P101	Water pump	1 to 80	15	Reciprocating Pump	Power = 0.27KW
P102	W31 pump	1 to 80	40	Reciprocating Pump	Power = 1.1 KW
P103	CO_2 pump	51 to 80	10	Reciprocating Pump	Power = 0.88 KW
E101	Heater H_2O	80	15 to 40	Shell and Tube Double pass	A = 0.17 m^2 L = 1.5 m Duty = 3.6 KW # pipes = 6
E102	Cooler fresh CO_2	51	15 to 0	Shell and Tube Double pass	A = 0.05 m^2 L = 0.8 m Duty = 1.37 KW # pipes = 4
E103	Heater CO_2	80	0 to 40	Shell and Tube Double pass	A = 2.54 m^2 L = 2 m Duty = 78.6 KW # pipes = 68
Spray Tower	Spray Tower	1	25	Cylinder	V = 0.69 m^3 L = 3.24 m Ø = 1.62 m
C101	1^{st} compressor recycle CO_2	5	140	Reciprocating compressor	Power = 34.33 KW
E104	Cooler CO_2 between compressor	5	133 to 40	Shell and Tube Double pass	A = 0.87 m^2 L = 0.5 m Duty = 25.6 KW # pipes = 32

C102	2st compressor recycle CO_2	20	150	Reciprocating compressor	Power = 30.7 KW
E105	Cooler CO_2 after compression	20	148 to -10	Shell and Tube Double pass	A = 0.74 m^2 L = 0.5 m Duty = 47.42 KW # pipes = 80
E106	Condenser CO_2	20	-10 to -20	Shell and Tube Double pass	A = 9.18 m^2 L = 3 m Duty = 87.21 KW # pipes = 162
V101	Liquid CO_2 vessel	20	-20	Pressurized vessel	V = 0.07 m^3
P104	Recycled CO_2 pump	51	-20	Reciprocating pump	Power = 0.84 KW

Table 57 - Equipment cost

ID	**ITEM**	**Estimated cost (k€)**
P101	Water pump	5.5
P102	W31 pump	5.5
P103	CO_2 pump	7.0
E101	Heater H_2O	1.5
E102	Cooler CO_2	0.7
E103	Heater CO_2	6.4
Static Mixer	Static Mixer	10.0
Spray Tower	Spray Tower	9.2
C101	Compressor CO_2	111.0
E104	Cooler CO_2	4.0
C102	Compressor CO_2	94.4
E105	Cooler CO_2	3.7
E106	Condenser CO_2	9.4

V101	Vessel liquid CO_2	18.5
P104	Pump CO_2	6.5

Table 58 - Breakdown of the total capital investment

Direct Costs	**(k€)**
Purchased equipment delivered	74.8
Purchased-Equipment installation	35.2
Instrumentation and controls (installed)	26.9
Piping (installed)	50.9
Electrical Systems (installed)	8.2
Building (including services)	13.5
Yard improvements	7.5
Service facilities	52.4
Total direct plant cost	269.4
Indirect Costs	
Engineering and Supervision	24.7
Construction expenses	30.7
Legal expenses	3.0
Contractor's fee	16-5
Contingency	32.9
Total indirect plant cost	107.8
Fixed-capital investment	754.3
Start-up Cost	8.2
Working capital (15% of total capital investment)	133.2
Total Capital investment	895.8

Refining the plant for the production of capsules and including cyclone and filters to make sure that no capsule enters the recycle stream of CO_2 the purchased equipment delivered cost is increased of around 20 k€, which brings the total capital investment in the order of 1.1 M€.

This does not affect the total added cost per unit, which slightly increases from 0.65 €/kg to 0.66 €/kg.

By increasing the production this effect is practically nullified: for a production of 100 ton/day the added unit cost is still 0.41 €/kg.

Table 59 - Breakdown of the cost for the estimation of total product cost and total added cost per unit

Item	Annual cost (k€)
Direct production cost	
W31 + H_2O	12006
CO_2	331
Utilities	107
Maintenance and repairs	53
Operating supplies	8
Patents & royalties	558
Operating labor	378
Supervision	57
Laboratory charges	57
Fixed charges	
Capital charges	75
Local taxes	15
Insurance	8
Plant overhead	293
Total product cost	13943
Total added cost per unit	0.65 €/kg

CURRICULUM VITAE

NAME: Luca Davico
DATE OF BIRTH: 23 June 1988
COUNTRY OF BIRTH: Italy

ACADEMIC QUALIFICATIONS

07/2013 – 12/2018 **PhD Candidate**
Ruhr University Bochum, Chair of Process Technology
Exchange period (10/2015 – 12/2015) at University of Valladolid, Faculty of Chemical Engineering and Environmental Technology

09/2012 – 02/2013 **Master Thesis**
T&I of SABIC Europe, Geleen, Netherlands

09/2010 – 03/2013 **Master of Science in Chemical Engineering**
Politecnico di Torino, Torino, Italy

07/2010 – 01/2011 **Bachelor Thesis**
Hysytech s.r.l., Torino, Italy

09/2007 – 04/2011 **Bachelor of Chemical Engineering**
Politecnico di Torino, Torino, Italy

09/2002 – 07/2007 **Secondary Education**
Liceo classico Cavour, Torino, Italy

WORK EXPERIENCE

07/2013 – 07/2017 **Research Assistant**
Ruhr University Bochum, Chair of Process Technology

09/2012 – 02/2013 **Internship**
T&I of SABIC Europe, Geleen, Netherlands

07/2010 – 01/2011 **Internship**
Hysytech s.r.l., Torino, Italy